

# Comparison of multistage thermoacoustic engines in serial versus parallel configurations

## Abstract

In industrial processes about 80% of the energy demand is in the form of heat. One of the problems of the industrial waste heat is the low temperature of this heat. The department of energy efficiency and infrastructure, 'E&I' of the Energy research Center of the Netherlands 'ECN' runs projects in order to use industrial waste heat with a thermoacoustic heat pump. Thermoacoustic engines can deliver the power to drive a thermoacoustic heat pump and can be driven by waste heat. The desired hot temperatures exceed the temperatures of the waste heat. It is believed that more than one thermoacoustic engine is necessary in order to gain sufficient temperature lift. In this study a parallel configuration of thermoacoustic engines is compared to a serial configuration of thermoacoustic engines. Additionally the losses in a coaxial thermoacoustic engine are analyzed.

In two sets of experiments two regenerator units were placed in parallel and serial configuration inside a symmetric resonator. The regenerators were heated with an electrical heater and cooled with cooling water. Power was subtracted with a load. The power that can be subtracted by the load is the same as the power that could be used in a heat pump. The main objective is to gain maximum load power with a hot regenerator temperature as low as possible.

The experiments show that the serial configuration produced more acoustic power in the load than the parallel configuration. In contrast the efficiency of the power produced in the resonator is found to be about the same for both configurations. This is because of the assumption that the power dissipated in the resonator is equal to twice the power dissipated in an empty half of the resonator, while in reality the power dissipated in the resonator depends also on the internal geometries in the resonator, and the internal velocity.

In the present experimental setup the pressure and velocity profile are not the same for serial and parallel configurations. The acoustic power measured in the load is used to compute the external efficiency. The internal efficiency is calculated from the resonator losses and the power measured in the load. The resonator losses were originally determined from two microphone measurements of an empty resonator half, without the consideration of internal geometries. Hence internal efficiencies of the two configurations can not be compared, whereas the external efficiencies can be compared to draw conclusions.

In the parallel configuration at a pressure of 19.9 bar, a drive ratio of 3.03 and a heater input of 324 W, 5.96 W of acoustic power can be subtracted while the hot regenerator temperature rises till 274 °C. In the serial configuration at a pressure of 19.5 bar, a drive ratio of 2.95 and a heater input of 367 W, 11.63 W of acoustic power can be subtracted while the hot regenerator temperature rises till 290 °C. This means the 2<sup>nd</sup> law external efficiency of the serial configuration is 47% better than for the parallel configuration. A calculation predicts that the serial configuration could perform as much as 80% better if the load was placed at the engine side.

In cooling, heating, and other processes where the external power is the useful power the serial configuration is the better configuration.

## Nomenclature:

$a$  = Speed of sound [m/s]  
 $A$  = Surface [m<sup>2</sup>]  
 $B$  = Volume porosity [-]  
 $C$  = Capacitance [s/Ω]  
 $c$  = Specific heat [J/(kgK)]  
 $D$  = Diameter [m]  
 $Dr$  = Drive ratio [%]  
 $E$  = Energy [J]  
 $e$  = Energy density [Wm<sup>-2</sup>]  
 $f$  = friction coefficient [-]  
 $F$  = View factor [-]  
 $g$  = Gravitational force [ms<sup>-2</sup>]  
 $G$  = Pressure multiplication factor [-]  
 $h$  = Convective constant [J/(m<sup>2</sup>Ks)]  
 $I$  = Current in ampère [A]  
 $i = \sqrt{-1}$   
 $J$  = Jacobian matrix derivative [-]  
 $K$  = Friction constant [-]  
 $k$  = Conductivity constant [J/(mKs)]  
 $l$  = Regenerator length [m]  
 $L$  = Inductance [Ωs]  
 $M$  = Specific molar weight [kg/mol]  
 $m$  = mass [kg]  
 $N$  = molflux [mol/s]  
 $n$  = constant value [-]  
 $Nu$  = Nusselt number [-]  
 $P$  = Pressure [10<sup>5</sup>N/m<sup>2</sup>]  
 $p$  = Pressure implied by the acoustic wave [10<sup>5</sup>N/m<sup>2</sup>]  
 $Pr$  = Prandtl Number [-]  
 $Q$  = Thermal energy [J]  
 $r$  = Radius [m]  
 $R$  = Resistance [Ω]  
 $Ra$  = Rayleigh number [-]  
 $Rr$  = Ideal gas constant [-]  
 $Rn$  = Reynolds number [-]  
 $T$  = Temperature [K]  
 $t$  = Time [s]  
 $U$  = Volumetric velocity [m<sup>3</sup>/s]  
 $u$  = Velocity [m/s]  
 $V$  = Volume [m<sup>3</sup>]  
 $v$  = Potential in Volt [V]  
 $W$  = Work [J]  
 $x$  = Distance [m]  
 $Y$  = Second order pressure derivative [Pa/s<sup>2</sup>]  
 $Z$  = Impedance [Ω]

$\Pi$  = perimeter [m]  
 $\beta$  = Thermal (isobaric) expansion coefficient [K<sup>-1</sup>]  
 $\delta$  = boundary layer [m]  
 $\varepsilon$  = roughness [-]  
 $\varphi$  = mass flow [kg/s]  
 $\gamma$  = Isentropic compression coefficient [-]  
 $\eta$  = efficiency [-]  
 $\lambda$  = wavelength [m]  
 $\mu$  = viscosity [kg/(ms)]  
 $\theta$  = phase difference [rad]  
 $\rho$  = density [kg/m<sup>3</sup>]  
 $\sigma = 5.67 \cdot 10^{-8}$  Boltzmann constant [W/(m<sup>2</sup>K<sup>4</sup>)]  
 $\tau$  = Ratio between hot, and cold temperature [-]  
 $\omega$  = frequency [s<sup>-1</sup>]  
 $\xi$  = Emissivity [-]  
 $\Psi$  = Position dependent amplitude [-]  
 $\Theta$  = Thermoacoustic engine index [K<sup>-1</sup>]  
 $\chi$  = Porosity [-]

subscripts:

$0$  = time averaged  
 $a$  = amplitude value  
 $c$  = cold  
 $car$  = Carnot  
 $crit$  = critical  
 $cs$  = cross sectional  
 $e$  = load entrance  
 $h$  = hot  
 $l$  = furthest aposing wall to the entrance  
 $m$  = mean  
 $p$  = constant pressure  
 $T$  = Thermal  
 $v$  = constant volume  
 $w$  = working fluid

Generally:

$$\dot{\alpha} = \frac{d\alpha}{dt}$$

$\text{Im}(\alpha)$  = Imaginary part of  $\alpha$

$\text{Re}(\alpha)$  = Real part of  $\alpha$

S\*.\* means Section \*.\*

$$\nabla^2 = \frac{\partial^2}{\partial x^2} + \frac{\partial^2}{\partial y^2} + \frac{\partial^2}{\partial z^2}$$

TBT = thermal buffer tube

## Contents

Nomenclature:	2
<b>1 Introduction</b>	
1.1 Brief history	7
1.2 Thermoacoustics at the Energy Research Center	8
1.3 Scope of the study	8
<b>2. Thermoacoustics</b>	
2.1 Acoustics	9
2.1.1 Standing waves	9
2.1.2 Traveling waves	11
2.2 Thermoacoustic effect	11
2.3 Analogy with electrical circuits	14
2.4 Comparison between single stage and different multistage configurations	16
2.5 DeltaEC	19
2.6 Nonlinear effects	19
<b>3 Experimental setup</b>	
3.1 Component overview	21
3.2 Experimental data processing	24
3.2.1 Determining the energy balance	24
3.2.4 Measurement of the acoustic power	25
3.2.2 Two microphone method	25
3.2.3 Measurement of the acoustic energy dissipated in the load	25
3.3 Relation between resonator power and operating conditions	28
3.4 Definition of efficiencies	29
3.5 Deviation of the results	29
<b>4. Results</b>	
4.1 Drive ratio based comparison between serial and parallel configurations	32
4.1.1 Drive ratio and heat input	32
4.1.2 Pressure dependency and comparison of efficiency	34
4.2 Internal efficiencies	35
4.3 External efficiency	36
4.4 Comparison of serial and parallel configurations	37
<b>5 Detailed Energetic Analysis</b>	
5.1 Additional Experiments to determine Irreversibilities	40
5.1.1 Heat losses due to natural convection and radiation at the outer resonator wall	40
5.1.2 Static internal losses determination by additional temperature sensors	41
5.1.3 Viscous flow losses around the unit	45
5.2 Results of detailed analysis	46
5.2.1 Environmental heat losses	46
5.2.2 Internal heat losses of the unit	47
5.2.3 Viscous losses around the unit	50

<b>6 Discussion</b>	
6.1 Configuration comparison	51
6.1.1 Correction-factor for the flange amplitude	51
6.1.2 Correction of the acoustic power	52
6.1.3 Correction of the load power	54
6.2 Irreversibilities from additional experiments	59
<b>7 Conclusions and Recommendations</b>	
7.1 Conclusions	61
7.2 Recommendations	62
References	63
Appendix A1: Temperature profiles single stage	I
Appendix A2: Heat losses	II
Appendix B: The DeltaEC program	III
Appendix B1: Predictions by DeltaEC	VII
Appendix B2: Parallel configuration	IX
Appendix B3: Serial configuration	XIII
Appendix B4: Serial configuration with load	XXI
Appendix C: Apparatuses dictionary	XXIX
Appendix C1: Two microphone method	XXXII
Appendix D: Heat images	XXXIV

## List of Figures:

Figure 1.1 Thermodynamic illustration of a thermoacoustic load driven by a thermoacoustic engine	7
Figure 2.1 Sondhauss tube	9
Figure 2.2 Different admittance at different eigenmodes in the tubes from Hall [11]	10
Figure 2.3 First mode in a Sondhauss tube.	10
Figure 2.4 One dimensional traveling wave.	11
Figure 2.5 Visualization of acoustic tubes	11
Figure 2.6 Creation of an acoustic wave in a stack	11
Figure 2.7 p-V Graph of a Stirling cycle.	13
Figure 2.8 Stirling engine.	13
Figure 2.9 The motion of a medium in the regenerator in a traveling wave.	14
Figure 2.10 The traveling wave of Ceperly (1979)	14
Figure 2.11 Schematic of the setup of Backhaus and Swift.	15
Figure 2.12 Torus and Coaxial	15
Figure 2.13 Representation of the torus shaped thermoacoustic system in an analog electrical circuit.	15
Figure 2.14 (a) double the effective area (b) serial engines in a coaxial setup.	17
Figure 2.15 The parallel setup will be constructed by using two units at two different resonator ends.	17
Figure 2.16 Relevant acoustic power in a serial multistage configuration.	18
Figure 3.1 The generator unit/engine	21
Figure 3.2 Resonator dimensions	22
Figure 3.3 Sensor locations; configuration in series	23
Figure 3.4 Sensor locations; configuration in parallel	23
Figure 3.5 Internal schematic in series	23
Figure 3.6 Internal schematic of parallel units.	24
Figure 3.7 Acoustic power	25
Figure 3.8 Simplified energy fluxes	26
Figure 3.9 Measurement of energy transported	26
Figure 3.10 Load power plotted against two microphone measured power at 19 bar in a parallel configuration	28
Figure 3.11 Acoustic engine power (a), and power losses dissipated in the resonator (b) verses load power	28
Figure 3.12 Data for determination of the relative standard deviation in resonator losses.	30
Figure 4.1 Engine power output and thermal efficiency against temperature of the hot side of the regenerator	31
Figure 4.2 Drive ratio squared against hot temperature.	32
Figure 4.3 drive ratio squared against total heat input.	33
Figure 4.4 Internal thermal efficiency as a function of hot regenerator temperature and drive ratio squared	34
Figure 4.5 Internal thermal efficiencies as a function of hot temperature of the regenerator and drive ratio	34
Figure 4.6 Experimental internal performance at 19 bar against hot regenerator temperature	35
Figure 4.7 External efficiency and power plotted against hot regenerator temperature	36
Figure 4.8 2nd law external efficiency against hot regenerator temperature (load side)	37
Figure 4.9 2nd law external efficiency against hot regenerator temperature (engine side)	37
Figure 5.1 Qualitative Energy flow diagram.	39
Figure 5.2 Thermal buffer tube and the heat processes	42
Figure 5.3 Slab theory	42
Figure 5.4 Single stage heat flux.	43
Figure 5.5 Heat image of a unit at 230oC	45
Figure 5.6 Geometries inside a resonator half.	45
Figure 5.7 (a) Calibration measurement	46
Figure 5.8 The temperature of the hot regenerator side is plotted against the dissipated heat	47
Figure 5.9 The temperature of the hot regenerator side is plotted against the dissipated heat	47
Figure 5.10 Heat input against hot regenerator temperature	48
Figure 5.11 Distribution of heat at 19 bar in dynamic (a 162°C) and static state (b 154°C)	48
Figure 5.11 Losses in the resonator and around a dummy	50
Figure 5.12 Regenerator friction losses of the serial configuration at different drive ratios at 19 bar	50
Figure 6.1 Middle microphones readings in series and in parallel against the flange microphone reading	52
Figure 6.2 Corrected pressure profile based on the phase shift of the two microphones in the middle.	52
Figure 6.3 Thermal internal regenerator efficiencies for serial and parallel configurations	53
Figure 6.4 Acoustic regenerator power produced in the different configurations	54
Figure 6.5 Acoustic regenerator power in load and no load conditions	56
Figure 6.6 Predicted 2 <sup>nd</sup> law external efficiency as a function of hot temperature	57

Figure 6.7 Data of acoustic power converted in the parallel configuration with the temperatures 16 K lower	57
Figure 6.8 volumetric velocity at end and start position of the unit under load conditions	58

# 1 Introduction

Thermoacoustics concerns the conversion of heat into acoustic energy and vice versa. Thermoacoustic systems have no moving parts and are not prone to wear and fouling. Thermoacoustic energy conversion can be used in a wide range of applications. Acoustic energy is a form of mechanical energy. Heat can be used to generate acoustic power that can be converted into electrical power, create cooling power, or used in a heat pump. A system is considered thermoacoustic when either the acoustic energy is generated by a temperature difference or acoustic power is converted into a temperature difference.

## 1.1 Brief history

The history of thermoacoustics [18] is complex in the sense that not always fundamental understanding has preceded technological developments. In the 18<sup>th</sup> century glassblowers discovered sound could be generated by placing glasses of different temperatures in contact with each other. This led to the development of the Sondhauss tube [5] in the 19<sup>th</sup> century. Rayleigh [1] was the first to qualitatively explain heat-driven oscillations in Sondhauss tubes (Section 2.1), which also occur in Rijke oscillations [6] and cavity combustion [11].

After attempts by Rayleigh and others Rott [2-4] described the mathematics of an oscillating gas in a channel with an axial temperature gradient. Rott did this in his cryogenic study. Urieli and Berchowitz [10] assumed sinusoidal time oscillations for all important variables and used complex numbers to account for time phase and amplitudes in Stirling engines.

In 1979 thermoacoustics was revived by Ceperly [7-8] who realized the time phasing between pressure and motion oscillation in the regenerator of a Stirling engine is that of an acoustic traveling wave (Chapter 2). Ceperly was not able to start his experimental setup, but knew how to solve it. Meanwhile Wheatley et al. [13-14] invented the first standing wave thermoacoustic refrigerator. Mikulin et al. created the Pulse tube refrigerator [9].

Backhaus and Swift [17] succeeded to develop the first acoustic traveling wave engine in Los Alamos in 1999 based on the improvements suggested by Ceperly.

Acoustic waves can be used for cooling, for separation of gas mixtures, for heating, and for mechanical power.

A thermoacoustic system can be divided into different components (examples are found in Table I). A system can be described as a thermoacoustic system when it involves a conversion from thermal into acoustic energy or vice versa. This component can either be the driver or the load (fig 1.1).

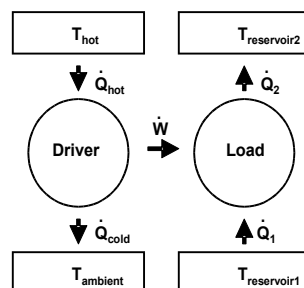


Figure 1.1 Thermodynamic illustration of a thermoacoustic load driven by a thermoacoustic engine

Table I shows the different energy conversion processes possible to and from acoustic energy. There are more possibilities than those shown. A detailed description of the thermoacoustic engine is given in appendix C.

Table I. Acoustic components. (A=Acoustic, E=Electrical, M=Mechanical, and T=Thermal)

Energy transfer	Driver name	Conversion Description	Load name	Conversion description
T→A/A→T	Engine	Temp. gradient into acoustic energy	Heat pump *	Acoustic energy into temp. gradient
E→A/A→E	Speaker	Electricity into acoustic energy	Piezoelectric	Acoustic energy into electricity
M→A/A→M	Displacer	Mechanical into acoustic energy	Displacer	Acoustic into mechanical energy
A	Resonators can be used for separation of gases			

\* Heat pump can be an actual heat pump or a refrigeration cycle

## 1.2 Thermoacoustics at the Energy Research Center

In industrial processes about 80% of the energy demand is in the form of heat. One of the problems in industrial waste heat is the low temperature of this heat. The aim of the Energy Research Center of the Netherlands 'ECN' department energy efficiency and Infrastructure is to reuse industrial waste heat. The research group 'Industrial Heat Technology' develops cost-effective technological solutions for upgrading or storing industrial waste heat. The temperature of the waste heat must be upgraded by a heat pump. Conventional compression heat pumps have a limited temperature range and lift related to the working fluid. Whereas the temperature lift and range in thermoacoustic heat pumps is limited by the temperature limits of the solid regenerator material.

The most efficient thermoacoustic engines use a traveling wave. ECN currently holds the world record in generation of acoustic energy from a thermal source, with an efficiency of 49% relative to Carnot. Multi-stage thermoacoustic engines may be necessary to obtain sufficient energy density in the system to create sufficient temperature-lift in a thermoacoustic heat pump.

This study is part of a larger study which was started at ECN in order to gain better understanding of the practical behavior of thermoacoustic systems. This study compares two configurations of a multistage engine, parallel and series. In the parallel configuration two engines are placed in opposite sides of the resonator. In the serial configuration two engines are placed in line close to each other facing the same direction.

## 1.3 Scope of the study

The first and most important aim of this study is to compare and analyze why and which configuration would deliver better performances, when a serial configuration is compared to a parallel configuration. An experimental comparison between serial and parallel configurations has never been reported in literature.

The second aim of the study is to widen the general knowledge on losses in thermoacoustic systems. Earlier studies have shown a big difference between theoretical and practical heat losses. This study aims to quantify these differences.

The methods that are currently used to measure the acoustic energy do not account for friction losses around a thermoacoustic engine. Therefore the real acoustic power output of the engine can not be determined. Including friction losses in the analysis will help to understand the differences in performance of the different configurations.

In chapter 2 the thermoacoustic phenomenon will be described. In chapter 3 the experimental setup will be described. Chapter 4 will present and compare the results. Then chapter 5 will be dedicated to the heat losses and friction losses. Chapter 6 will discuss and combine the different results of this study. Finally chapter 7 will formulate the conclusions and recommendations.

## 2. Thermoacoustics

Thermoacoustic systems convert sound into a temperature gradient or a temperature gradient into sound. The energy transport is done by an acoustic wave in a working fluid. In thermoacoustics there is a combination of temperature, heat, displacement, and pressure oscillations in the medium. Rayleigh [1] stated: “If heat be given to the air at the moment of greatest density or be taken from it at the moment of greatest rarefaction, the vibration is encouraged “. The medium is always a fluid with a lower heat capacity than the solid material that is in contact with the medium.

Swift [18] stated “The thermoacoustic approach begins with the assumptions that the oscillations of pressure, temperature, density, velocity, and entropy can be though small and that they are adequately represented as sinusoidal function of time.” The mathematical description of harmonic oscillations is

$$\alpha(t) = \alpha_0 + \alpha_a \exp^{i\omega t} \quad (2.1)$$

where  $\alpha$  stands for any oscillating property,  $t$  is time,  $i = -1^{0.5}$ , and  $\omega$  is the angular frequency.

### 2.1 Acoustics

An acoustic wave is a combination of displacement and pressure oscillation in a medium. It is a combination of kinetic and potential energy with the anomaly of oscillation.

#### 2.1.1 Standing waves

The Sondhauss tube is a tube filled with air and heated at the closed side, see figure 2.1

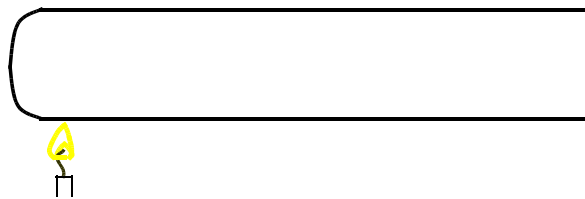


Figure 2.1 Sondhauss tube

Sondhauss tubes produce sound waves. Glass is a bad conductor, so the air is heated only locally at the closed end. At the closed end the pressure can differ from the environmental pressure, while at the open end the pressure is always environmental. There is no volume flow through the closed end, but through the open end gas can move freely. Posing the boundary conditions that are present in the Sondhauss tube on the time independent wave equation or Helmholtz equation [27] we obtain

wave equation: 
$$\frac{\partial^2 u}{\partial t^2} = a^2 \nabla u$$

Boundary conditions:  $x = 0 \Rightarrow U = 0 \Rightarrow \vec{u} = 0$

$$x = L \Rightarrow p = p_o \quad (2.2)$$

Solutions: 
$$U = U_a \sin\left(\frac{(1+2n)\pi x}{2L}\right) \sin(2\pi\omega t)$$

$$p = p_o + p_a \cos\left(\frac{(1+2n)\pi x}{2L}\right) \cos(2\pi\omega t)$$

with  $n$  being any natural number (0,1,2,3,...)

$\nabla^2$  is the Laplacian operator, which is the sum of the second derivatives in all specified dimensions,

$p_a$  stands for oscillating pressure amplitude,  $L$  is the length of the open tube,  $U_a$  is the oscillating volumetric velocity amplitude,  $\omega$  is the frequency,  $u$  is a scalar function,  $a$  is the speed of sound, and  $\vec{x}$  is the velocity vector.

Different solutions are possible for solving the boundary conditions in the Sondhauss tube. The one dimensional standing wave (only evaluated in one direction) has therefore different frequency modes with a different admittance profile. The admittance is the inverse of the impedance (the impedance is the resistance to an alternating potential). In figure 2.2 a mathematically derived example is shown for a special kind of Sondhauss tube with two closed ends.

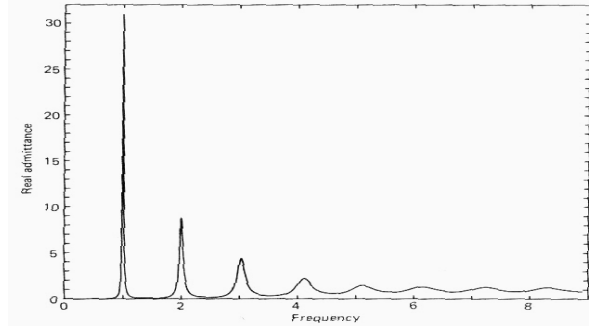


Figure 2.2 Different admittance at different eigenmodes in the tubes from Hall [11] the frequency is given as a multiplication of the constant  $a/2L$ . The admittance is the Amplitude times the ratio between radii of the tube.

Figure 2.3 shows the pressure and velocity of the oscillating fluid particles in the first mode that has the highest energy content. The pressure and velocity evolve with a  $90^\circ$  phase, or  $1/4 \lambda$  wavelength difference.

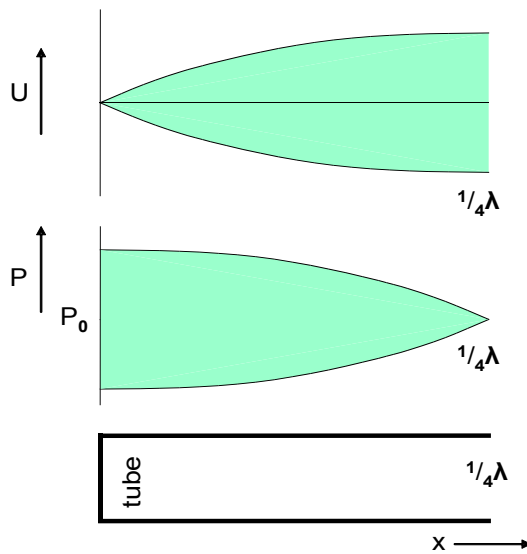


Figure 2.3 First mode in a Sondhauss tube.

Where  $p_0$  is the time averaged pressure. The closed end has a pressure antinode, while a node can be found at the open end at atmospheric pressure. The length is always  $1/4 \lambda$ , where  $\lambda$  is the wavelength. The frequency is equal to the sound velocity divided by  $\lambda$ . Thus the length of the tube will determine the frequency of the modes.

The Energy flow in an acoustic wave is given by

$$\dot{E}_{acoustic} = \frac{1}{2} p_a U_a \cos \mathcal{G} \quad (2.3)$$

$\mathcal{G}$  being the phase difference between velocity and pressure in time

The energy contents is equivalent to the product of  $p$  times  $U$ , which is the highest halfway (at  $1/8 \lambda$ ).

### 2.1.2 Traveling waves

If the pressure and velocity amplitudes are in phase, it is called a traveling wave. Solid tubes are used to constrain the acoustic power in one direction in order to maintain a high energy density. In a traveling wave (fig.2.4) the length of the tube is infinite, so there are no boundary conditions in this direction.

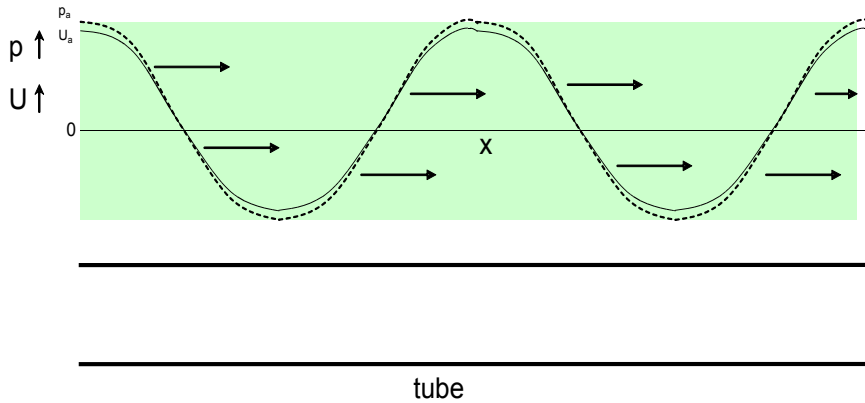


Figure 2.4 One dimensional traveling wave.

### 2.2 Thermoacoustic effect

In this section the standing wave will be explained in a stack and the traveling wave in a regenerator, although traveling waves can also exist in stacks.

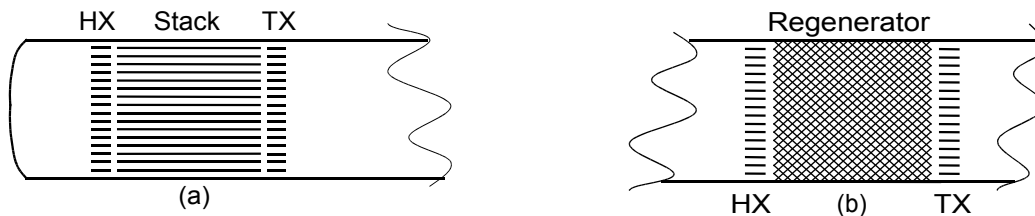


Figure 2.5 Visualization of acoustic tubes with the hot heat exchanger HX and ambient heat exchanger TX.

Figure 2.5a is similar to the Sondhauss tube, heating is done at the closed end. The stack consists of a number of channels in order to increase the surface area and thus the thermoacoustic effect. The regenerator (fig.2.5b) is made of porous material with very thin pores, so the medium and solid temperature in the regenerator can be assumed to be equal.

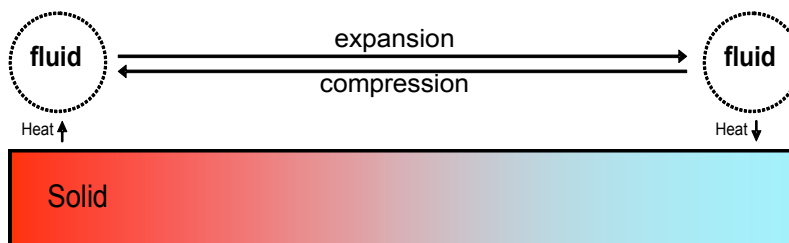


Figure 2.6 Creation of an acoustic wave in a stack the black arrows represent the heat flow, and the horizontal arrows give the direction of motion. Red represents hot and blue cold. When the parcel moves to the left it expands by heating, while the movement causes compression of the gas between the stack and the closed end, and vice versa.

In the creation of a standing wave by a temperature difference along a solid wall (fig.2.6) a fluid parcel that is heated will expand as it heats up, building up pressure because there is a closed end placed after the hot side (fig.2.5). The parcel gets pushed towards the cold side because of the pressure built up at the hot side. When the fluid cools down as it moves in the opposite direction it contracts, further away from the cold side the pipe is open (fig.2.3) and the pressure is constant. The contraction of the fluid at the cold side will result in a low pressure at the hot side, thus creating the conditions where the fluid is pulled towards the hot side and so on. This oscillation of the fluid accompanied by the acoustic wave is a form of mechanical energy, because the mass of the fluid is not equal to zero.

In the reversed process an acoustic (standing) wave is forced through the stack and the pressure builds up at the side of the closed end. This compression will create heat while the expansion at the other side will create cooling.

The medium that is further away from the wall outside the viscous boundary layer, but within the thermal penetration depth, suffers less viscous losses, a moving parcel can have a different temperature than a parcel near the solid wall. Heat exchange is better at locations of lower velocities because there the medium has a uniform temperature.

There is a finite layer thickness of the medium that is effective for thermal transport in an oscillating acoustic wave. This is called the thermal boundary layer thickness of the working medium[19]

$$\delta_r = \sqrt{\frac{2k}{\rho c_p \omega}} \quad (2.5)$$

where  $k$  is the thermal conductivity of the fluid,  $\rho$  is density of the fluid, and  $c_p$  is the heat capacity of the fluid. In regenerators the hydraulic radius should not exceed the thermal boundary layer.

The losses are mainly viscous losses. The viscosity of the working fluid also determines the thickness of the layer which is not effective because of the dissipation of kinetic energy, Tijani et al. [20].

$$\delta_v = \sqrt{\frac{2\mu}{\rho\omega}} \quad (2.6)$$

where  $\mu$  is the viscosity. The optimum medium has a small viscous boundary layer, and a large thermal boundary layer thickness. The ratio between these layers is expressed by the Prandtl number  $Pr$  given by

$$Pr = \frac{\delta_v^2}{\delta_r^2} = \frac{\mu c_p}{k} \quad (2.7)$$

For the use in thermoacoustics fluids with the lower Prandtl number are favorable. Helium ( $Pr=0.70$ ) is used often, because of the low viscous losses. Nitrogen ( $Pr=0.69$ ) and Argon ( $Pr=0.68$ ) are used as more inert variants of air ( $Pr=0.68$ ). Some researchers use air to overcome pressurization issues.

Because of the better theoretical efficiency of the traveling wave, the focus in this study is on traveling waves.

The traveling wave thermoacoustic cycle is similar to a Stirling cycle where an acoustic wave replaces the pistons. The Stirling engine was originally invented in 1816 as an external heat driven engine. The basic form involves two pistons of which one is the driver located at the heated side, and the other, the displacer, is placed on the cold side (fig.2.8). The medium is the same on both sides and moves from one side to the other through a thermal buffer which is also called regenerator.

The Stirling cycle could be divided into two isochoric processes and two isothermal processes as shown in figure 2.7a. In reality there is overlap in the occurrence of these processes (fig.2.7b).

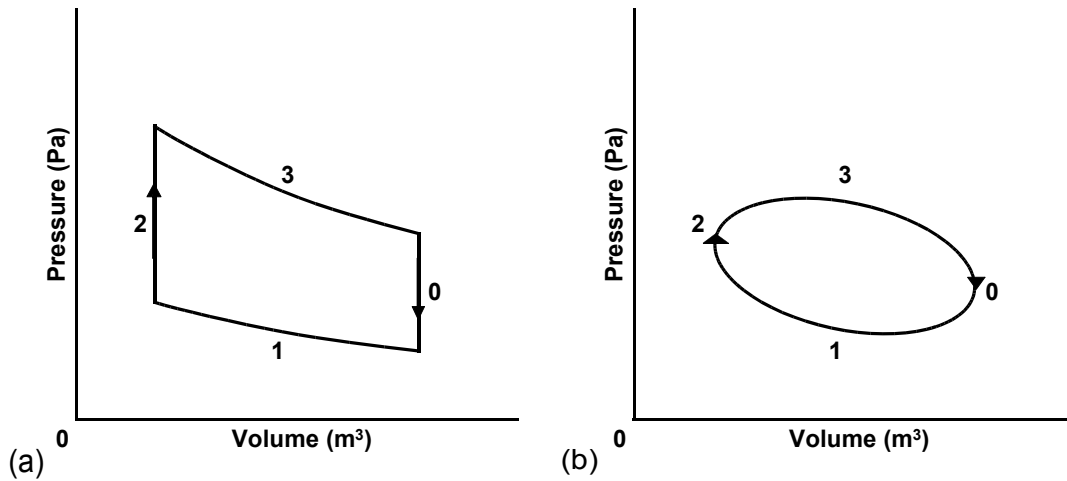


Figure 2.7 p-V Graph of a Stirling cycle. (a) The isothermal and isochoric process (b) The real Stirling cycle

In the Stirling cycle (fig.2.7 & 2.8) step 0 and 2 are isochoric, while 1 and 3 are isothermal. Figure 2.8 illustrates the working of a Stirling cycle. Numbers correspond with the left side of figure 2.7.

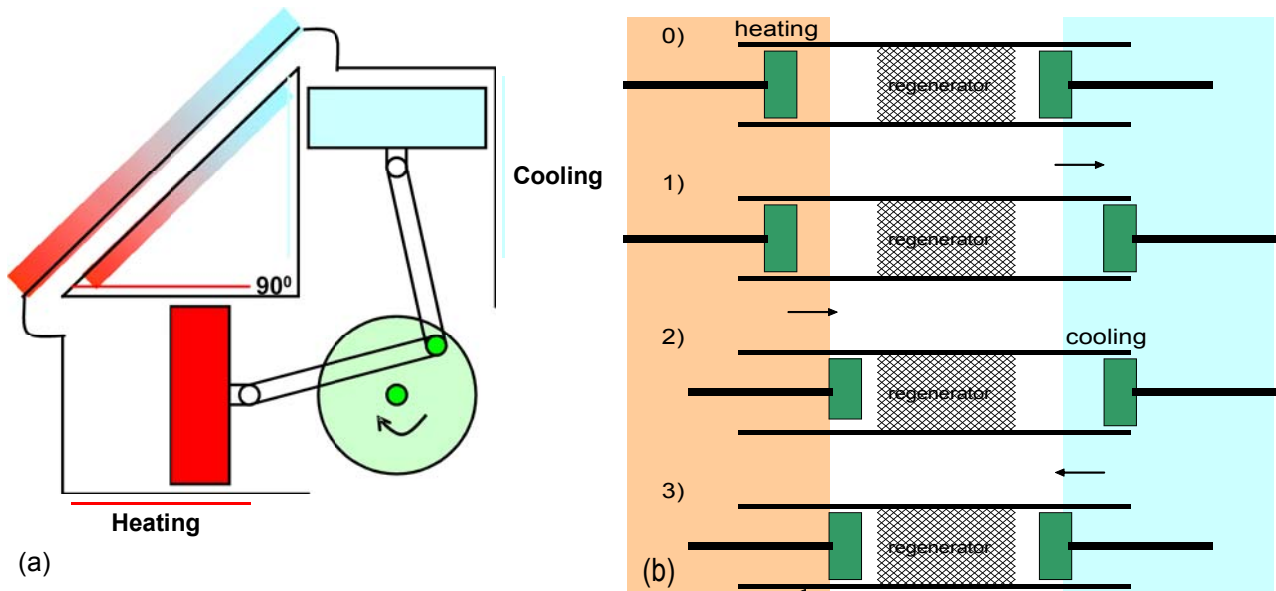


Figure 2.8 Stirling engine. (a) A simple example of a Stirling engine. The green wheel turns on a shaft in the midpoint, while two rods are attached to a second shaft on the wheel. The two pistons are exposed on one side to the same medium, and on the other side to environmental conditions. (b) The driver is the left piston, while the right piston is free. The first step 0) is heating, followed by an expansion 1) followed by cooling 2) followed by compression 3).

When there is more fluid in the heated part (fig.2.8) the fluid expands and drives the shaft that will suck fluid to the cooled side. The fluid is already cooled on its way to the cooled side. Further decrease of the fluid volume at the cold side drives the same shaft that now expands the volume at the hot side changing the direction of the fluid. The fluid is heated as it moves towards the hot side, and so on. In a perfect Stirling engine the velocity and pressure are in phase.

In figure 2.9 a piece of a complex network of pore-channels of the regenerator is simplified as two straight solids. In a traveling wave when a temperature difference is applied along the regenerator, a moving parcel of fluid will subsequently be displaced, heated, and expanded. This will create higher pressures that reverse the flow direction, the fluid will be displaced in the opposite direction, cooled and shrunk. During this cycle the gas is being shrunk at low temperature, while expansion takes place at high temperature. This means that work is performed on the fluid. The effect of this work is that the pressure amplitude of the sound wave is increased.

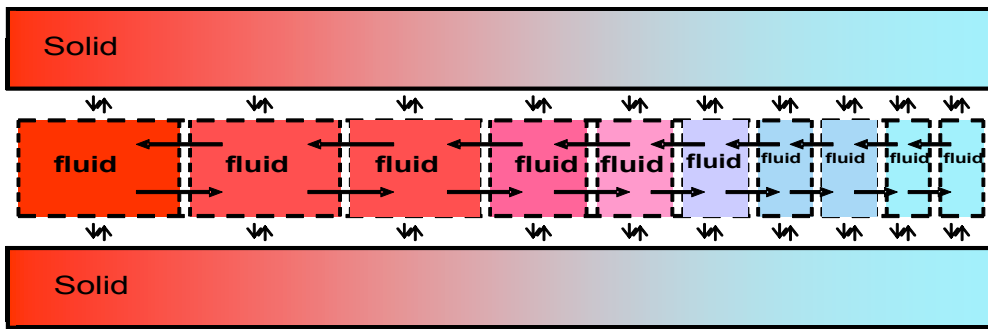


Figure 2.9 The motion of a medium in the regenerator in a traveling wave.

Heat can be exchanged between the working fluid and the solid material equally well at all times and locations, because of good thermal contact.

Volumetric velocity and pressure are in phase, the compression and expansion are maximal when the medium velocity is maximum.

In the reverse process an acoustic (traveling) wave is forced through the regenerator and heats up as the pressure builds up because of compression. The expansion at the other side will create cooling. By fixing the hot or cold temperature the regenerator can be respectively a cooler or heater.

Ceperly [7-8] tried to create a thermoacoustic cycle using a traveling wave (fig.2.10). He used a regenerator and two heat exchangers in a looped pipe, but failed to start the acoustic wave. The regenerator dissipated too much power. The flow through the regenerator would always cause more friction than the increase in power would have been

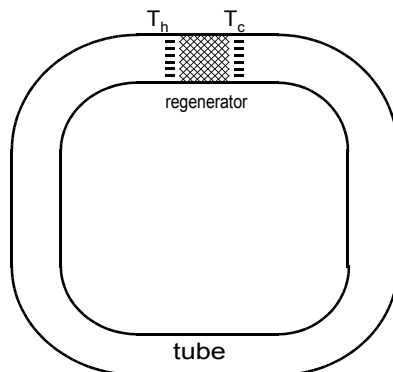


Figure 2.10 The traveling wave of Ceperly (1979)

### 2.3 Analogy with electrical circuits

The analogy for comparison between multistage parallel and serial configurations of thermoacoustic engines is derived by using the analogy between acoustic and electrical circuits. Backhaus and Swift [17] improved the traveling wave engine designed by Ceperly by attaching a resonator. The resonator dictates the frequency and decreases the local fluid velocity in the loop (fig.2.11). Like in electricity transport where a high voltage is applied in order to reduce the current through the power lines, analogously they intended to increase the pressure in order to reduce the volumetric flow. In a Sondhauss tube high pressures and low velocities are found at the closed end, so the loop is placed at the end of a resonator (fig.2.11). Unfortunately the resonator also dissipates acoustic energy.

In figure 2.11 a traveling wave is preserved in the left loop while a standing wave is preserved in the resonator. The controlled environment is a buffer volume. It simulates an open end and enables to control the pressure. The (generator) unit inside the loop is introduced as the combination of a regenerator, heat exchangers, thermal buffers, and anything between these apparatuses.

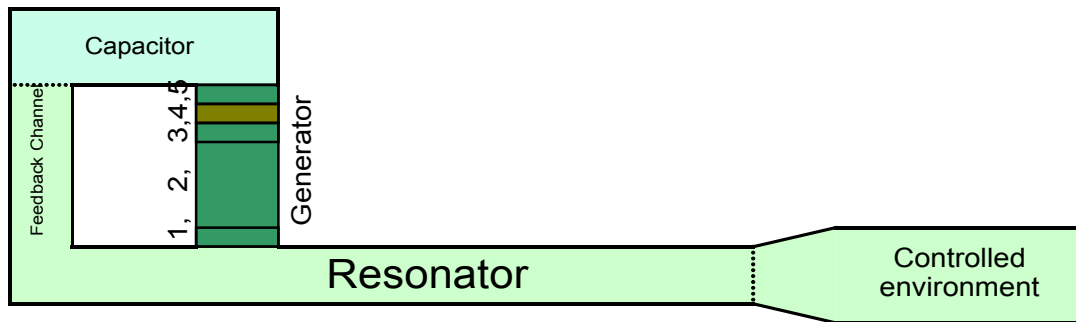


Figure 2.11 Schematic of the setup of Backhaus and Swift. The generator consists of: 1; cold heat exchanger, 2; thermal buffer tube, 3; hot heat exchanger, 4; regenerator, and 5; cold heat exchanger. The medium can move freely within the colored elements but is sealed off from the environment.

In the torus shape the feedback channel, capacitor volume and unit are placed in a sequential loop. The coaxial configuration has the unit placed inside the feedback channel and capacitor (fig.2.12).

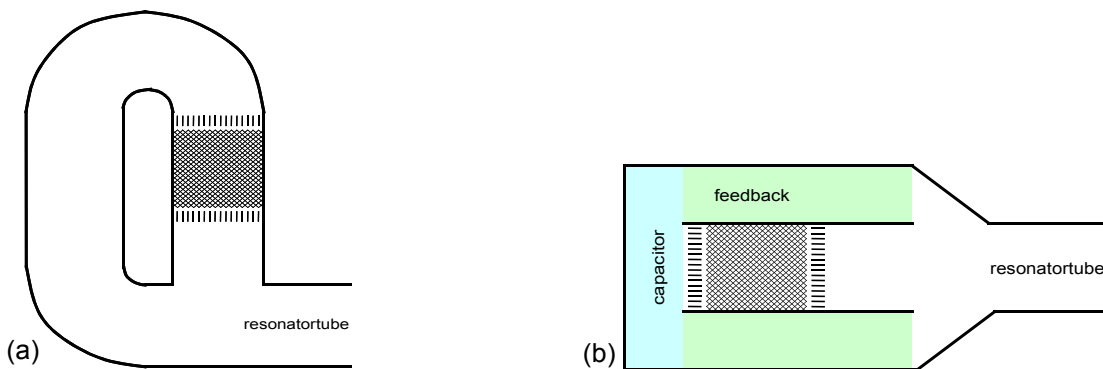


Figure 2.12 Torus and Coaxial (a) torus shape (b) coaxial shape

In an electrical analogy represented in figure 2.13, which is the same system as figure 2.11, can be shown that the phase in the resonator and the regenerator can be different. The standing wave on the right is effectively a frequency control while the left side contains the working parts, and operates a traveling wave.

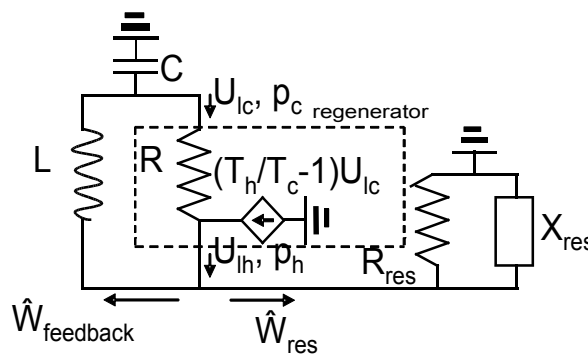


Figure 2.13 Representation of the torus shaped thermoacoustic system in an analog electrical circuit.

In figure 2.13 there are two resistances  $R$  drawn. The left one being the regenerator, and the right one is the resonator.  $U_{lc}$ ,  $U_{lh}$ ,  $p_c$ , and  $p_h$  are respectively volumetric velocity before the regenerator, volumetric velocity after the regenerator, pressure before the regenerator, and pressure after the regenerator.  $L$  is the constant value of the inertia of the feedback channel.  $X_{res}$  is a reactive impedance (purely complex impedance value).

An impedance contains a real and an imaginary value. A purely real value is also known as resistance, while complex values affect the phase.

The frequency dependent impedance of the components generator, feedback channel, and capacitor equals respectively  $R$ ,  $\omega L$ , and  $1/\omega C$ .

The regenerator acts as acoustic amplifier with the amplification factor [7]  $\tau$  equal to

$$\tau = \frac{T_h}{T_c} \quad (2.8)$$

where  $T_h$  and  $T_c$  are respectively the temperature of the hot side of the regenerator and the temperature of the cold side of the regenerator. So that

$$\dot{W}_{out} = \frac{T_h}{T_c} \dot{W}_{in} \quad (2.9).$$

where  $\dot{W}$  stands for the acoustic power.

In order to operate at temperatures below 200°C for which the amplification factor is low, multistage thermoacoustic engines are expected to be necessary. The idea is to use multiple thermoacoustic engines driven by industrial waste heat as a driving force to generate sufficient acoustic power to create higher temperature lifts in a thermoacoustic heat pump.

From a simplified model based on analogy with electrical circuits, Ceperly [7] and Backhaus and Swift [17] could derive the pressure amplitude of the acoustic wave.

$$p_c^2 = \frac{2R}{T_h/T_c \omega^2 LC} \dot{Q}_h \quad (2.10)$$

where  $\omega$  is the frequency of the acoustic wave,  $p_c$  is the pressure amplitude at the cold side of the regenerator,  $\dot{Q}_h$  being the heat flux inserted on the hot side.  $L$ ,  $R$ , and  $C$  respectively the inertance of the feedback channel, the resistance of the regenerator and the capacitance of the capacitor volume (fig.2.11).

They further derived the volumetric velocity amplitude of the acoustic wave inside the regenerator.

$$U_{1c} = \frac{\omega^2 LC}{R} \frac{p_c}{1 + i\omega L/R} \quad (2.11)$$

where  $U_{1c}$  is the volumetric velocity at the cold side of the regenerator. They concluded that in the regenerator  $p_a$  and  $U_a$  are in phase when  $\omega L \ll R$ .

Because at low frequencies the wave is more effective,  $\omega$  is small and the impedance  $\omega L$  is small. In this experimental setup the frequency is in the range of 60 to 70 Hertz.

## 2.4 Comparison between single stage and different multistage configurations

The original question for thermoacoustic engineering which is strongly related to the choice between parallel and serial configuration was the determination of the optimum geometry of the regenerator in terms of diameter 'A' and thickness 'B'. Increasing the thickness reduces the temperature gradient for the same heat source and increases the internal regenerator friction, but reduces the conduction of heat through the regenerator. Increasing the cross sectional area should result in a linear increase of the system power, provided losses don't increase in the feedback channel.

Because the optimum thickness can be mathematically determined once the friction losses and

conductivity are known, and engines are likely to be built in a modular way, the optimization issue was pushed towards the comparison between serial (fig.2.14b) and parallel (fig.2.15) multistage engines. Parallel engines should suffer similar friction losses as serial engines, because the feedback has the same geometry (fig.2.15). When friction losses are not considered the comparison can be visualized as in figure 2.14.

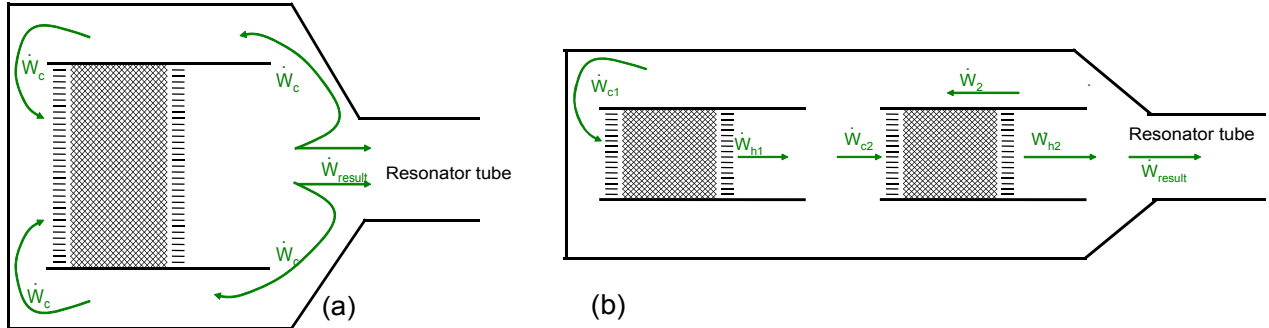


Figure 2.14 (a) double the effective area (b) serial engines in a coaxial setup.

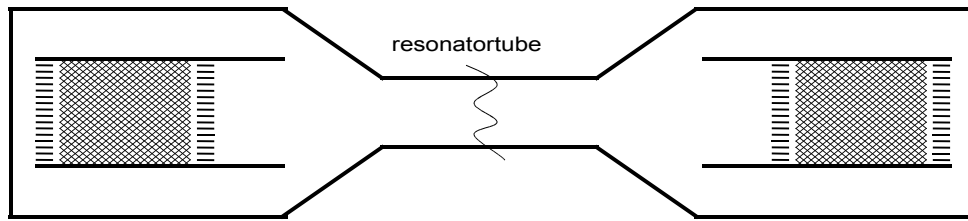


Figure 2.15 The parallel setup will be constructed by using two units at two different resonator ends.

The relation between temperature and amplification (of Ceperly [8]) is

$$\dot{W}_h \approx \tau \dot{W}_c \tag{2.12}$$

where  $\tau$  is the ratio between hot and cold temperature,  $\dot{W}_h$  is the acoustic power on the hot side, and  $\dot{W}_c$  is the acoustic power on the cold side. Eq. 2.12 can be used to determine the relation between the cold power input and the resulting output power, assuming for simplicity all losses only take place in the resonator tube.

For the parallel configuration a doubled cross sectional area means double entering energy with the same acoustic wave and double the leaving energy at the hot side

$$\begin{aligned} \dot{W}_{result, parallel} &= 2\dot{W}_h - 2\dot{W}_c \\ \dot{W}_{result, parallel} &= 2\dot{W}_c (\tau - 1) \end{aligned} \tag{2.13}$$

In the serial configuration there are 6 unknown acoustic power values (fig.2.14b) and only four constitutive equations

$$\begin{aligned} \dot{W}_2 &= \dot{W}_{h2} - \dot{W}_{result} \\ \dot{W}_{h1} &= \dot{W}_{c1} \tau \\ \dot{W}_{h2} &= \dot{W}_{c2} \tau \\ \dot{W}_{c1} &= \dot{W}_{h1} - \dot{W}_{c2} + \dot{W}_2 \end{aligned} \tag{2.14}$$

This could be used to derive

$$\begin{aligned}
\Rightarrow \dot{W}_{c2} &= \dot{W}_{c1}\tau + \dot{W}_{c2}\tau - \dot{W}_{result} - \dot{W}_{c1} \\
(1-\tau)\dot{W}_{c2} &= (\tau-1)\dot{W}_{c1} - \dot{W}_{result} \\
\dot{W}_{c2} &= \frac{\dot{W}_{result}}{(\tau-1)} - \dot{W}_{c1}
\end{aligned} \tag{2.15}$$

This leaves two different approaches to solve the problem. Either an assumptive relation must be introduced on how the added power between both units relate, or the radial acoustic power transfer from and to the capacitor between the two units can be assumed zero.

For equal added power for both units

$$\begin{aligned}
\dot{W}_{h1} - \dot{W}_{c1} &= \dot{W}_{h2} - \dot{W}_{c2} \Rightarrow (\tau-1)\dot{W}_{c1} = (\tau-1)\dot{W}_{c2} \Rightarrow \dot{W}_{c1} = \dot{W}_{c2} \\
\dot{W}_{result} &= 2(\tau-1)\dot{W}_{c1}
\end{aligned} \tag{2.16}$$

the same relationship is found as in the parallel configuration.

A volume in an acoustic system acts the same way as a conductor in an electrical system. The DeltaEC simulation (Appendix B) predicts that as the volume between the two engines becomes smaller the overall efficiency improves. When the compliance volume decreases the power leak decreases until effectively  $\dot{W}_{c1} = \dot{W}_{c2}$ . Then the acoustic powers can be redrawn as in figure 2.16. This will result in equation 2.17.

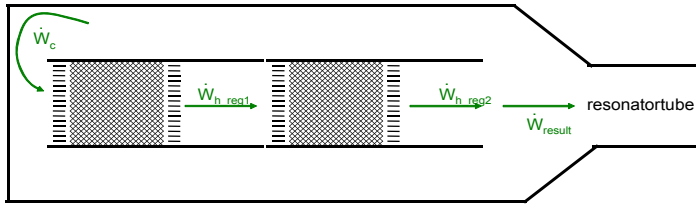


Figure 2.16 Relevant acoustic power in a serial multistage configuration.

$$\begin{aligned}
\dot{W}_{h1}\tau &= \dot{W}_{h2} \\
\dot{W}_c &= \dot{W}_{h2} - \dot{W}_{result} \\
\dot{W}_c\tau &= \dot{W}_{h1} \\
\Rightarrow \dot{W}_c\tau^2 &= \dot{W}_{h2} \Rightarrow \dot{W}_c - \dot{W}_c\tau^2 = -\dot{W}_{result} \\
\dot{W}_{result} &= \dot{W}_c(\tau^2 - 1)
\end{aligned} \tag{2.17}$$

The real amplification factor for the “serial configuration” should be somewhere in between  $(\tau^2 - 1)$ , and  $2(\tau - 1)$ .

To obtain the same drive ratio for both parallel and series and consequently the same conditions, the outgoing work divided by the ingoing work should be equal (see eq.2.13 and 2.17)

$$\tau^2 - 1 = 2\tau - 2 \Rightarrow \tau^2 - 2\tau + 1 = 0 \Rightarrow (\tau - 1)^2 = 0 \tag{2.18}$$

Meaning for  $\tau > 1$ , which is always true, series will produce better power amplifications.

Note that this is no statement regarding the efficiency. Nevertheless the efficiency greatly depends on the drive ratio, which is the pressure amplitude divided by the average pressure, when the amplification factor is higher, this would benefit high drive ratios with better efficiencies.

The efficiency of a series of coaxial multistage thermoacoustic engines was quantified in recent

years. Parallel combinations were not studied because it was believed to be unfavorable to have separate generator units, when the same effect could follow from increasing the diameter.

A simulation (appendix B and Chapter 4) showed that serial units would operate better than parallel units with the same hot temperature. The predicted efficiency of both configurations was the same, but serial units produced more acoustic power.

## 2.5 DeltaEC

In the development of thermoacoustic systems the DeltaEC software tool is commonly used. DeltaE was created for the Los Alamos national laboratory by Ward, Clark, and Swift. DeltaEC stands for design environment for Low-amplitude thermoacoustic energy conversion.

DeltaEC numerically integrates a one-dimensional wave equation over any defined geometry with a selected working fluid. The program solves the one dimensional wave equation through each of the user defined elements, called “segments”, such as volumes, ducts, heat exchangers and regenerators, base on the periodic wave equation and the Navier Stokes equation. DeltaEC calculates the thermoacoustic equations, conduction equations, and respects all conservation laws. DeltaEC ensures that the pressure and volumetric flow rates, both real and imaginary components, are matched at the boundaries of each segment. DeltaEC also checks and shows the acoustic power and energy flow between segments.

DeltaEC ignores some areas of acoustic dissipation, like flow straightening screens, the friction around complex geometries, some heat related power dissipation (it does include conduction related heat dissipation in the regenerators, and the thermal buffer tube), and non-linear effects.

## 2.6 Nonlinear effects

A traveling wave system is a very close approximation to the Stirling-, or ideal cycle, and therefore traveling wave systems are often considered reversible. In a fully reversible process the second law efficiency also called efficiency relative to Carnot would be 100% (see Section 3.4)

The irreversibilities are due to thermo-viscous and nonlinear effects in the system. Nonlinear effects can be subdivided in four different effects, which will be further discussed in this section.

### Gedeon Streaming

Traveling waves don't suffer from boundary conditions, they oscillate freely. The freedom of movement through the regenerator, while the pressure drop between the resonator and the capacitor is different through the feedback channel than through the unit, will result in a steady mass flux as a second order effect. This current is called 'Gedeon streaming' which is, because of the similarities between a thermoacoustic system and an alternating current, a direct current (DC) streaming.

### Rayleigh Streaming

In a standing wave and in anything less than a perfect traveling wave, the gas between the parcels oscillating furthest from and nearest to the solid wall has a different temperature during the motion of the parcel between the hot side and the cold side, due to the phasing between temperature and motion. Because the viscosity depends on temperature, the drag experienced by the parcel is different in different directions. The parcel does not come back to its initial position.

The resulting direct current in thermoacoustics is referred to as Rayleigh streaming, as described by Olsen and Swift [28].

In the regenerator the temperature of the working fluid, and the solids can be assumed equal. A direct current will push gas with an environmental temperature to the cold side and push hot gas out of the hot side. The sum of these two heat losses could be expressed as

$$\dot{Q} = \|\varphi_m \cdot c_p (T_h - T_c)\| \quad (2.22)$$

where  $\varphi_m$  is the mass flux of the DC streaming in kg/s.

The DC losses can be very high and are easily prevented. Common practice is the use of a non permeable flexible membrane. This was also used in the experiments reported in this study. Jet pumps deliver an alternative solution (Appendix C).

### Jet Streaming

Jet streaming occurs when the gas volume passes a more narrow or wider part (like the entrance and exit of the regenerator) driven by an acoustic wave. The gas undergoes a sudden expansion or compression. This effect creates turbulence that is defined as jet streaming.

### Turbulence

A completely different situation from direct current streaming, but still a negative nonlinearity to the system is turbulent streaming that can occur in the case of excessive natural convection. This is a common phenomenon right after the heat exchanger that operates with a different temperature than the controlled environment. The losses occur in three ways:

1. Convective heat losses
2. Increased viscous losses
3. Inertia losses, because of the turbulent medium.

# 3 Experimental setup

This chapter describes the experimental setup that was used to determine the performance of parallel and serial configurations.

## 3.1 Component overview

The regenerator is placed inside a unit and is insulated by a Teflon layer. The hot temperature of the regenerator should not exceed 270°C.

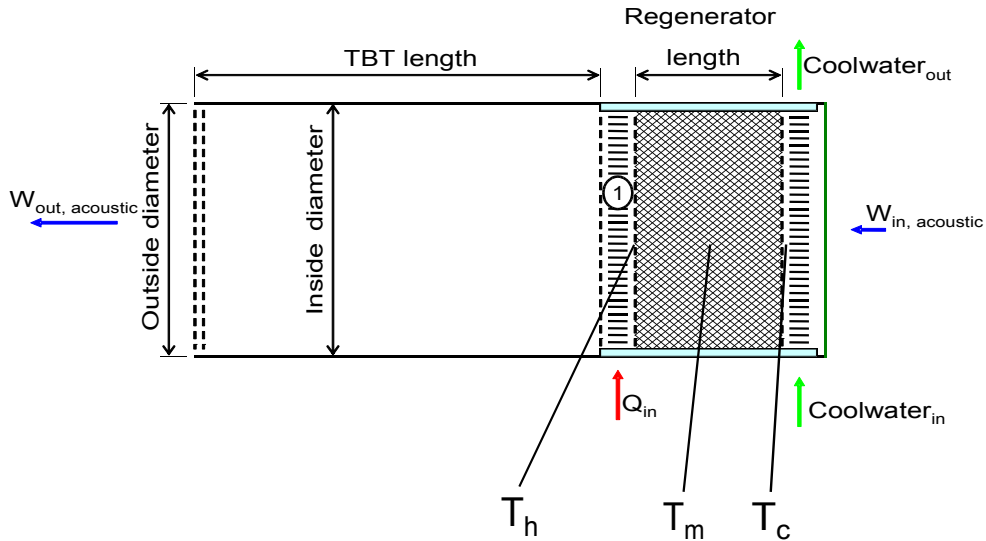


Figure 3.1 The generator unit/engine with instrumentation (TBT=thermal buffer tube)

In figure 3.1 the left dotted lines represent a flow straightener. On the left is the thermal buffer tube (appendix C). The number ① is an electric heater packed between two porous protection sheets, followed on the right side by the regenerator surrounded by Teflon insulation, the ambient heat exchanger and a flexible latex lid called the membrane (green) are on the far right. The metal border of the unit will also be referred to as the casing. There are three thermocouples placed in the regenerator ( $T_c$ ,  $T_m$ , and  $T_h$ ) one in the middle and two at the ends.

The units have an outside diameter of 58.6 mm. The inside diameter is 56.5 mm at the TBT side and 55mm at the regenerator side, where the metal wall is 0.35 mm thick. The Teflon is 1.4 mm thick. An overview with dimensions of unit components is given in Table II for serial configuration and Table III for parallel configuration.

The heat is exchanged through a cross-flow cold heat exchanger, and an electrical coil (heater). Some volumes contain solids that reduce the gas volume  $V_{gas}$ . The porosity is

$$\chi = \frac{V_{gas}}{A_{cs} \Delta x} \tag{3.1}$$

where  $\Delta x$  is the axial length, and  $A_{cs}$  the cross sectional area.

Table II Units of the serial multistage configuration (see figure 3.1).

Series	Internal Diameter	Length( $\Delta x$ )	Material Thickness	Porosity( $\chi$ )
Thermal buffer tube 1	56.5 mm	84 mm	1 mm	1
Thermal buffer tube 2	56.5 mm	62 mm	1 mm	1
Regenerator 1	55 mm	15 mm	30 $\mu\text{m}$	0.78
Regenerator 2	55 mm	13.2 mm	30 $\mu\text{m}$	0.78
Heaters	55 mm	3.6 mm	-	0.38
Cold heat exchangers	55 mm	15 mm	-	0.34

Table III Units of the parallel multistage configuration (see figure 3.1).

Parallel	Internal Diameter	Length( $\Delta x$ )	Material Thickness	Porosity( $\chi$ )
Thermal buffer tubes	56.5 mm	84 mm	1 mm	1
Regenerators	55 mm	14.5 mm	30 $\mu\text{m}$	0.78
Heaters	55 mm	3.6 mm	-	0.38
Cold heat exchangers	55 mm	15 mm	-	0.34

The regenerator consists of a stack of weaved slabs of stainless steel wire mesh with a diameter of 30  $\mu\text{m}$  and has an overall porosity of 78%.

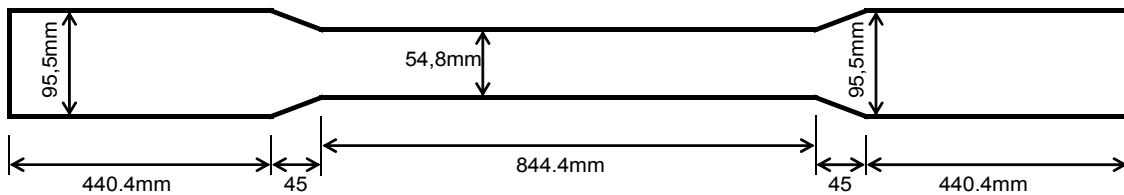


Figure 3.2 Resonator dimensions

The dimensions of the resonator are given in figure 3.2. The horizontal arrows are internal lengths and the vertical arrows are internal diameters. The medium (see also section 2.2) is nitrogen.

The set of experiments for both configurations is done in the same resonator tube with two coaxial ends (fig.3.2). At the left (load side) an extension is placed to create a variable acoustic load consisting of a controllable valve (resistance) and volume (capacitance) of 0.001  $\text{m}^3$ .

The thermoacoustic unit (fig.3.1) consists of a membrane, a cold water cooled heat exchanger, a regenerator, electrical heating, a thermal buffer tube, and a flow straightener. The cold water runs through the flange parallel to the cylindrical resonator wall along the wires for thermocouples and electric heating. In each regenerator three temperatures are measured at both ends and in the middle. On one of the thermal buffer tubes the outside wall temperatures are measured at both ends, and in the middle. Five microphones are placed as in Figure 3.3 and 3.4, while their signal is analyzed using a lock in amplifier, which can measure the AC voltage, and the phase compared to a reference signal. The flange pressure is chosen as the reference signal. The pressure sensor at the flange is also used for determination of the average pressure. The transformer for the heater reads the energy input to the heater.

Because ultimately the engines would be driven on waste heat, the hot temperatures in the regenerator are the same for both units in order to create characteristics that are representative for waste heat usage. A good characterization of the performance of the engines also involves measurements at much higher temperatures than can be achieved with waste heat in order to analyze the trend. Besides heat exchangers, insulation, and surfaces are not optimized, so in a final

design better thermoacoustic efficiencies are expected.

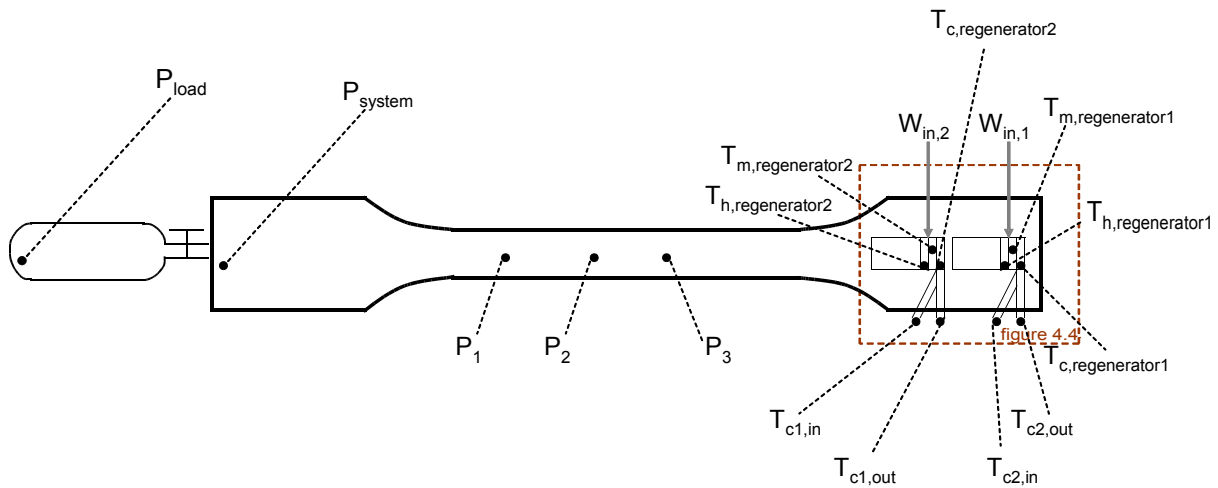


Figure 3.3 Sensor locations; configuration in series

The setup is changed into a parallel configuration (fig.3.4) where the same measurements are taken.

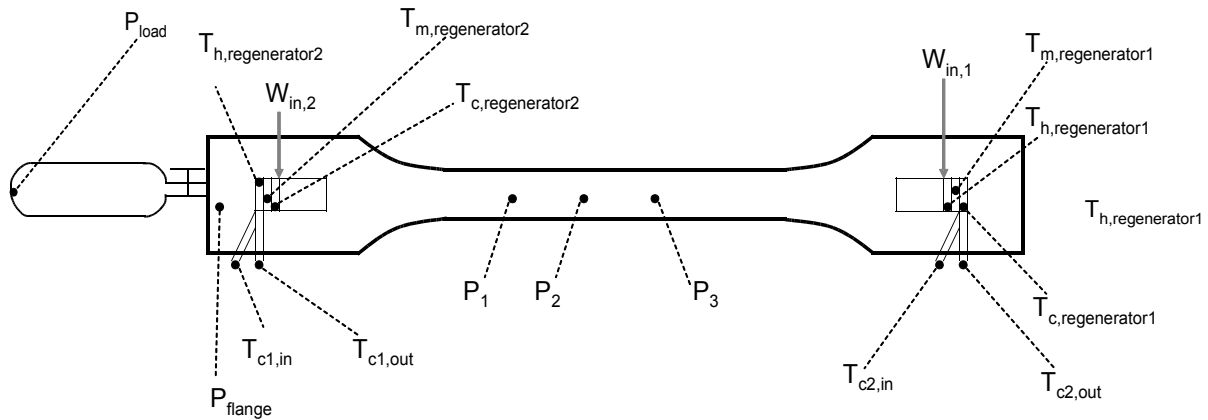


Figure 3.4 Sensor locations; configuration in parallel

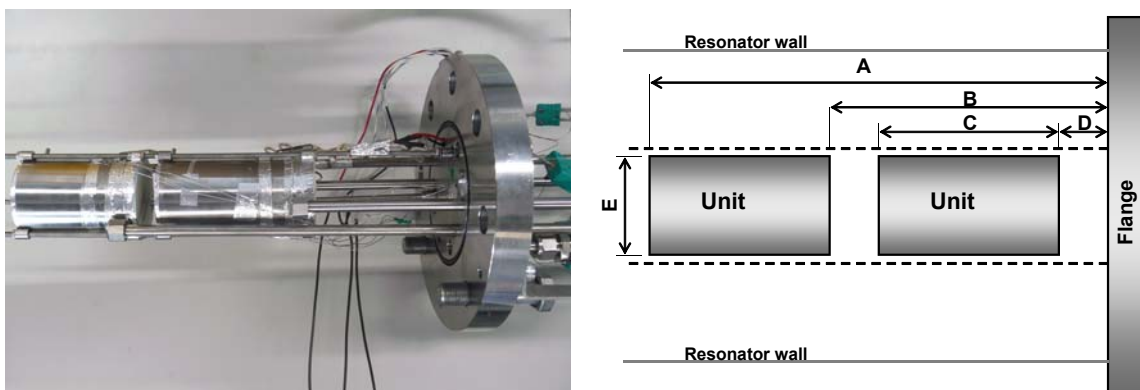


Figure 3.5 Internal schematic in series The positioning of the units in series is described by four lengths A-D and one diameter E.

In figure 3.5; A is the cumulative length of both units and capacitors, B is the cumulative length of both capacitors and the first unit, C is the length of the unit (fig.3.1), D is the length of the capacitor, and E stands for the external diameter of the units. In figure 3.6 (the parallel setup) the capacitors are identical for both engines and both units have the same length and diameters. The values of the dimensions in figure 3.5 and 3.6 are given in Table IV.

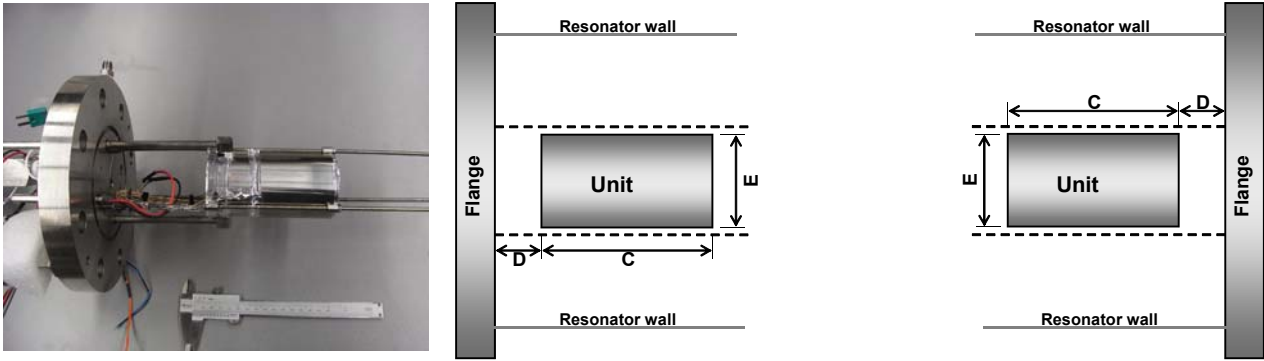


Figure 3.6 Internal schematic of parallel units. The positioning of the units in parallel is described by two lengths C and D and one diameter E.

Table IV Internal positioning of the units

		Specific sizes, A,B,C,D,E (Figure 3.4 & 3.5)				
		A	B	C	D	E
1	Series	352 mm	251 mm	128 mm	113 mm	58.6 mm
2	Parallel no load side	-	-	128 mm	113 mm	58.6 mm
3	Parallel load side	-	-	128 mm	113 mm	58.6 mm

In the test sequential units (series) are compared against parallel units. In both configurations the units are placed at optimum position and have the same average regenerator size.

### 3.2 Experimental data processing

The resonator tube is a closed system built for testing the effect of different parameters on the behavior of thermoacoustic systems. A map of the energy flows in the system needs to be made for analysis.

ECN aims to reduce the high temperatures required for operation of the system and to increase the overall efficiency. Therefore we need to measure the temperatures of the hot side and sufficient data to allow for calculation of the energy balance. Temperatures are measured by thermocouples.

#### 3.2.1 Determining the energy balance

An electric heater heats the hot side of the different regenerators.

The electrical current  $I$  and potential  $v$  are measured and to determine the ingoing heat flux

$$\dot{Q}_{in} = vI \quad (3.2)$$

The cooling power is measured by the flow of cooling water, and the entering, and exiting temperature

$$\dot{Q}_{cooling} = (\rho c_p U \Delta T)_{water} \quad (3.3)$$

### 3.2.2 Two microphone method

The acoustic power is the power contents of an acoustic wave. The two microphone method measures the acoustic energy transported through a cross sectional area. The velocity, the mean pressure, and the pressure difference could be derived from just two pressure sensors, as long as pressure amplitude, phase, and average pressure can be separated.

The determination of acoustic energy in this matter was developed by Fusco et al. [16]. For a viscous medium the derived equation was further simplified by Backhaus and Swift [17]

$$\dot{W}_{2mic} = \frac{A_{cs}}{2\omega\Delta x} \left(1 - \frac{\delta_v}{r}\right) |p_1||p_2| \sin \varphi + \frac{\delta_v}{2r} (|p_1|^2 - |p_2|^2) \quad (3.4)$$

where  $\delta_v$  is the viscous penetration depth,  $\varphi$  is the phase difference between the pressure amplitudes  $p_1$  and  $p_2$ ,  $\Delta x$  is the distance between the points of the pressure measurements orthogonal to the cross sectional area  $A_{cs}$ , and  $r$  is the radius of cross section.

### 3.2.3 Measurement of the acoustic energy dissipated in the load

The acoustic power dissipated by the acoustic load can be determined when the load is considered a compliance with a volume  $V$  [16]:

$$\dot{W}_{load} = \frac{\omega V}{2p_0} \frac{c_p}{c_v} p_e p_l \sin \phi \quad (3.5)$$

where  $c_v$  is the heat capacity at constant volume,  $\Phi$  is the phase difference between the entrance pressure  $p_e$  and the pressure at the furthest opposing wall  $p_l$ .

### 3.2.4 Measurement of the acoustic power

The thermoacoustic engine produces acoustic power. The two microphone method can measure acoustic power after the data is displayed by a lock in amplifier for a single frequency. The acoustic power dissipated in the load is equal to the power that can be used in a heat engine. The methods used in this study result in five stages for full quantification of the system. The load power, which is the useful power of the system, is directly measured. The acoustic power that is derived from measurements of the resonator losses with the two microphone method will be called the measured (acoustic) power. This can also be called engine power when the losses in and around the unit are chosen to be part of the engine and the losses in the resonator are chosen not to be part of the engine (fig.3.7).

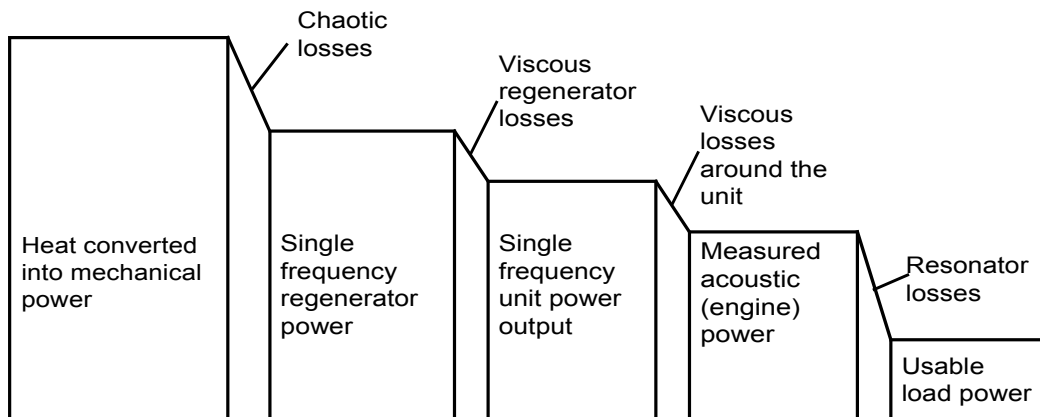


Figure 3.7 Acoustic power

The two microphone method measures the acoustic power transported through a cross section. This section is about the relation between the two microphone power, the load power, the measured (acoustic) engine power, and resonator power.

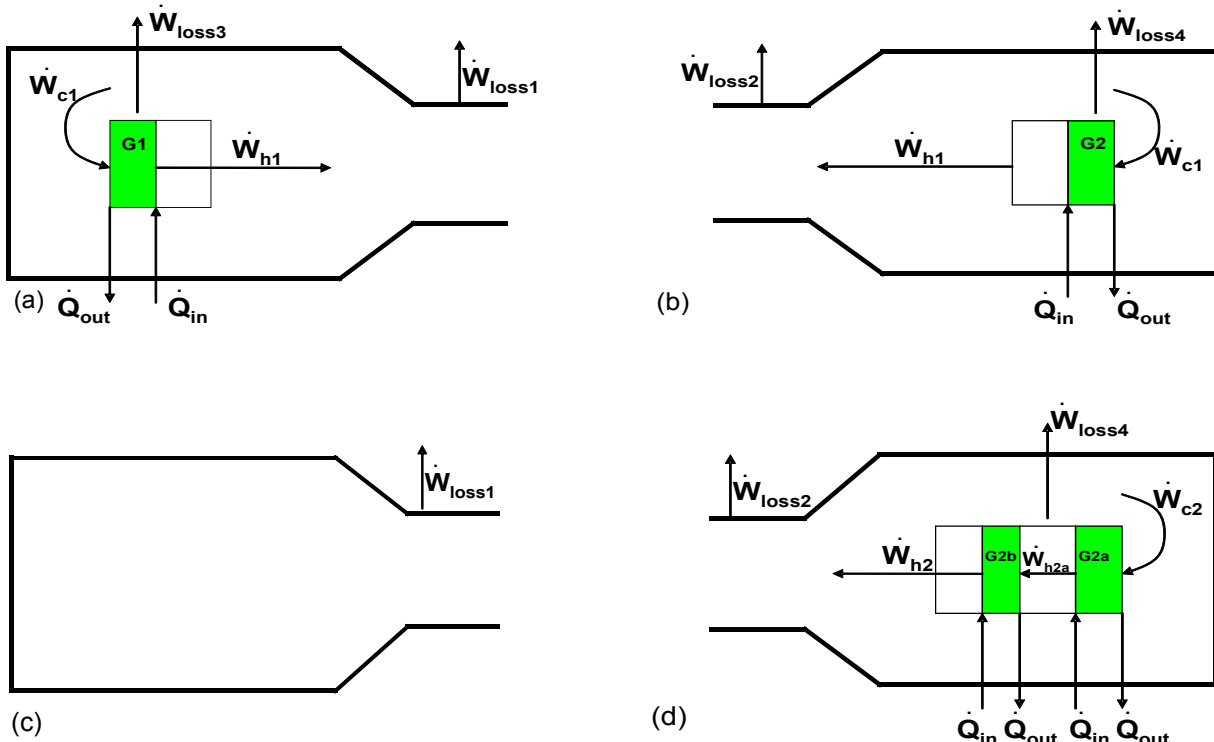


Figure 3.8 Simplified energy fluxes (a) and (b) single units in a parallel configuration, (c) and (d) in a serial configuration

Figure 3.8 shows the energy flows in a resonator half with a single unit or a “serial configuration”.  $\dot{W}_{loss1} / \dot{W}_{loss2}$  and  $\dot{W}_{loss3} / \dot{W}_{loss4}$  are respectively the losses in the resonator and the viscous losses in the regenerator added by the viscous losses around the unit. The work converted by the regenerator or single frequency regenerator power equals

$$\dot{W}_{G1} = \dot{W}_{h1} - \dot{W}_{c1}, \text{ and } \dot{W}_{G2} = \dot{W}_{h2} - \dot{W}_{c2} \quad (3.6).$$

The complete picture of acoustic energy fluxes can be simplified to create Figure 3.9. Only the load is asymmetrical. The two microphone method measures the power that is distributed to compensate a power imbalance. It is good to realize the losses in the resonator of this setup are higher than the produced load power.

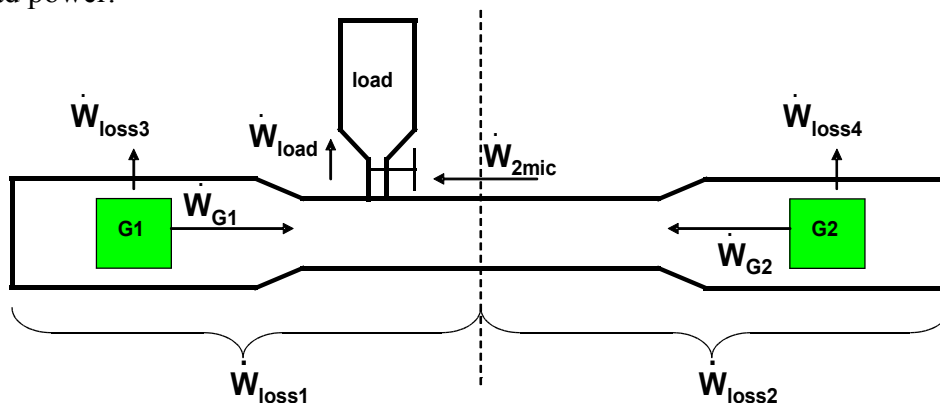


Figure 3.9 Measurement of energy transported

In Figure 3.9 there are two sides of the resonator that contain G1 and G2. There is a volume and a controlled valve that form the external load. In case of a multistage “parallel configuration” G1 and

G2 are both single units. In series G2 consists of two units while G1 is absent. Losses 3 and 4 occur only because of the units. The power dissipated as  $\dot{W}_{loss1}$  and  $\dot{W}_{loss2}$  are the losses on the half of the symmetrical resonator without losses around the units.  $\dot{W}_{loss,res}$  is defined as the total resonator loss and is the sum of  $\dot{W}_{loss1}$  and  $\dot{W}_{loss2}$ . Through symmetry

$$\left(\dot{W}_{loss1}\right) = \left(\dot{W}_{loss2}\right) \quad (3.7)$$

, and  $\dot{W}_{loss,res} = 2\dot{W}_{loss1}$

The measured acoustic power is

$$\dot{W}_{loss,res} + \dot{W}_{load} \quad (3.8)$$

where the resonator losses are determined by the two microphone method and the load power is measured directly.

The energy balance is given by

$$\dot{W}_{G1} + \dot{W}_{G2} = \dot{W}_{loss1} + \dot{W}_{loss2} + \dot{W}_{loss3} + \dot{W}_{loss4} + \dot{W}_{load} = \dot{W}_{load} + \dot{W}_{loss,res} + \dot{W}_{loss3} + \dot{W}_{loss4} \quad (3.9)$$

$\dot{W}_{2mic}$  is the power distributed through acoustics measured with the 2 microphone method.

$$\begin{aligned} \dot{W}_{2mic} &= \left| \dot{W}_{G2} - (\dot{W}_{loss2} + \dot{W}_{loss4}) \right| \\ \dot{W}_{2mic} &= \left| \dot{W}_{G1} - (\dot{W}_{loss1} + \dot{W}_{loss3}) - \dot{W}_{load} \right| \end{aligned} \quad (3.10)$$

In serial configuration the energy measured by the two microphone measurement can be derived from the energy balance

$$\begin{aligned} \dot{W}_{G1} + \dot{W}_{G2} - \dot{W}_{loss,res} - \dot{W}_{load} - \dot{W}_{loss3} - \dot{W}_{loss4} &= 0 \\ \dot{W}_{G1} &= 0, \text{ and } \dot{W}_{loss3} = 0 \\ \dot{W}_{G2} - \dot{W}_{loss4} &= \dot{W}_{loss,res} + \dot{W}_{load} \\ \dot{W}_{2mic} &= \dot{W}_{G2} - \dot{W}_{loss4} - \frac{1}{2}\dot{W}_{loss,res} \\ \dot{W}_{2mic} &= \dot{W}_{load} + \frac{1}{2}\dot{W}_{loss,res} \end{aligned} \quad (3.11)$$

In parallel configuration the energy measured by the two microphone measurement can be derived from the energy balance

$$\begin{aligned} \dot{W}_{G1} + \dot{W}_{G2} - \dot{W}_{loss,res} - \dot{W}_{load} - \dot{W}_{loss3} - \dot{W}_{loss4} &= 0 \\ \dot{W}_{G1} &= \dot{W}_{G2}, \text{ and } \dot{W}_{loss3} = \dot{W}_{loss4} \\ 2(\dot{W}_{G2} - \dot{W}_{loss4} - \frac{1}{2}\dot{W}_{loss,res}) &= \dot{W}_{load} \\ \dot{W}_{G2} &= \dot{W}_{loss4} + \frac{1}{2}\dot{W}_{loss,res} + \frac{1}{2}\dot{W}_{load} \\ \dot{W}_{2mic} &= \dot{W}_{G2} - \dot{W}_{loss4} - \frac{1}{2}\dot{W}_{loss,res} \\ \dot{W}_{2mic} &= \frac{1}{2}\dot{W}_{load} \end{aligned} \quad (3.12)$$

Note that neither configuration can be used for the quantification of  $\dot{W}_{loss3}$ , and  $\dot{W}_{loss4}$ .

In figure 3.10 the experimental two microphone power is plotted against the experimental load power in a parallel configuration.

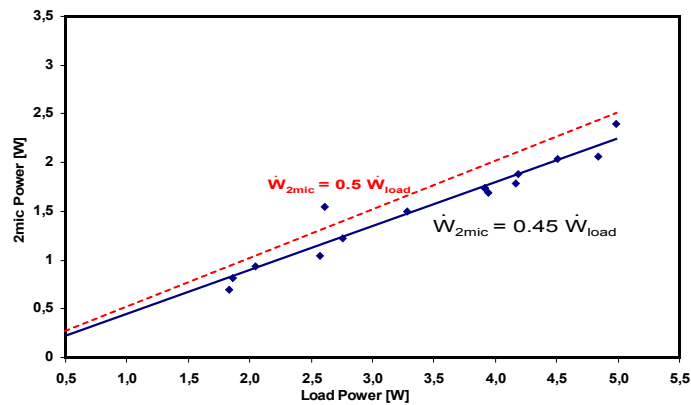


Figure 3.10 Load power plotted against two microphone measured power at 19 bar in a parallel configuration

The two microphone method measures the power that is distributed from the engine opposite the load to the engine that is placed closest to the load. When there are more viscous losses between the engine opposite the load and the load than between the engine closest to the load and the load, the two microphones measure less acoustic power than half the load, because the engine furthest from the load can distribute less power to the load (fig.3.10). This explains why experimentally a slightly smaller value has been measured than expected from equation 3.12.

### 3.3 Relation between resonator power and operating conditions

To determine the amount of acoustic power produced by a parallel engine one needs to know the acoustic power dissipated in the resonator. In a parallel configuration the power dissipated by the resonator can not be determined (see eq.3.12). In figure 3.11(a) the measured acoustic power (see eq.3.8 and 3.11) in a serial configuration is plotted against the applied load power. In figure 3.11(b) the corresponding power losses dissipated in the resonator are plotted against the applied load power.

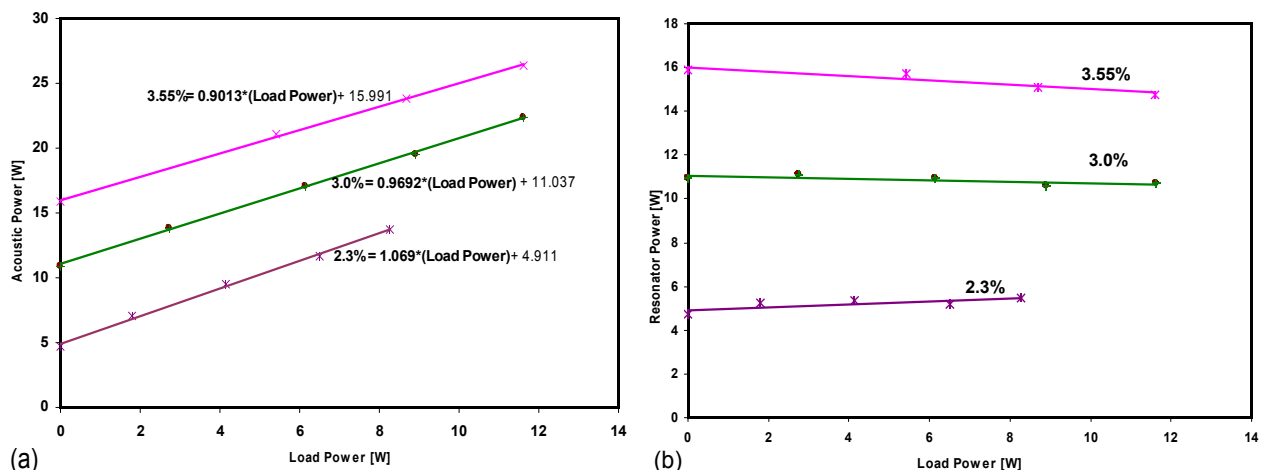


Figure 3.11 Acoustic engine power (a), and power losses dissipated in the resonator (b) versus load power for the drive ratios of 2.3%, 3.0%, and 3.55% at 19 bar.

Figure 3.11 shows that the power dissipated in the resonator and load power are not correlated. The power dissipated in the resonator is not dependent on the power distributed through the resonator by the load. The dissipated power in the resonator is constant when the drive ratio  $Dr$  is constant.

$$Dr = \frac{P_a}{P_0} \quad (3.13)$$

The acoustic power in figure 3.11a is

$$\dot{W}_{acoustic} = \dot{W}_{resonator} + \dot{W}_{load} \quad (3.14)$$

Useful load power can be produced at a specific drive ratio when the temperature exceeds the temperature necessary to obtain this specific drive ratio. Higher drive ratios require higher start temperatures, which means less excess temperature is available to produce load power. Although higher drive ratios are in general correlated to better efficiencies, an increase of the drive ratio means less excess (load) power can be produced.

### 3.4 Definition of efficiencies

The maximum mechanical power that can be gained from a temperature difference is described by Carnot. The performance of a thermoacoustic component or system can be described relative to the second law efficiency

$$\eta_{2nd\_law} = \frac{\eta_{thermal}}{\left(1 - \frac{T_c}{T_h}\right)} \quad (3.15)$$

, and

$$\eta_{thermal} = \frac{\dot{W}_{useful}}{\dot{Q}_{in}} \quad (3.16)$$

where  $T_c$  is the temperature of the ingoing cooling water and  $T_h$  is the temperature of hot side of the regenerator that is in contact with the heater.

In an acoustic system there are two important energy values, namely the present acoustic power and the load power. The acoustic power measured or engine power generated is the sum of the power dissipated in the resonator and the load power subtracted from the system.

The **internal efficiency** analyzes the power converted into acoustic power. In the results (chapter 4) this will be the measured acoustic power dissipated in the resonator added by the power that is dissipated by the load, this describes the performance of the engine as a subsystem. Note that viscous losses around the unit and in the regenerator are not included in the comparison experiments. In chapter 5 these losses will be analyzed to find the acoustic power present (fig.3.7).

In the analysis of the **external efficiency** the useful power is considered the power dissipated by the load, this describes the performance of the system. The resonator power is an unwanted loss that is necessary to feed power back to the regenerator at the right frequency.

### 3.5 Deviation of the results

The accuracy of the thermocouples and microphones used in the experiments does not significantly influence the obtained experimental data. When the load power changes rapidly by adjustment of the valve the pressure amplitude is changed over time. Different pressure amplitudes can coexist in the resonator although they will eventually level out. A deviation in resonator power can result from these and other conditions.

In this study the acoustic power dissipated in an empty half of the resonator is used to determine a numerical relation between resonator power and drive ratio squared. The relative error that can be made in reading the acoustic power is the relative standard deviation. In the results that were used

for the objective of this study the relative standard deviation is 4.7% (fig.3.12)

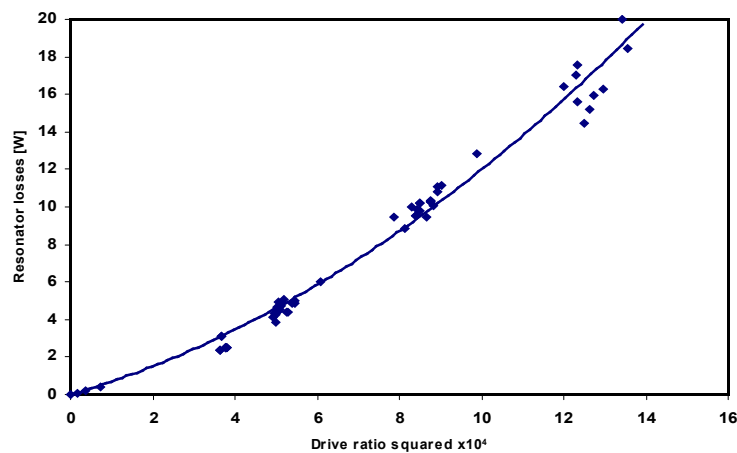


Figure 3.12 Data for determination of the relative standard deviation in resonator losses.

The biggest uncertainties can be found in the cooling water power. When the temperature difference between ingoing and outgoing cooling water is only 0.07 K a 0.01 K misread of the temperatures would result in an error would be about 28.6%.

All in all the engine power and the load power can be measured quite accurately by the two microphone method, because of the choices made in determination of the boundaries of the engine as a subsystem. The engine power is less than the power converted into acoustic energy by the regenerators. The losses dissipated in the resonator is determined from the losses measured in an empty resonator half.

# 4. Results

The main objective of this study is the comparison between serial and parallel configurations. At ECN DeltaEC simulation models have been developed for these computations. The DeltaEC simulation was done without the consideration of a load and without thermal losses other than conduction through the thermal buffer tube. In this chapter the results of the simulations and the experiments that are related to the comparison of the different configurations are presented. DeltaEC simulations (appendix B) show that the serial configuration has a slightly higher efficiency and produces more power than the parallel configuration (fig.4.1) for the same temperature on the hot side of the regenerator (hot regenerator temperature).

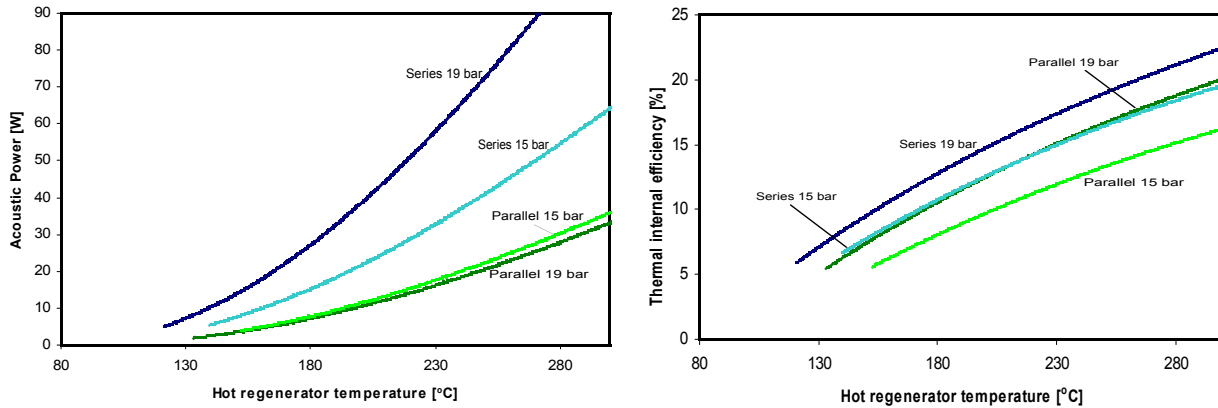


Figure 4.1 Engine power output (a) and thermal efficiency (b) against temperature of the hot side of the regenerator

The differences between parallel and series configurations can be summarized by four conditions as in table V.

Table V Different conditions in different configurations.

	<b>Serial Configuration</b>	<b>Parallel configuration</b>
<i>Amplification Factor*</i>	Between $2(\tau-1)$ and $(\tau^2-1)$	$2(\tau-1)$
<i>Local Dr at load side</i>	7% lower than on engine side	
<i>External heat losses (Ch.5)</i>	~18% less than parallel	~18% more than series
<i>Viscous losses</i>	Velocity squared around the unit times length of the unit is twice as much for the second unit as it is for the first unit	Velocity squared around the unit times length of both units is the same as for the first unit in series

\* $\tau > 1$

The second engine in a serial configuration is placed in a location of higher velocity amplitudes. A mathematical equation shows a better amplification factor in serial configurations if the temperatures are the same. A better amplification factor means that more power is produced at the same temperature gradient.

The load is placed on the opposite side of the engines in series, where the viscous transport losses through the resonator have reduced the power and drive ratio. In the parallel configuration one engine can supply the load directly.

Because of the local velocities, the serial configuration will suffer higher viscous losses around the

second unit and in the second regenerator.

The supply of nitrogen to the load under load conditions may increase the velocity near the load. Then the viscous losses would increase more in a parallel configuration due to viscous losses around the unit at the load side.

The serial configuration has two heat sources close to each other, this will result in a high local gas temperature which reduces heat losses from the engine.

In this chapter the experimental results are shown in three parts, the comparison between experimental results without load at different pressures, the internal efficiencies, and the external efficiencies.

#### 4.1 Drive ratio based comparison between serial and parallel configurations

In the first part a set of experiments compares the obtained drive ratio in the resonator as a result of heat input in both configurations at different pressures.

##### 4.1.1 Drive ratio and heat input

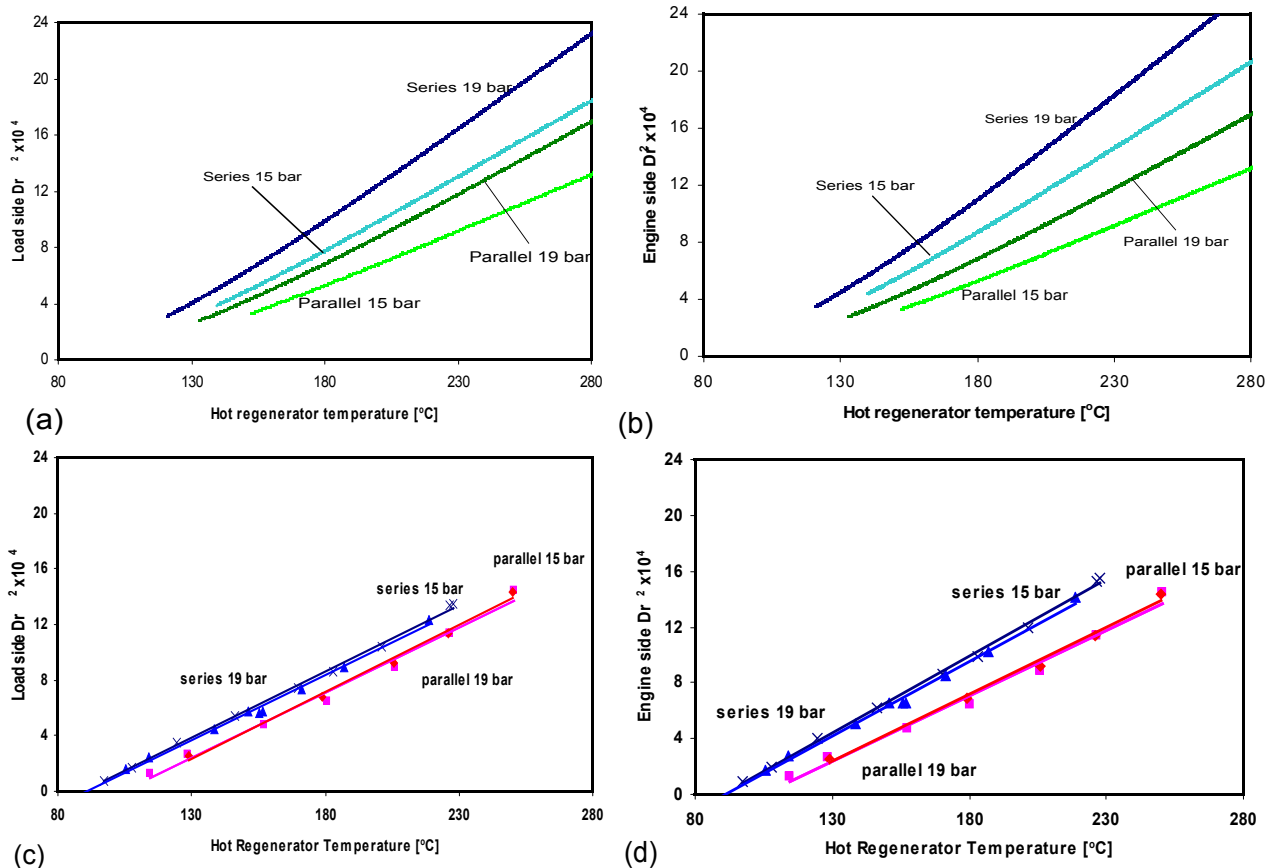


Figure 4.2 Drive ratio squared against hot temperature. (a) and (b) are generated using deltaEC, (c) and (d) are measured data.

In figure 4.2 the relation between hot regenerator temperature and drive ratio is given. The maximum drive ratio occurs at the pressure node, this is at the flange of the resonator. The resonator has two flanges when the parallel configuration is applied the conditions are equal on both sides. In the serial configuration the pressure amplitudes are higher on the engine side than on the load side<sup>1)</sup>. In figure 4.2c the same drive ratio at the load side can be obtained in the parallel configuration as in the serial configuration when the hot regenerator temperature is approximately 16 K higher. The difference in drive ratio between the serial and parallel configuration was predicted higher by the simulation than the experimental results show. This is not surprising considering the viscous losses

related to connections to the unit that are not considered in the simulation model. The velocity amplitudes at the unit that is placed closer to the center of the resonator are much higher. The experimental results show higher drive ratios (squared) can be obtained at low temperatures with serial configurations (fig.4.2c and d). The simulation model (fig.4.2a-b) also shows better drive ratios for the serial configuration. The experimental results don't show better drive ratios at a lower average pressure as the simulation predicted. The quantitative relation between hot regenerator temperature and the drive ratios found in the simulation are close to the quantitative relation found in the experiments. The simulation predicts 55% higher drive ratio squared values for the serial configuration on the engine side at 200°C, in the experiments the serial configuration has about 30% higher drive ratio squared at the engine side.

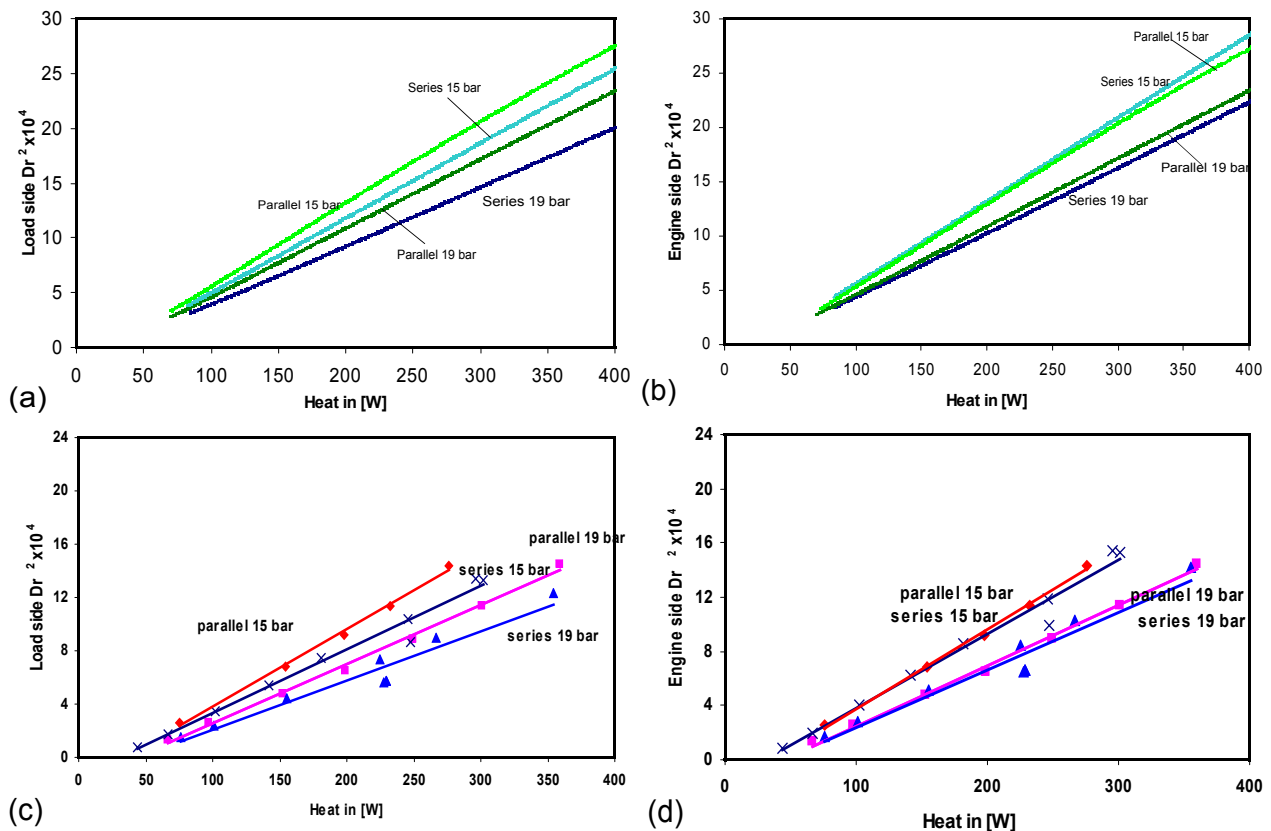


Figure 4.3 drive ratio squared against total heat input. (a) and (b) are generated using deltaEC. (c) 'serial configuration' and (d) 'parallel configuration' are measured values.

Figure 4.3 presents the relation between heat input and drive ratios squared. When the pressure is lower, the same drive ratio can be obtained with lower pressure amplitudes and therefore with less power input. In the simulation and in the experimental results the drive ratio depends more on the pressure than on the type of configuration. When for the load side drive ratio the simulation is compared to the measurements the trends show a reasonable fit. In the experiments and in the simulation the serial configuration produces as good a drive ratio on the engine side as the parallel configuration with the same heat input at the same pressure (fig.4.3b and d).

The relation between heat input and drive ratio squared shows lower drive ratios are found than the simulation predicted (the scale of the y-axis in fig.4.3a and b exceeds the scale of the y-axis in fig.4.3c and d by 25%). The relation between pressure or configuration and drive ratio is similar. By comparing figure 4.2 and 4.3 it shows the serial configuration has more heat input at the same hot temperature as the parallel configuration.

1) Even if there is no load applied, the side where there is no engine in series will be referred to as load side. The drive ratio on the load side and the engine side was taken from simulation results with simplified geometries. A reflection on this method can be found in section 6.1.1.

### 4.1.2 Pressure dependency and comparison of efficiency

In this section the internal thermal efficiency of the engine is compared for different drive ratios and different average pressures. The theory shows that the efficiency depends greatly on the drive ratio because a large pressure difference is helpful in forcing the working fluid through the regenerator where the viscous losses are high. Figure 4.4 shows the thermal internal efficiency as a function of the hot temperature and drive ratio. The thermal efficiency for a certain drive ratio doesn't depend on the configuration. The serial configuration shows higher thermal efficiencies than the parallel configuration for the same hot regenerator temperature. The simulation models shows efficiencies up to 21% at 280°C.

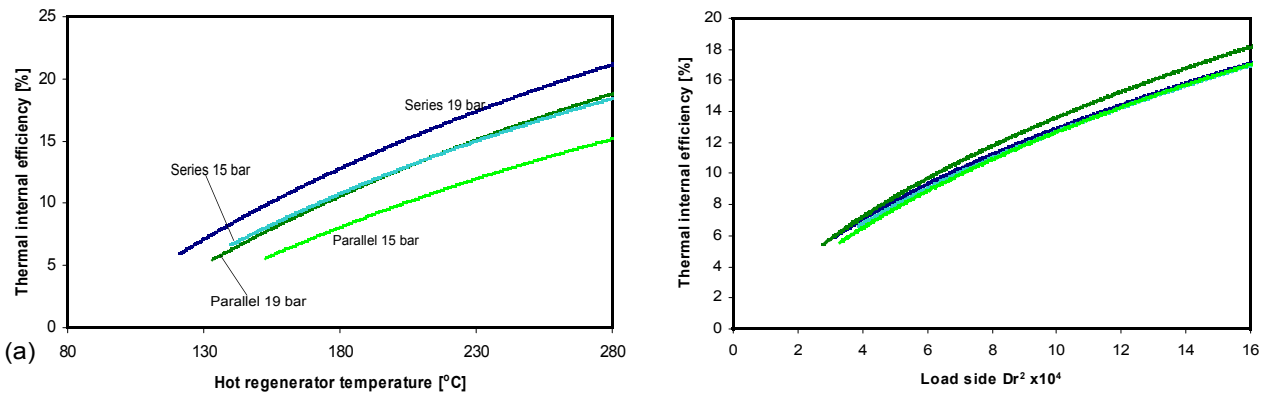


Figure 4.4 Internal thermal efficiency as a function of (a) hot regenerator temperature and (b) drive ratio squared calculated in the DeltaEC simulation.

The same thermal internal efficiencies with the same drive ratio were expected and found in both configurations.

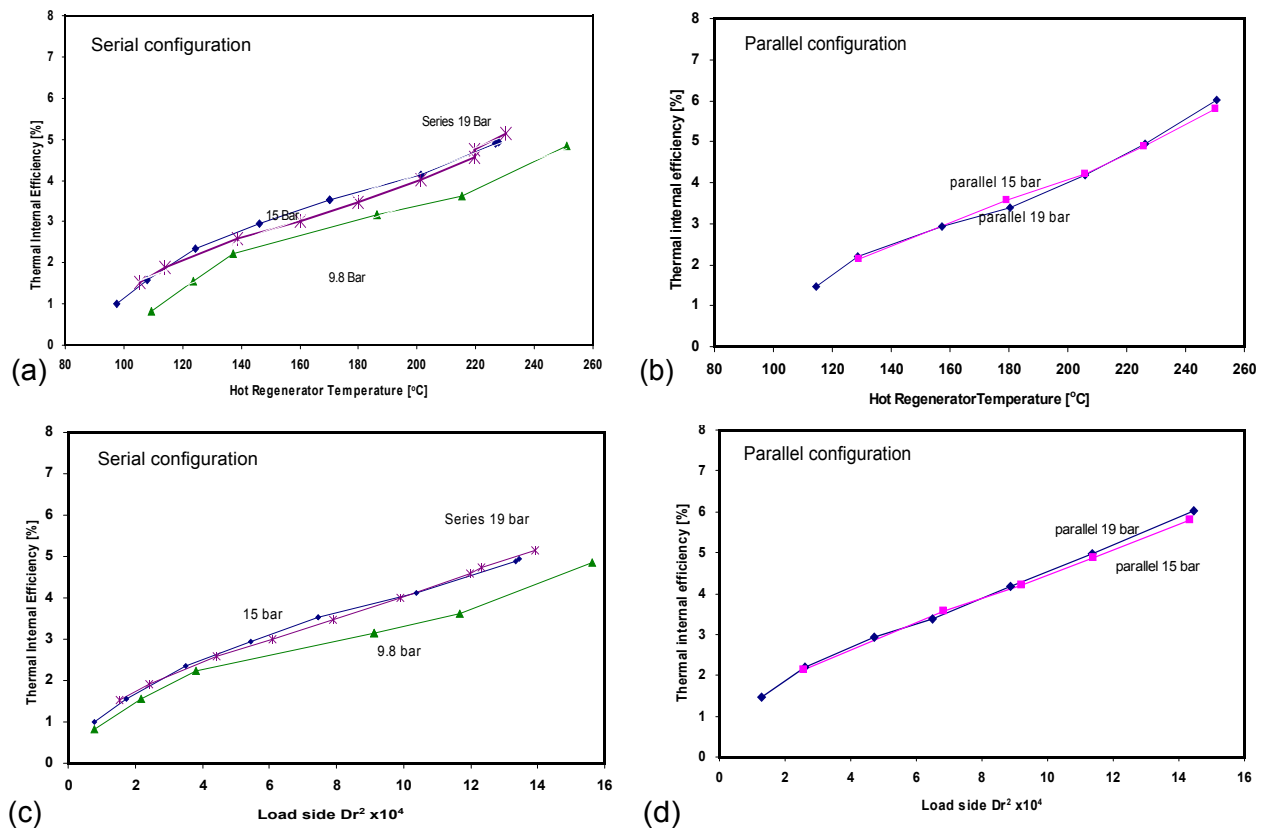


Figure 4.5 Internal thermal efficiencies as a function of hot temperature of the regenerator (a & b) and drive ratio (c & d) for series and parallel configurations at different pressures. (a) series (b) parallel (c) series (d) parallel

The relation between drive ratio squared and thermal efficiency in figure 4.5 corresponds with the model trends. Serial configurations (fig.4.5c) showed the same thermal internal efficiencies as parallel configurations (fig.4.5d). Note that the power dissipated in the resonator, which is equal the engine power when there is no load applied, is the same for both configurations.

The simulation model (fig.4.4a) predicted serial configuration to have higher efficiencies at the same temperature of the hot side of the regenerator. There is hardly any difference found for 15 and 19 bar except at low temperatures. The difference in thermal efficiency (fig.4.5a and b) between the configurations at the same drive ratio is smaller than the simulation predicted (fig.4.4a).

## 4.2 Internal efficiencies

In the second set of experiments an external load is applied and the pressure is constant. Here the performance of the system is analyzed in different conditions. The results are given in sections 4.2 and 4.3.

The sum of the load power and the power dissipated in an empty resonator is the power produced by the engine that can be found with the two microphone method. In this section the measured engine performance is shown for different temperatures and different operating conditions.

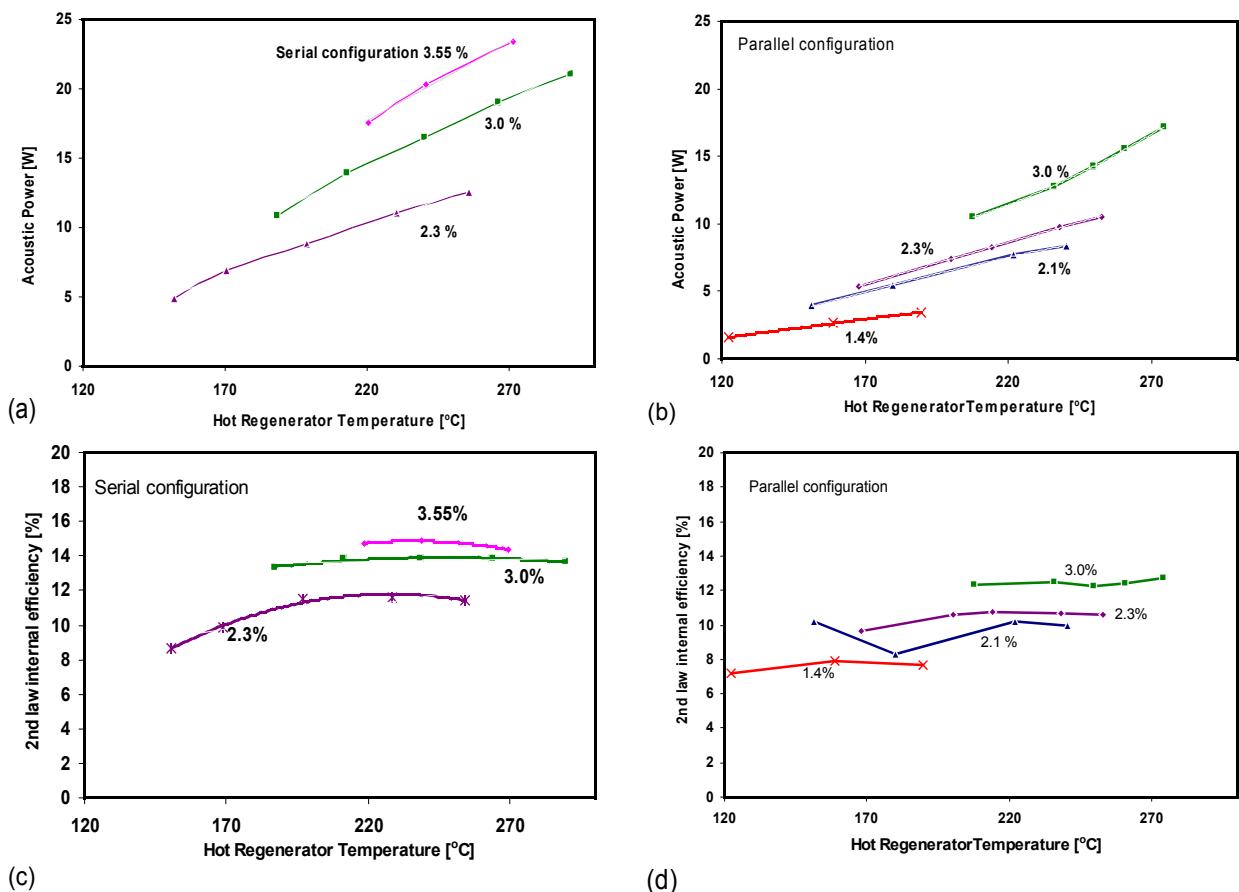


Figure 4.6 Experimental internal performance at 19 bar against hot regenerator temperature for different drive ratios. (a) Acoustic engine power in serial configuration (b) Acoustic engine power in parallel configuration (c) 2<sup>nd</sup> law internal efficiency in serial configuration (d) 2<sup>nd</sup> law internal efficiency in parallel configuration

In the temperature range of the experiments the serial configuration measures higher powers and higher 2<sup>nd</sup> law efficiencies (fig.4.6). The increase in power as a function of the hot regenerator temperature in figure 4.6b is surprisingly steady considering the temperature of the cold side of the regenerator also increases with the increase of temperature on the hot side.

As predicted by the model in figure 4.1 There is a higher energy content in serial configurations

than in parallel configurations, although the difference shown in figure 4.6 is much smaller than predicted. This may be due to higher losses related to the location of the units in the serial configuration. The viscous losses in the serial configuration are higher, because of the higher velocity amplitudes in and around the second unit. Therefore the power difference between the power converted in the unit and the measured acoustic engine power in the serial configuration is more than in the parallel configuration. The internal efficiencies of the unit in the serial configuration are then higher than in the parallel configuration.

### 4.3 External efficiency

The useful power of a thermoacoustic system is the power that can be dissipated by the load. The load was placed on the flange and the power dissipated in the load was controlled by a valve.

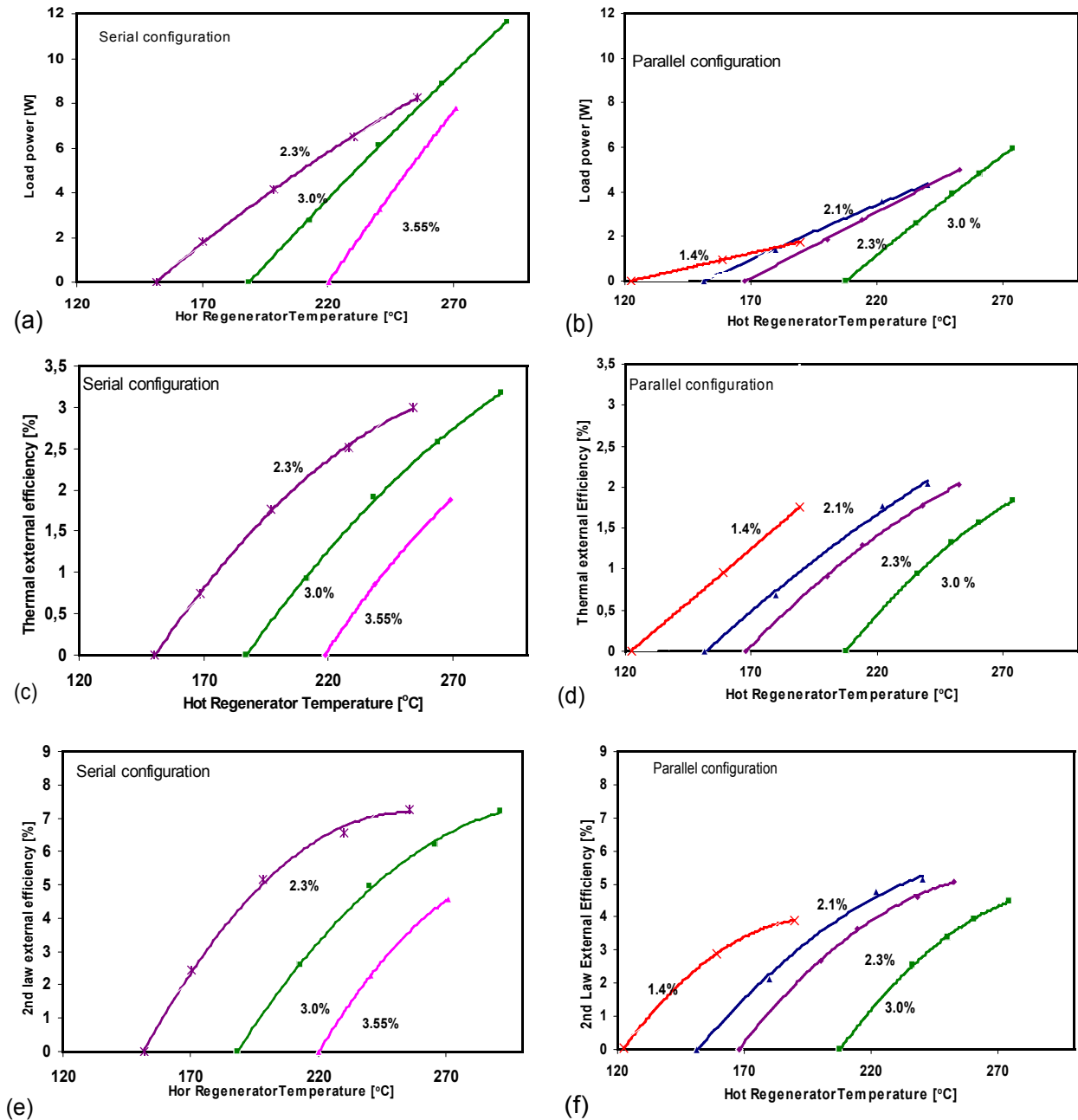


Figure 4.7 External efficiency and power plotted against hot regenerator temperature (a) Useful load power in serial configuration (b) Useful load power in parallel configuration (c) Thermal external efficiency in serial configuration (d) Thermal external efficiency in parallel configuration (e) 2<sup>nd</sup> law external efficiency in serial configuration (f) 2<sup>nd</sup> law external efficiency in parallel configuration

Figure 4.7a and b show that it is possible to dissipate the same amount of load power at the same temperature but at different conditions (drive ratios). This is due to the different start conditions. The corresponding figures (4.7 c and d) show that the heat input in these cases was different, otherwise the thermal efficiencies would also have been the same.

The experimentally determined efficiency of the dissipated power in the load (thermal and relative/ 2<sup>nd</sup> law) is given in figure 4.7e and f. The same drive ratio can be obtained at a lower hot temperature in the serial configuration than in the parallel configuration. More power can be dissipated by the load at the same temperature and load side drive ratio in the serial configuration than in the parallel configuration. Both thermal (fig.4.7c and d) and 2<sup>nd</sup> law efficiencies (fig.4.7e and f) are better for the serial configuration.

#### 4.4 Comparison of serial and parallel configurations

The relationship between hot regenerator temperature and 2<sup>nd</sup> law external efficiency is by far the most important. In figure 4.8 & 4.9 the 2<sup>nd</sup> law external efficiencies of serial and the parallel configuration are plotted in the same graph for the same drive ratio. The drive ratio in figure 4.8 was measured at the load side.

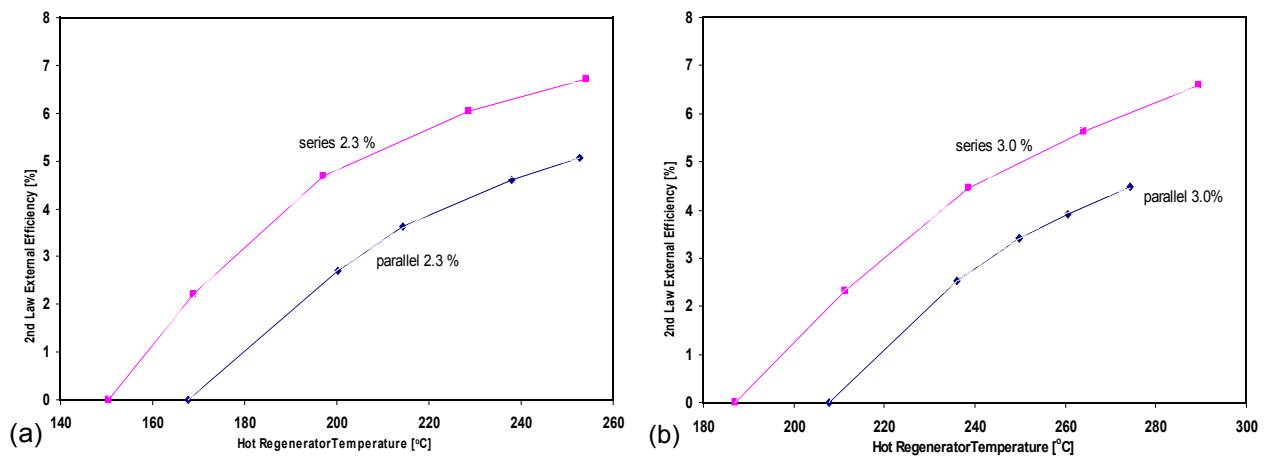


Figure 4.8 2<sup>nd</sup> law external efficiency against hot regenerator temperature (Dr load side) (a) Series (b) Parallel.

The DeltaEC simulation predicts the drive ratio on the engine side in a serial configuration exceeds the drive ratio on the load side by 7.15%. By linear interpolation the drive ratio of 3.0% on the engine side in the serial configuration can be compared to the same drive ratio in the parallel configuration (fig.4.9).

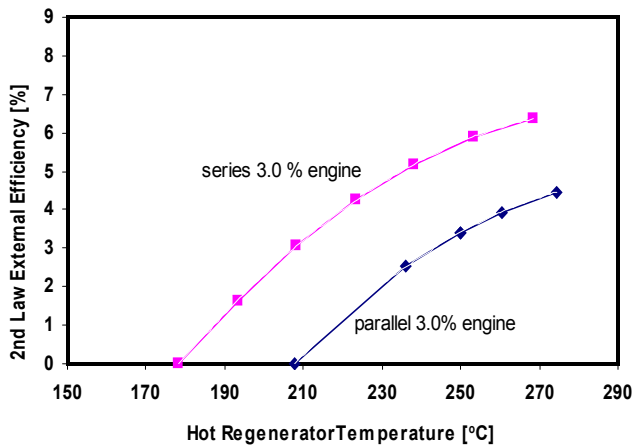


Figure 4.9 2<sup>nd</sup> law external efficiency against hot regenerator temperature (Dr of the engine side)

The efficiency of the serial configuration at a drive ratio of 3% at the engine side (fig.4.9) was about 47% more at a hot regenerator side temperature of 270°C. The difference is larger at lower temperatures down to 205°C. At this temperature no power can be subtracted from the parallel configuration.

## 5 Detailed Energetic Analysis

The predicted internal engine efficiencies by the DeltaEC model are much higher than the efficiencies found in the experimental results. This chapter will analyze the losses that occur in the experimental setup. These losses can be divided in heat losses and viscous losses. The heat losses can be analyzed at the boundary between the resonator and the environment, and between the unit and the inside of the resonator. Viscous losses in the resonator are included in the measurements and the model, but the measurements do not include the viscous losses around the unit and inside the regenerator. For determination of these losses a number of small experiments was carried out. First the experiments will be shortly described. Then the results will follow.

The process of heat that is transferred into acoustic energy can be drawn as in figure 5.1.

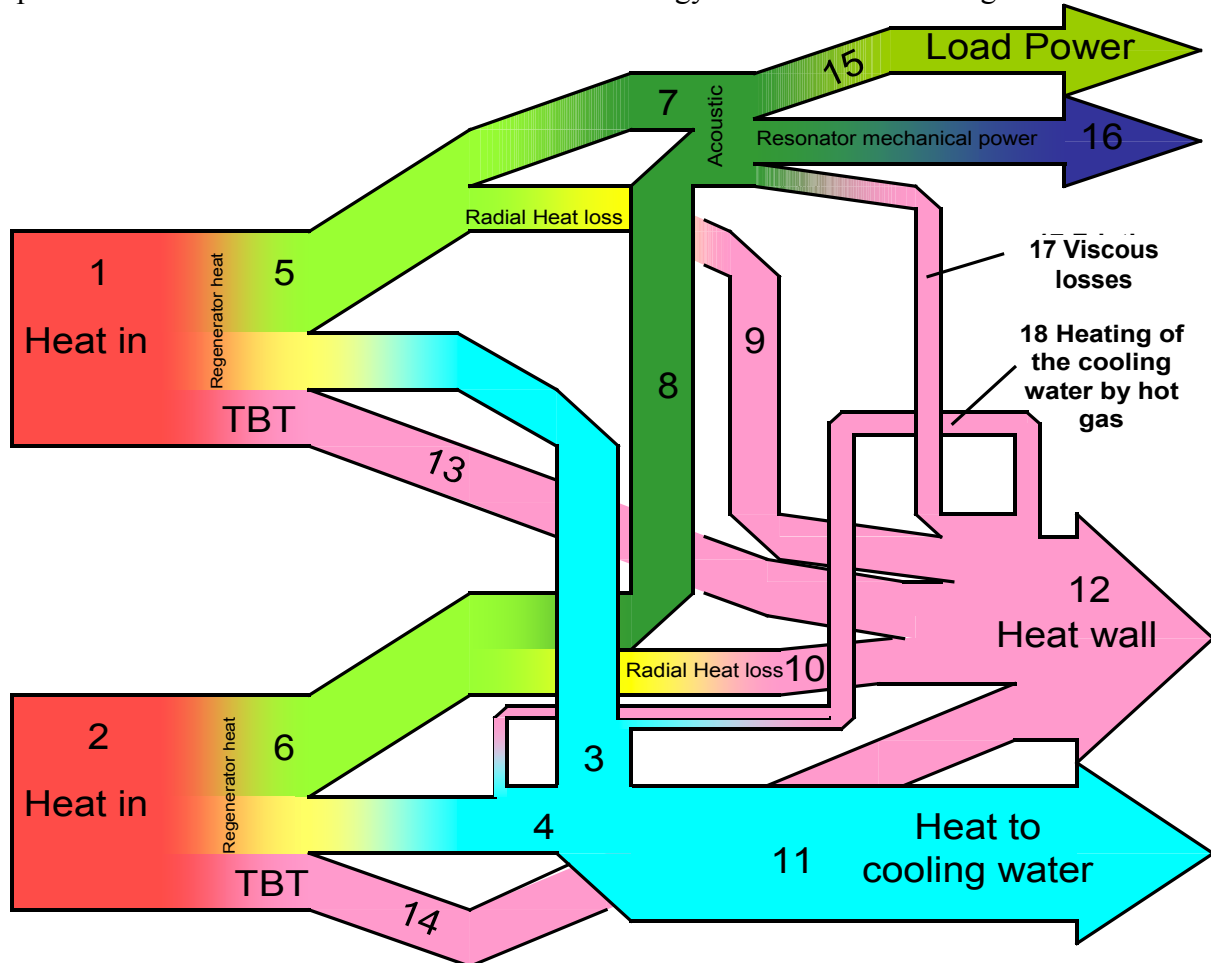


Figure 5.1 Qualitative Energy flow diagram.

First there are two heat flows entering the system, 1 & 2. The electrical power input of the heaters is known. The heater is coiled around a plate and heat is assumed to spread in two directions. Heat flows through the thermal buffer tubes (13 & 14) is dissipated through the gas to the resonator wall. Heat flowing in the useful direction is called regenerator heat. Heat-flows 3 and 4 are the outgoing heat flows through the cooling water (11). The heating of the cooling water is partly due to the conduction of the regenerator, partly due to heat exchange with the hot gas, and enhanced by the acoustic wave by viscous losses in the regenerator and by heat transport. In the regenerator there are also radial heat losses 9 & 10, which are unwanted and are reduced with insulation. The acoustic power is presented by 7 & 8. Mechanical losses 16 and 17 are the resonator power. Viscous losses 17 consist of the internal viscous losses in the regenerator 17a (mostly dissipated by the cooling water) and the resonator viscous losses 17b around the unit, along the resonator wall, through the

flow straightener, and by the membrane. The losses in 17b have been experimentally determined. Heat flow 12 is the total heat loss to the environment. The mechanical load power 15 has been measured. Heat flow 18 is the heating of cooling water by the hot gas.

### 5.1 Additional Experiments to determine Irreversibilities

Three additional sets of experiments have been done to quantify the different losses.

- Heat images of the external temperature of the resonator at different conditions (S5.1.1 & S5.2.1).
- Static experiments are experiments for which the presence of acoustic oscillations is prevented. In dynamic experiments there is an acoustic wave. The temperatures are measured at different points of the unit casing in static and dynamic experiments (S5.1.2 & S5.2.2).
- Quantification of viscous losses in and around the unit (S5.1.3 & S5.2.3).

Table VI Energy fluxes in a multistage thermoacoustic system.

Flux	Calculation	Measurements
1	$q = \eta_{\text{electrical\_heater}} v I$	v, and I
2	$q = \eta_{\text{electrical\_heater}} v I$	v, and I
3	$q = \phi c_p \Delta T$	$\phi$ , and $\Delta T$
4	$q = \phi c_p \Delta T$	$\phi$ , and $\Delta T$
5	1-(3+13)	none
6	2-(4+14)	none
7	1-(3+13+9)	none
8	2-(4+14+10)	none
9	From experiments	S5.1.2
10	From experiments	S5.1.2
11	3+4	none
12	Through experiment and heat flow equilibrium	S5.1.1
13	From experiments	S5.1.2
14	From experiments	S5.1.2
15	Two microphone method	P_flange, P_load, and relative phases
16	1+2-(11+12+15)	none
17a	From experiments	S5.1.3
17b	Calculated by DeltaEC	none
18	From experiments	S5.1.2

#### 5.1.1 Heat losses due to natural convection and radiation at the outer resonator wall

At the resonator wall there are mechanical losses by resonance, and there are heat losses (thermal losses). In all systems there is conservation of energy. The energy fluxes are dependent on the location of the boundaries. When the heat transfer between the resonator and the environment is analyzed by thermal images a rough figure can be found. It will, in combination with other quantities, give a first indication of the quantity of work that is done by vibration of the direct environment. Because the acoustic energy lost in the resonator is known, a rough estimation of the total sum of mechanical losses can follow.

$$\begin{aligned}\dot{W}_{mechanical\_external\_loss\_resonator} &= \sum \dot{Q}_{in} - \sum \dot{Q}_{out} - \dot{W}_{load} = Flow16 \\ \sum \dot{Q}_{in} &= Flow1 + Flow2 \\ \sum \dot{Q}_{out} &= Flow11 + Flow12 \\ \dot{W}_{load} &= Flow15\end{aligned}\tag{5.1}$$

For radial heat losses from the resonator the losses by radiation are neglected, because of the low temperatures.

$$\dot{Q}_{radial,radiation} = \sigma \xi A_{wall} (T_1^4 - T_2^4)\tag{5.2}$$

For natural convection around a cylinder the Nusselt number Nu was derived by Churchill and Chu, cit.[29].

$$\begin{aligned}\overline{Nu}_D &= 0.36 + \frac{0.518 \cdot Ra_D^{1/4}}{(1 + (0.559 / Pr)^{9/16})^{4/9}} ; \quad 10^{-6} < Ra_D < 10^9 \\ \overline{Nu}_D &= \left[ 0.60 + 0.387 \left( \frac{Ra_D}{(1 + (0.559 / Pr)^{9/16})^{16/9}} \right)^{1/6} \right]^2 ; \quad Ra_D > 10^9\end{aligned}\tag{5.3}$$

$$Ra = \frac{\beta \Delta T g D^3}{(\mu / \rho)^2} ; \quad Pr = \frac{c_p \mu}{k}$$

Here Ra is the Rayleigh number, and Pr is the Prandtl number, and g is the gravitational force. Convection consists of two terms of  $\Delta T$ ;  $\Delta T$  and  $\Delta T^{1.25}$ . When the velocity around the resonator is low the relation between heat losses and temperature differences is similar to conduction.

A more simple and effective method is the comparison of the temperatures of the resonator wall against the temperatures when the heat losses are known. For comparison a validation measurement is done without presence of an acoustic wave (static experiment) where the heat fluxes  $\dot{Q}$  are defined by:

$$\dot{Q}_{resonatorwall\_out} = \dot{Q}_{in\_unit1} + \dot{Q}_{in\_unit2} - \dot{Q}_{out\_coolwater\_unit1} - \dot{Q}_{out\_coolwater\_unit2}\tag{5.4}$$

### 5.1.2 Static internal losses determination by additional temperature sensors

One major effect on the effectiveness of the regenerator is the heat loss that occurs in the surroundings of the hot heat exchanger. The heat flux out of the hot heat exchanger consists of axial heat flux in two directions. Useful heat runs through the regenerator towards the cold heat exchanger. A part of the useful heat is lost by conduction and a part of the heat is carried by the medium to the cold heat exchanger in axial direction. The radial losses in regenerator merge with the axial losses towards the thermal buffer zone in the casing connection and the surrounding gas.

We assume the axial heat flux through the regenerator is measured by the heat increase of the cooling water. The radial heat loss and losses in the thermal buffer zone need to be derived from the temperature profile on the thermal buffer tube and the temperatures inside the regenerator. The simplified temperature profile of the unit is optically verified by heat images (fig.5.5).

The heat transport through the regenerator to the cooling water consists of a static and a dynamic term. In order to determine the dynamic term it is necessary to determine the static term, which is the static heat conduction through the regenerator. Ideally this is done under the same temperature conditions as in the dynamic measurements, so that there is no need to adjust the numbers according to radial heat flows in the regenerator. However there is only a small temperature range where increase of the adjustable load can prevent an acoustic wave to form.

In the thermal buffer zone and around the thermal buffer tube the heat flux is more complicated as illustrated in figure 5.2.

The unit is hung on three long bolts that are attached to the flange. On the underside of the unit at the end of the thermal buffer tube a pin is welded to keep the unit in place.

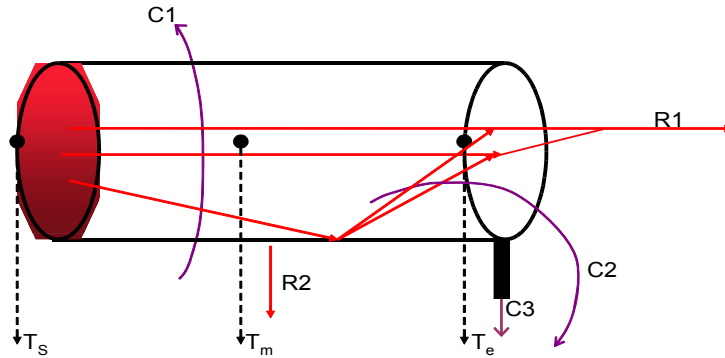


Figure 5.2 Thermal buffer tube and the heat processes. C1 is the external convection between the medium and the TBT, C2 is the internal convection between the medium and the thermal buffer zone, C3 is conduction through the pin, R1 is the combination of direct and indirect radiation from the hot side to the environment, and R2 is radial radiation.

Three thermocouples are installed on the outer wall of the thermal buffer tube to determine the temperature profile near the heater  $T_s$ , at the end  $T_e$ , and half way  $T_m$  (fig.5.2 and 5.5) in a set of experiments. Five different data-sets can be obtained.

Set I Dynamic experiments without additional insulation.

Set II Static experiments without additional insulation.

Set III Static experiments with the inside fully filled with insulation material.

Set IV Static experiments with the outside fully filled with insulation material.

Set V Static experiments with insulation material fully filling both sides of the thermal buffer tube.

### Assumptions

All calculations are numerically solved by dividing the 128 mm long casing into 1mm slabs. First the radiation in axial and radial direction is determined using an emissivity of 0.36 for steel, and 1.0 for the hot heat exchanger. The temperatures are assumed radially symmetric (fig.5.3). In dynamic the Doppler effect is expected to reduce chaotic losses. Finally the statements for single stage are assumed to hold for multistage systems.

The conduction properties of metal and the conduction properties of the insulation material are known. This is used to determine the heat losses by conduction. The heat loss by convection is found by subtraction of other well defined heat fluxes.

In Figure 5.3 the radial radiation is represented by purple arrows, the axial conduction by red arrows, and the convection by orange arrows. When the inside of the thermal buffer tube is filled completely with insulation material and the outside is not, the total convection losses outside are the difference between the initial and final heat conduction reduced by the radiation losses.

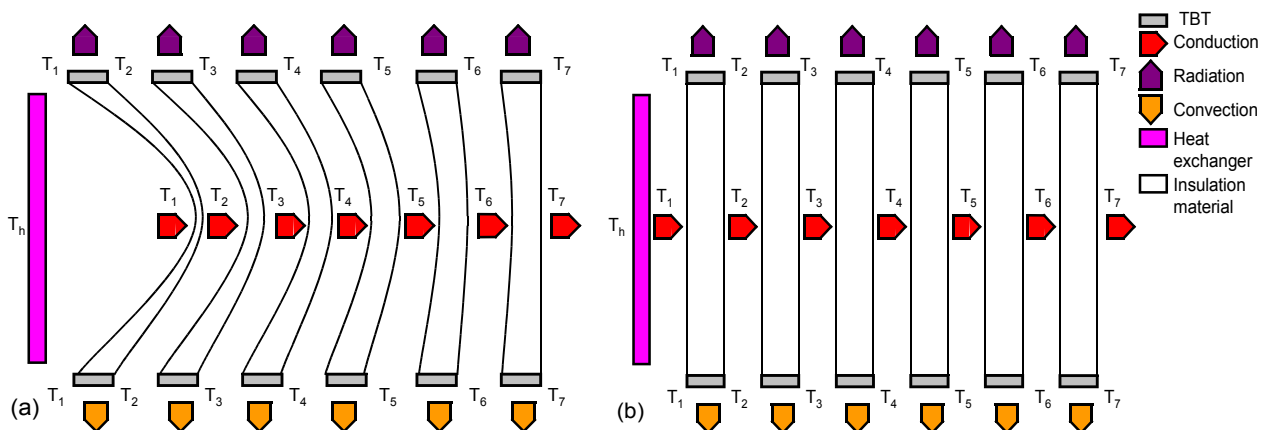


Figure 5.3 Slab theory (a) the expected temperature profile (b) the simplified temperature profile.

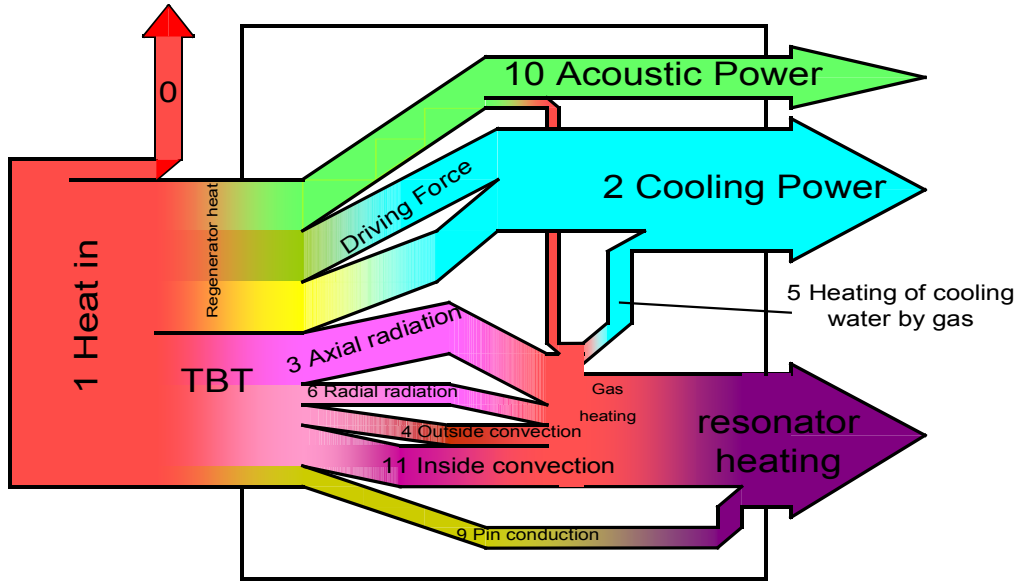


Figure 5.4 Single stage heat flux. See table VII for reference to the numbers (0 is the loss in the electricity lines)

Table VII Detailed energy flows in the analysis of a single stage engine (right see Fig.5.2).

	name	Representing	Fig. 5.2
1	Q_in	Total heat flux in	
2	Q_cw	Total heat flux out by the cooling water	
3	Q_rad_rad	Heat flux by radiation in radial direction of the casing	R2
4	Q_conv	Heat loss through convection along the thermal buffer tube	C1
5	Q_in_m	Heat absorbed by the cooling water from the heated gaseous medium	
6	Q_rad_ax	Heat radiation through the thermal buffer tube exit	R1
7	Q_conduction	Radial heat conduction from the casing through insulation	
8	Q_axial cond	Heat conduction in axial direction	
9	Q_pin	Heat conduction through the spacer pin at the thermal buffer tube exit	C3
10	Power	Acoustic engine power	
11	Q_inn_conv	Heat loss through forced convection inside the thermal buffer tube	C2
12	deviation	$1+5-(2+3+4+6+7+8+9+10+11)$	

In table VII the following equation apply:

$$1) vI\eta_{electrical} = vI \frac{R_{heater}}{R_{wire} + R_{heater}} \quad (5.5)$$

$$2) \varphi_{m,cw} c_{p,cw} \Delta T \quad (5.6)$$

$$3) \sum_1^{103} \xi \sigma \Pi \Delta x (T_{wall}^4 - T_{gas}^4) \quad (5.7)$$

Where  $\sigma$  is the Steven Boltzmann constant,  $\Pi$  is the perimeter of the thermal buffer tube,  $\Delta x$  is 1mm, and  $\xi$  is the emissivity of steel (the hot side of the unit is 103 mm).

$$4) \sum_1^{103} \left\{ \frac{(k_{metall} A_{tube} + k_{insulation} A_{cs})}{\Delta x} \Delta T - \xi \sigma \Pi \Delta x (T_{wall}^4 - T_{gas}^4) \right\} \quad (5.8)$$

Note that eq.5.8 only applies for set III with internal insulation and no external insulation. A correlation between the hot temperature and the convection is derived with similar temperature dependency as eq.5.13 for  $10^{-6} < Ra_D < 10^9$  by fitting the heat fluxes found at different temperatures. This equation is then applied on set I and II without outside insulation.

5) It is assumed the convection on the cold side of the unit behaves in a similar way as convection around the hot side of the unit. This heat flux is very small and can be neglected in the total heat balance. However it should be subtracted from the total heat flow through the cooling water in order to find the heat flow through the regenerator. The latex lit (membrane is a good insulator. The membrane is assumed to be the average temperature between the gas in the unit and outside the unit. The heat transfer per area of membrane is half as high as in the outside convection when the inside temperature is considered equal to the temperature of the cooling water.

$$6) F_{13} \sigma A_{cs,intern} (T_{hot}^4 - T_{gas}^4) + (1 - F_{13})(1 - \xi) \sigma A_{cs,intern} (T_{hot}^4 - T_{gas}^4) \quad (5.9)$$

Here  $F_{13}$  is the view factor between the flow straightener and the heater.

$$7) \frac{k_{insulation} \bar{A}_{casing \& resonator} \Delta T}{(d_o - d_i)} \quad (5.10)$$

$$8) \frac{(k_{metal} A_{tube} + k_{insulation} A_{cs})}{L_{tube}} (T_{hot} - T_{gas}) \quad (5.11)$$

$$9) \approx \frac{(k_{metal} A_{pin})}{L_{pin}} (T_{end} - T_{resonator}) \quad (5.12)$$

A multiplication constant close to unity is applied, because the assumption that the temperature is independent from the distance to the pin does not hold.

10) Is explained in section 3.2 along the two microphone method.

11) The value is the last to be determined. The outside convection can only be determined in Set III The inside convection is determined using subtraction of all the known fluxes in Set II and IV.

For natural convection from a first cylindrical shape to a second parallel more wide and hollow cylindrical shape is stated as an increase in conduction [29]

$$\frac{h_{eff}}{(D_o - D_i)k} = 0.386 \left( \frac{Pr}{0.861 + Pr} \right)^{1/4} Ra_{cyl}^{1/4} \quad (5.13)$$

$$\text{where: } Ra_{cyl} = \frac{(\ln(D_o / D_i))^4}{L^3 (D_i^{-3/5} + D_o^{-3/5})^5} Ra_L$$

where  $h_{eff}$  is the effective convection. The heat losses expected by equation 5.13 are compared to the experimentally derived heat convection losses in equation 5.8.

The experiments are carried out with one unit in the resonator at 19 bar and at 13 bar. 19 bar is the same pressure as was used in the experiments for the comparison between parallel and serial configurations. 13 bar was chosen as a considerable lower pressure that could still produce enough acoustic power to be correctly detected.

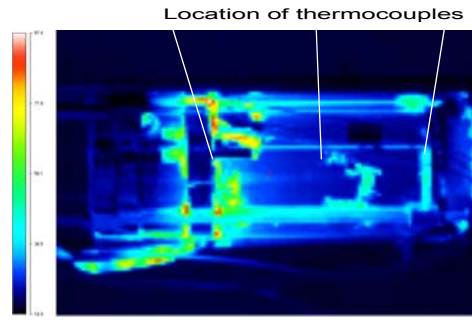


Figure 5.5 Heat image of a unit at 230°C

### 5.1.3 Viscous flow losses around the unit

The power dissipated by the resonator was experimentally determined from an empty resonator half in a serial configuration. In figure 3.4 and 3.5 the tubes for the cooling water, the thermocouple wires and the mechanical supports are shown. These will all create additional viscous losses. The complex shape of the units makes it preferable to derive the friction around the unit from experiments. When two engines are placed in parallel and one engine is heat-driven and the other engine is not, the other engine will function as a heat pump. In order to find the friction with the two microphone method without power losses due to heat pump, the regenerator is removed. This creates a dummy with identical geometries as the unit. The viscous losses in a resonator half with dummy (fig.5.6b) are compared against an empty resonator half (fig.5.6a). The serial configuration has one resonator half with two units. The viscous losses around the second unit (fig.5.6c) are mathematically derived (see also section 6.1.2).

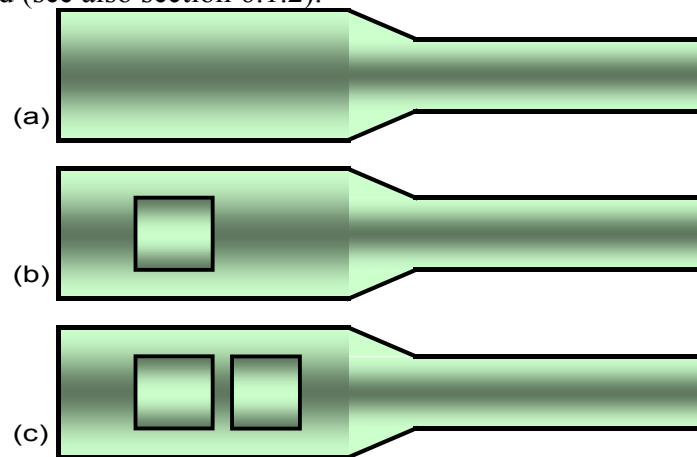


Figure 5.6 Geometries inside a resonator half.

The viscous losses that occur inside the regenerator depend on the viscosity of the working fluid, the velocity, the cross sectional area of the regenerator, the thickness of the regenerator, and the hydraulic diameter. These mathematical relations are part of the program DeltaEC that is used in determination of the viscous losses inside the regenerator. The viscous losses in the regenerator are heating the regenerator. In the program the heat added in the regenerator can only be transferred to the cooling water. When heat conduction through the regenerator in the model is set to zero

$$\begin{aligned} \dot{Q}_{out,coolwater} &= \dot{W}_{viscous\_loss,reg} + \text{proceeds heat} + \dot{Q}_{out,conduction,reg} \\ \text{proceeds heat} &= \dot{Q}_{heater\_to\_gas} \frac{T_{solid,cooler}}{T_{solid,heater}} \end{aligned} \quad (5.14)$$

$$\dot{W}_{viscous\_loss,reg} = \dot{Q}_{out,coolwater} - \dot{Q}_{heater\_to\_gas} \frac{T_{solid,cooler}}{T_{solid,heater}} + 0$$

where  $\dot{W}$  is the power.

## 5.2 Results of detailed analysis

### 5.2.1 Environmental heat losses

The temperatures and acoustic conditions were measured simultaneously from heat images (Appendix D). The heat image camera reading could deviate from the actual temperature. Pictures were taken together with thermocouple readings as reference values (fig.5.7) in order to calibrate the heat camera. At the time figure 5.7b was taken the lab temperature measured 19.38°C and the internal temperature was 200°C.

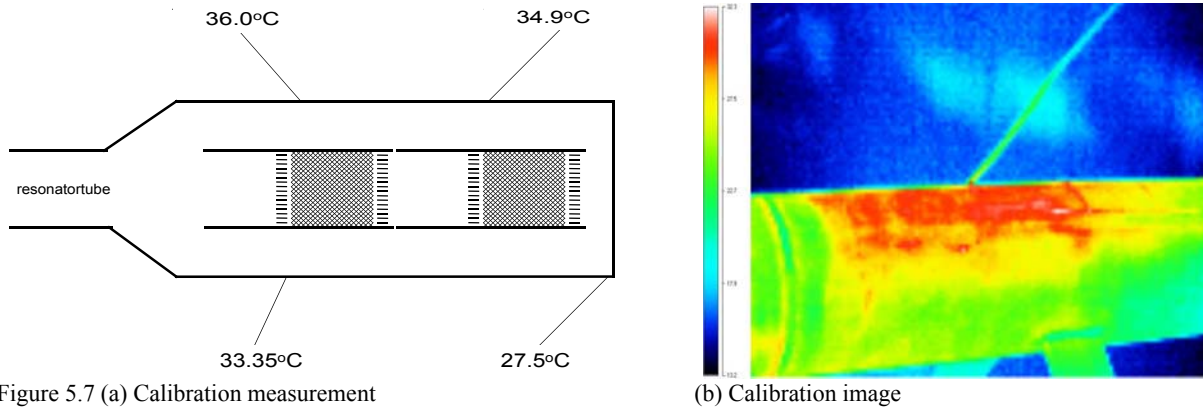


Figure 5.7 (a) Calibration measurement

(b) Calibration image

Appendix D3 shows heat images of the system boundaries when the heat losses to the environment are known to be equal to the difference between the heat input and the extracted heat by the cooling water. The temperature difference between the environment and the surface of the resonator was used to create a correlation.

The results give an estimate of the relation between the type of configuration and the dissipated heat. The difference between ingoing and outgoing heat is very interesting, because it should represent the mechanical losses.

Table VIII System analysis by heat images of the resonator.

$T_{\text{hot regenerator}}$	$T_{\text{environment}}$	$\Delta T$	$q_{\text{in}}$	$q_{\text{coolwater}}$	$q_{\text{in}} - q_{\text{out}}$	$q_{\text{environment}}$
Static*	[°C]	[°C]	[W]	[W]	[W]	[W]
100,30	16,50	3,55	30,69	5,96	0,00	24,73
124,60	17,10	4,83	39,60	8,45	0,00	31,15
<b>Parallel</b>						
180,50	18,50	6,28	197,01	110,36	44,42	<b>42,22</b>
200,50	17,00	7,13	293,83	178,68	67,25	<b>47,90</b>
219,00	17,27	9,54	362,84	201,29	97,40	<b>64,14</b>
<b>Series</b>						
179,85	18,83	5,48	253,24	155,09	61,36	<b>36,79</b>
200,34	20,00	6,18	302,94	199,59	61,80	<b>41,55</b>
219,63	19,43	6,95	353,93	197,03	110,19	<b>46,70</b>

\*parallel configuration with one heated engine

Table VIII shows that the heat losses to the environment in the parallel configuration are an average 18% higher than in serial configuration. Furthermore the mechanical losses were found to be much higher than the acoustic power (over 4 times the engine power). On average the power in the serial

configuration was higher than in the parallel configuration. This is consistent with the better performance and the lower start temperatures of the serial configuration. The uncertainties in the differences between ingoing and outgoing heat fluxes of table VIII are mainly caused by the uncertainties in the amount of heat removed by the cooling water (see section 3.5).

### 5.2.2 Internal heat losses of the unit

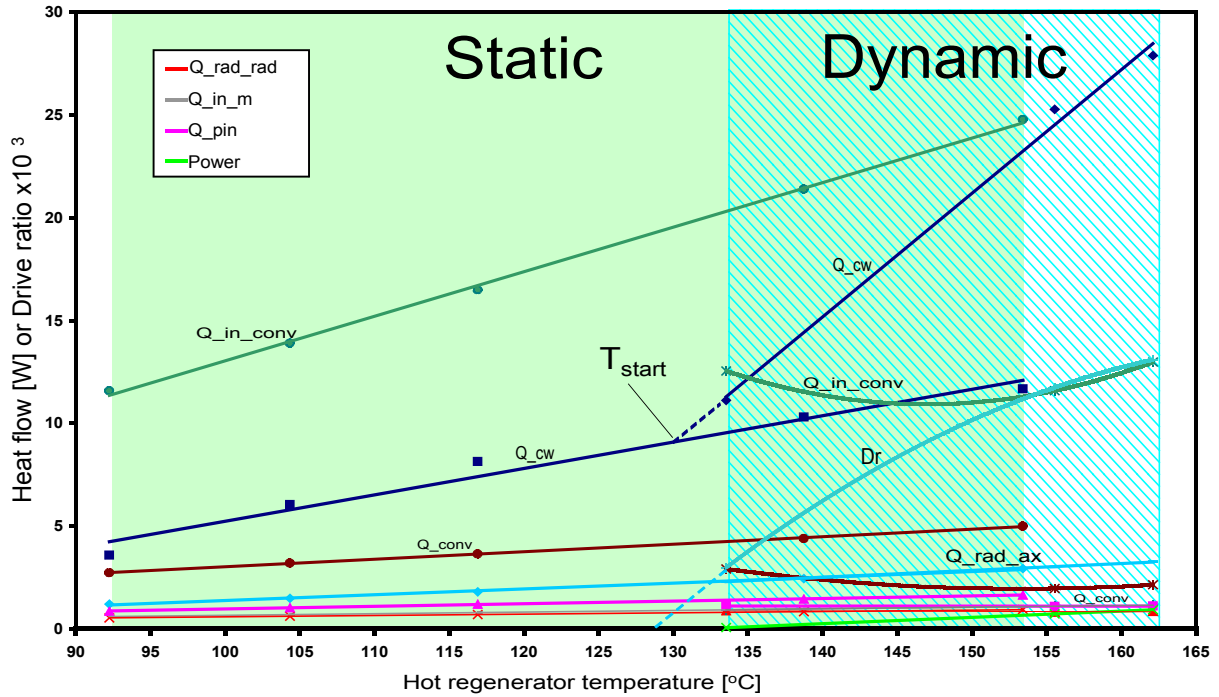


Figure 5.8 The temperature of the hot regenerator side is plotted against the dissipated heat at 19 bar. The drive ratio (Dr) is in tenth of a percent. See table VII for indexes.

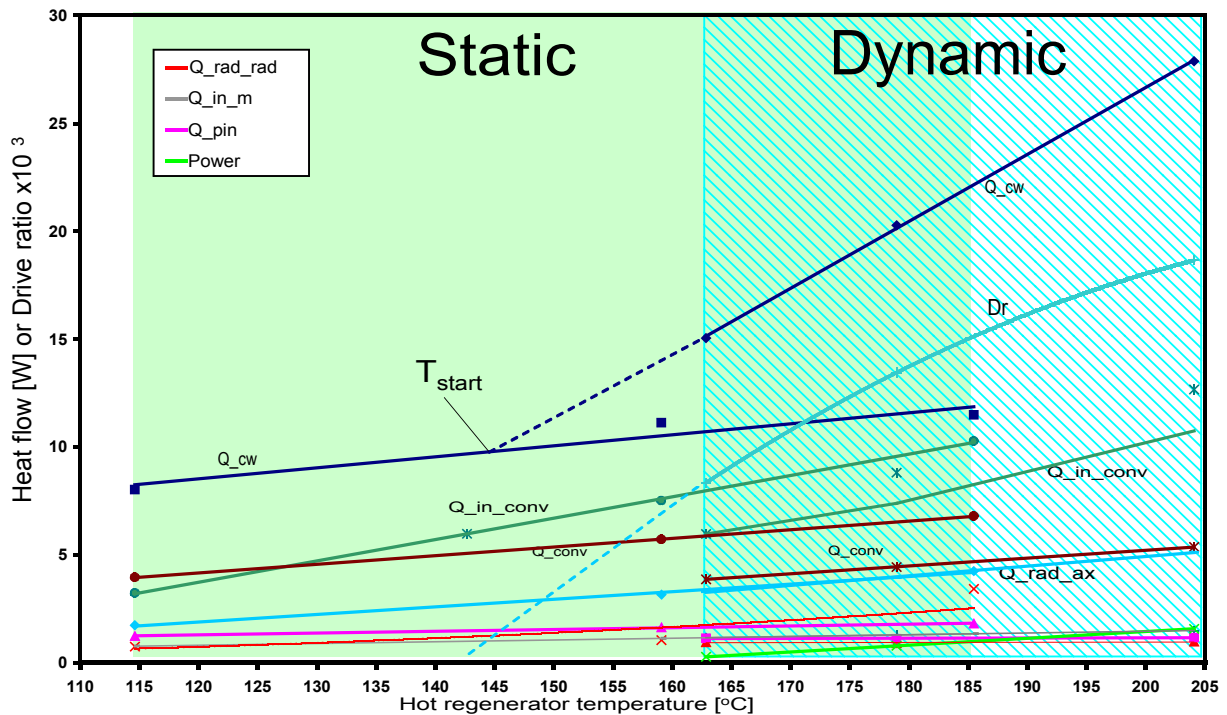


Figure 5.9 The temperature of the hot regenerator side is plotted against the dissipated heat at 13 bar. The drive ratio (Dr) is in tenth of a percent. See table VII for indexes.

In figures 5.8 and 5.9 the heat dissipation is plotted against the temperature of the hot side. The static and dynamic trend lines of the heat removed by the cooling water meet each other at the same temperature ( $T_{start}$ ) as where the drive ratio curve crosses the x-axis. This is the activation or start temperature, which is around 14 K higher for 13 bar than for 19 bar. The start temperature is higher than in multistage configurations.

The outer convection was found to be 2.2 times higher than the predicted natural convection (eq.5.13).

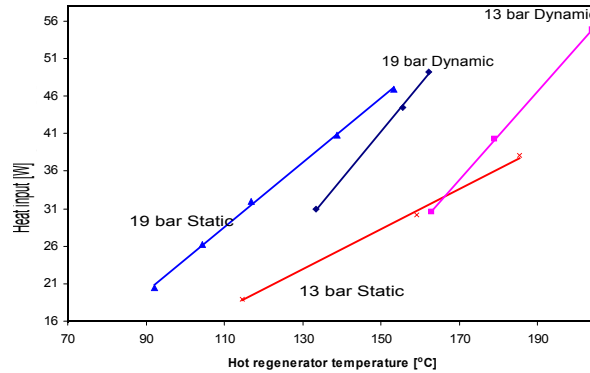


Figure 5.10 Heat input against hot regenerator temperature in heat related experiments with a single unit.

Figure 5.8 and 5.9 further show a big difference between the inner convection of 19 bar and 13 bar, figure 5.10 confirms that far more heat is extracted at 19 bar. Because the heat conduction properties of nitrogen hardly changes between 13 and 19 bar, and the heat extracted by the cooling water is similar (fig.5.8 and 5.9) a mechanical losses must be involved. The Jet streaming, Rayleigh streaming and Gedeon streaming (see also section 2.6) are thermoacoustic effects that are only present in dynamic state. The inner convection was calculated by subtraction of all the other heat losses and does therefore include mechanical losses. Therefore the inner convection losses are much higher than the literature suggests.

The decrease of the inner convection losses when the acoustic wave starts, and thus the velocity in and around the thermal buffer tube increases, suggests some effects similar to the Doppler effect, mechanical losses caused by a highly chaotic motion are suppressed by an organized motion. When the acoustic wave increases in strength mechanical losses increase again because of the increase in Jet streaming.

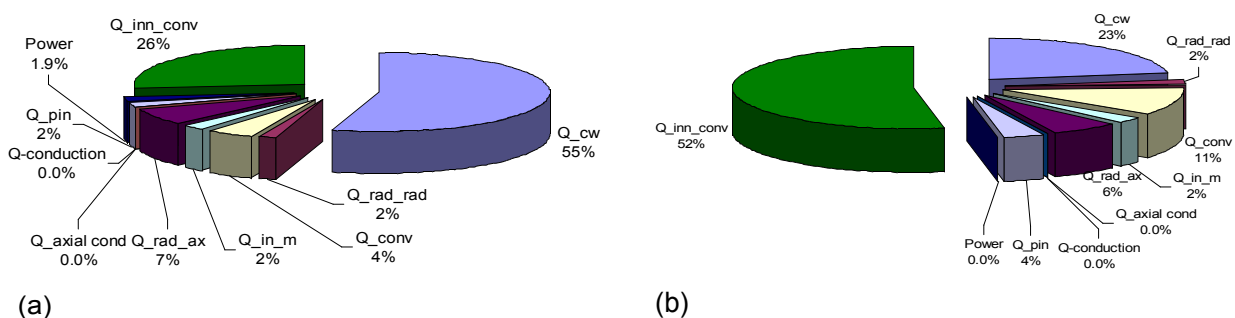


Figure 5.11 Distribution of heat at 19 bar (a) in dynamic (162°C) and (b) static state (154°C) See table VII for indexes

### Heat losses to the environment of a serial configuration compared to a parallel configuration.

The theoretical heat losses in a serial configuration where one unit has a thermal buffer tube of 84mm and one unit has a thermal buffer tube of 62mm are compared against the theoretical heat losses a parallel configuration with two thermal buffer tubes of 84mm. Because the temperature of the thermal buffer tube can be considered uniform (fig.5.5) the heat losses are expected to decrease when the length of the thermal buffer tube decreases from 84 to 62 mm. The axial radiation loss is

expected to increase roughly 25% [29, Appendix C3a] of 7% (fig.5.11) and the inner convection losses are expected to reduce by the same absolute value as the outer convection losses. The heat distribution to the cooling water and the heat used in power production ( $Q_{cw}$ ,  $Q_{in\_m}$ , and Power) don't have a linear relation to the length of the thermal buffer tube. The heat losses that are expected to reduce evenly with the reduction of the length of the thermal buffer tube are the convection losses, the radial radiation losses and, the conduction losses through the pin. The reduction of losses

(twice the convection losses found on the outside + radial radiation losses +

$$\text{conduction losses through the pin}) \frac{\text{decrease in length}}{\text{initial length}} \quad (5.15)$$

$$(2 \cdot Q_{conv} + Q_{rad\_rad} + Q_{pin}) \frac{L_0 - L}{L_0} = 13\% \frac{84 - 62}{84} = 3.4\%$$

The heat losses to the environment are the same as the heat input reduced by the heat distributed to the cooling water and the engine power. In dynamic state (fig.5.11b this is 100%-55%-2%=43%. In a shorter thermal buffer tube the heat losses to the environment are expected to reduce by 3.4% because of the reduction in area and increase by 1.75% because of the change in view factor between the heat source and the environment. The overall reduction is ((43%-41.35%)/43%) 3.85% at 162°C.

In a serial configuration one unit has this shorter thermal buffer tube. The proximity of both engines increases the local gas temperature. A higher local gas temperature in combination with one shorter thermal buffer tube reduces the heat flux from the unit to the gas and therefore the heat losses to the environment by approximately  $(-1 + 42.22/36.79)$  14.8% (see section 5.2.1). This would mean that the effect of increase in heat reduction because of the higher local temperature is more dominant.

The experiments show that higher temperatures could be obtained in the parallel configuration with less heat input. More heat is necessary in the serial configuration because more heat is lost by conduction in the second engine with a thinner regenerator

$$\frac{k_{series}}{k_{parallel}} = k_{single\_unit} \frac{L_{su} + L_{su}}{L_{u1} + L_{u2}} = \frac{15 + 15}{15 + 13.2} = 1.064 \quad (5.16).$$

The heat conducted through a 15mm thick regenerator is 23% at 154°C (fig.5.11). The heat distributed to the cooling water in the serial configuration would be

$$\left( \frac{k_{parallel} + \frac{k_{series}}{k_{parallel}} - 2k_{parallel}}{2k_{parallel}} \right) \frac{Q_{conduction,reg}}{Q_{total}} = \frac{1 + 1.064 - 2}{2} 23\% = 0.74\% \quad (5.17)$$

of the total heat input more than in the parallel configuration.

In the data sets with a drive ratio of 2.3% and 3.0% (from the experiments discussed in chapter 4) the temperature difference between the cold regenerator side of the second unit and the cooling water in the serial configuration is about 40% more than in the units of the parallel configurations and the first unit in the serial configuration. An increase of 40% of the temperature difference in a single heat exchanger increases the overall heat losses by conduction to the cooling water of two identical heat exchangers by 20%. The heat losses to the environment are about 18% less in the serial configuration (see section 5.2.1). In dynamic state about 60% of the heat is lost to the cooling water and 40% is lost to the environment (fig.5.8 and 5.11). The total heat dissipated in the serial configuration therefore is about  $(0.6 \cdot 20\% - 0.4 \cdot 18\%)$  4.8% higher than in the parallel configuration at the same temperature. The heat dissipation increase in the second unit because of conduction is much lower than the increase in heat dissipated by the second unit, the high viscous losses in the second regenerator are transferred back into heat.

The total heat dissipation does not contribute to a better performance of the serial configuration, but the localized hot gas temperature does.

### 5.2.3 Viscous losses around the unit

In order to find the viscous losses around the unit, the viscous losses in a resonator half with dummy was measured with the two microphone method and compared against the viscous losses in an empty resonator half (fig.5.6). The measurements with an empty resonator half are done in the serial configuration. On the x-axis the drive ratio squared is used, because the local velocity is not measured.

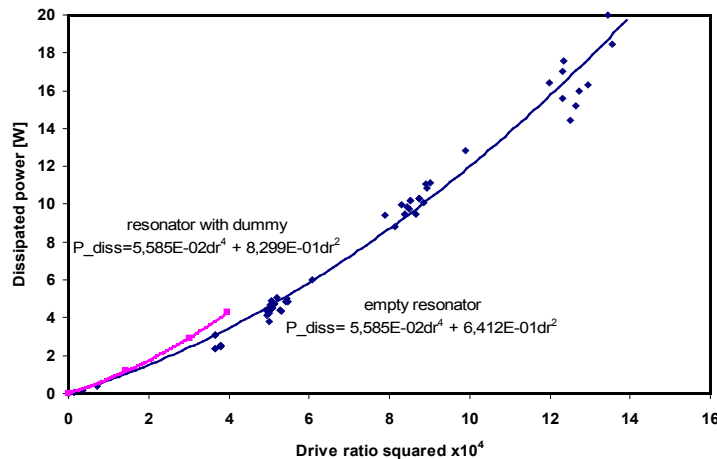


Figure 5.11 Losses in the resonator and around a dummy

Figure 5.11 can be interpreted in two ways. In reality there is a laminar and a turbulent region in the resonator, dependent on position and internal drive ratio, although the velocities in the resonator are not uniform the shift from laminar to turbulent is smooth. This relationship was used in the determination of the resonator friction losses in the parallel setup. The measured power dissipated around a dummy unit of 128mm are 0.1887 Watt at a standardized drive ratio squared of  $10^{-4}$  more than an empty resonator half.

The viscous losses in the regenerator are well defined in DeltaEC (fig.5.12).

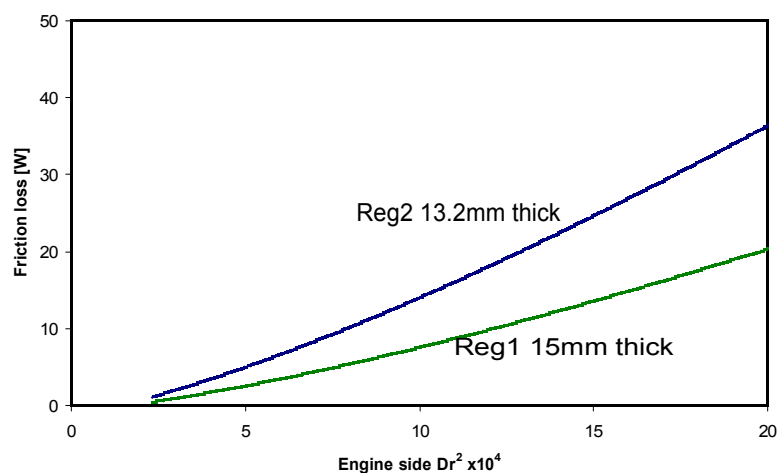


Figure 5.12 Regenerator friction losses of the serial configuration at different drive ratios at 19 bar

In figure 5.12 the drive ratios are similar to the drive ratios in the experiments. The viscous losses in the regenerator depend on the location, the drive ratio, the hydraulic diameter, the cross sectional area, and the thickness. The location, the hydraulic diameter, and the cross sectional area are the same for the regenerators in the parallel configuration as for Reg1 (fig.5.12), but the thickness and therefore the viscous losses are 3.33% less (compare Table II and III) than Reg1 in figure 5.12.

# 6. Discussion

## 6.1 Configuration comparison

The results of the comparison between serial configurations and parallel configurations show three important differences:

- I. The serial configuration reaches more favorable, higher, drive ratios with the same temperature differences.
- II. The efficiencies of the serial configuration are better than of an equivalent parallel configuration.
- III. The serial configuration is able to produce more useful power than the parallel configuration.

These statements are drawn from measurements where the friction losses around the engine were considered as a inherent part of the power produced by the engine. The engine power is derived from an empty half of the resonator. In reality the units have to produce more acoustic power to overcome all viscous losses. The viscous losses in the serial configuration are higher because the velocity amplitudes are higher around the second engine.

An increase of the flow velocities near the flange may occur due to flow to and from the load. Then the unit placed near the load will dissipate more viscous losses. This could lead to a reduction in the power that could be dissipated by the load in a parallel configuration.

Another issue which is less straightforward involves the effect of the higher pressure amplitude in the engine side of the serial configuration. This implies the viscous losses that the engine overcomes were higher, because the losses in the resonator are not symmetrical and only the losses on the load side were determined.

The question that should be answered is whether the external performance of serial configurations is much better due to better performance of the units or due to friction losses around the asymmetric load.

In section (6.1) adjustments on the measured values will be implemented in order to answer this question.

### 6.1.1 Correction-factor for the flange amplitude

The drive ratio is measured at the load side, which is for the serial configuration the opposite side of the engines. In parallel the engines are placed on both sides. In the results the drive ratio at the engine side was derived from the correlation in DeltaEC between the pressure amplitude on the engine side and the load side.

The drive ratio is an important parameter, therefore it is better to derive the difference in drive ratio between the engine and the load side for the serial configuration from the test results. In a simple resonator with two closed ends the pressure amplitude in the first mode could be expressed by

$$p_a = p_{a,\max} \left( 1 - \sin \left( \frac{\pi x}{L} \right) \right). \quad (6.1)$$

The velocity amplitude in the resonator has a 90° phase difference with the pressure amplitude. Because the friction/ viscous losses are related to the velocity squared it is good to express the velocity squared.

$$\vec{u}_a^2 = \vec{u}_{a,\max}^2 \sin^2 \left( \frac{\pi x}{L} \right) \quad (6.2)$$

The pressure amplitude that is read in the middle of the resonator will be higher than zero because it

is measured at the wall, then 6.1 and 6.2 become

$$P_a(x) = (P_{a,max\_loadside} - \alpha_{wall}) \left( 1 - \sin\left(\frac{\pi x}{L}\right) \right) + K_f(x) \sin^2\left(\frac{\pi x}{L}\right) + \alpha_{wall} \quad (6.3)$$

$$P_a(x) \approx P_{a,max\_loadside} \left( 1 - \sin\left(\frac{\pi x}{L}\right) \right) + K_f(x) \sin^2\left(\frac{\pi x}{L}\right)$$

where  $K_f(x)$  is the friction factor and  $\alpha_{wall}$  is a function to compensate for the minimum amplitude.

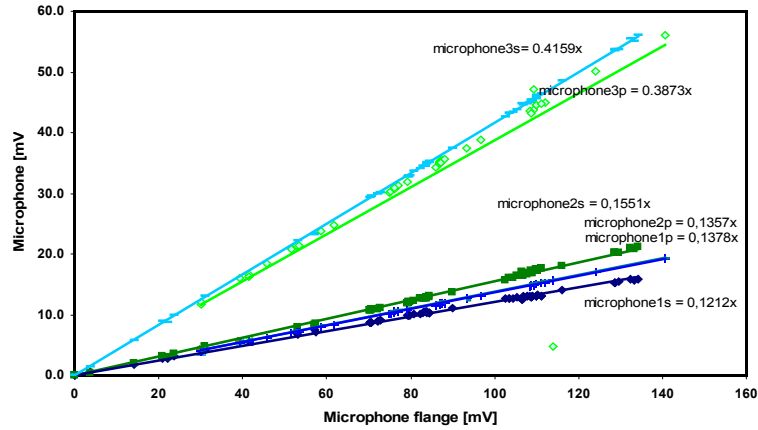


Figure 6.1 Three middle microphones readings in series 's' and in parallel 'p' against the flange microphone reading.

In figure 6.1 the readings of the pressure sensors in the middle of the resonator during serial configuration are plotted against the flange pressure. In figure 6.2 a numerical fit of the first and second microphone was made according to eq.6.3. This resulted in a pressure amplitude 19% higher on the engine side than on the load side. The third microphone however didn't match the fit. Therefore the pressure correction of 7.15% more pressure amplitude on engine than on load side in series from the DeltaEC model will be used in the correction of the acoustic power. In reality the pressure amplitude on the engine side could be higher then the corrected value.

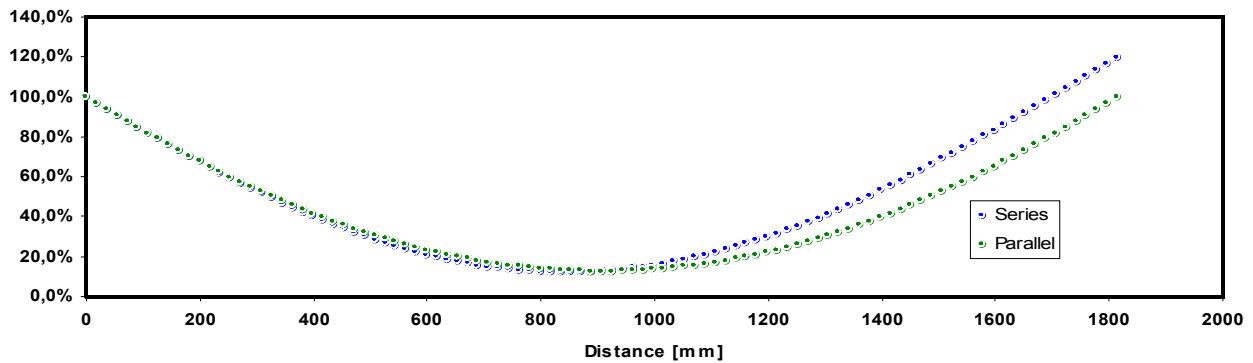


Figure 6.2 Corrected pressure profile based on the phase shift of the two microphones in the middle.

### 6.1.2 Correction of the acoustic power

In this study and previous studies the viscous losses around the unit and in the regenerator were considered as a part of the coaxial thermoacoustic engine. The power converted in the regenerators has to be higher to overcome these viscous losses. In this section power converted in the regenerators in the first mode is estimated using the viscous losses determined in section 5.2.3.

$$\text{Viscous losses per length of the unit} = K \cdot \bar{u}^2$$

Losses in the resonator are related to  $Dr^2$  (fig.3.12)

Losses in the resonator are described in section 5.2.3

The first mode acoustic power produced by the regenerators at the same pressure is

$$\left( \underbrace{\frac{\bar{u}^2}{\bar{u}_{ref}^2} \frac{L_{unit}}{L_{dummy}} K(Dr_{load})}_{\text{Viscous losses around the units}} + \underbrace{\frac{Dr_{loadside}^2 + Dr_{engineside}^2}{2Dr_{loadside}^2} K(Dr_{load})}_{\text{Losses in the resonator}} + \underbrace{K(Dr_{engine})}_{\text{Viscous losses in the regenerator}} \right) + \dot{W}_{load} \quad (6.4)$$

where  $L$  is the length of the unit,  $K(Dr)$  is a drive ratio dependent friction function in Watt.

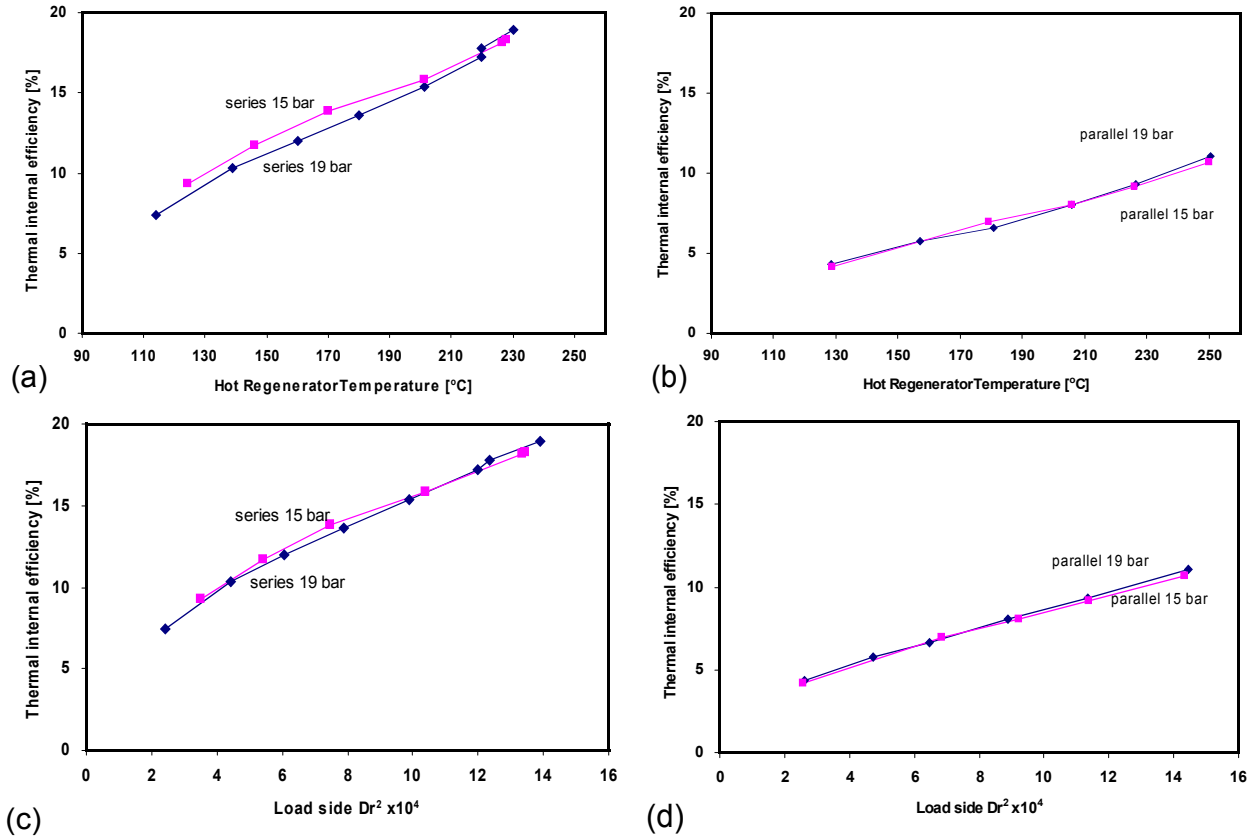


Figure 6.3 Thermal internal regenerator efficiencies for serial and parallel configurations. (a) Serial configuration, function of hot regenerator temperature (b) Parallel configuration, function of hot regenerator temperature (c) Serial configuration, function of drive ratio (d) Parallel configuration, function of drive ratio.

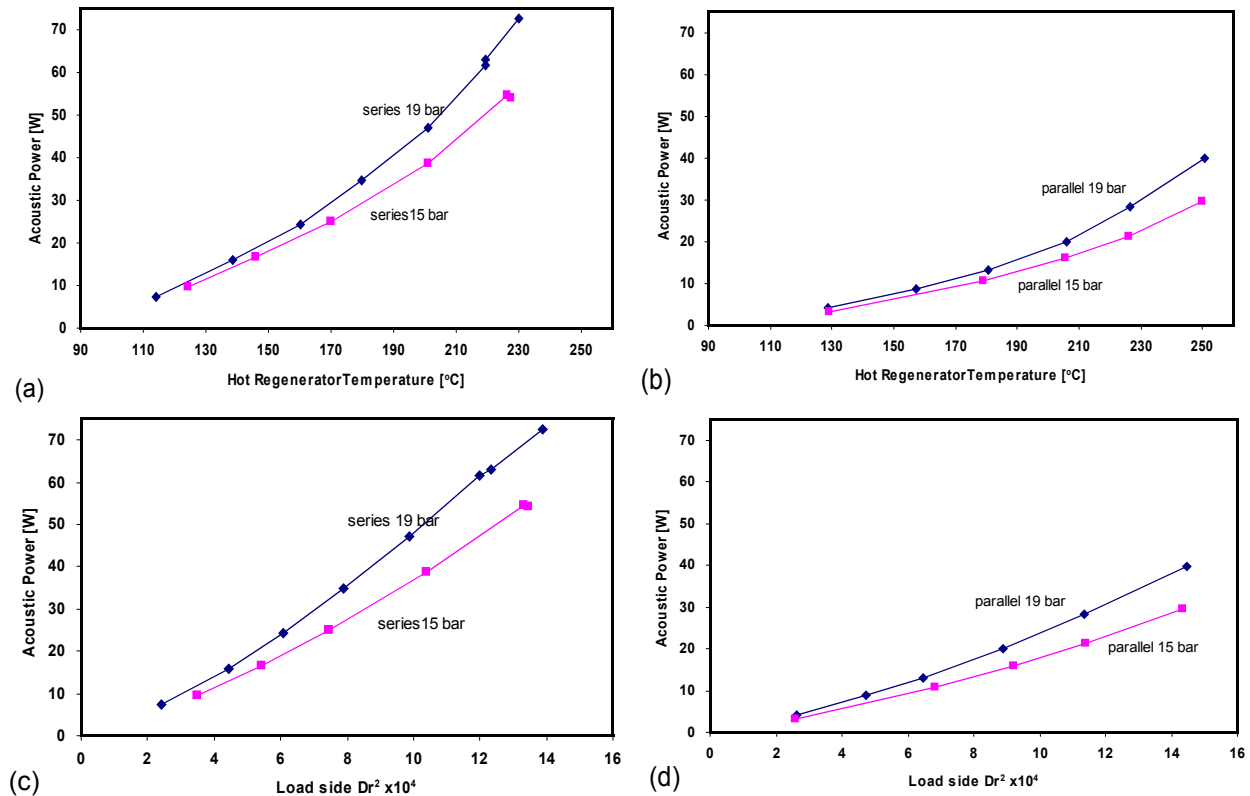


Figure 6.4 Acoustic regenerator power produced in the different configurations (a) Serial configuration, function of hot regenerator temperature (b) Parallel configuration, function of hot regenerator temperature (c) Serial configuration, function of drive ratio (d) Parallel configuration, function of drive ratio.

The thermal internal efficiency of the regenerators is plotted against hot temperature and drive ratio in figure 6.3. Figures 6.3 and 6.4 show that there is about 80% more acoustic power generated in the serial configuration than in the parallel configuration. If the internal efficiencies of the regenerators were similar to the internal efficiencies of the engines (fig.4.5) the differences in the external efficiency could not have been explained. When the external efficiency (fig.4.7) is combined with the internal efficiency of the regenerators (fig.6.3), the serial configuration is consistently better.

Quantitatively figure 6.3 and figure 4.7 don't match. It could be the viscous losses around the second unit are overestimated, because when two units are placed in close proximity the flow losses that occur because of the sharp edges are reduced. Furthermore increased acoustic power production would also increase losses in the regenerator. Therefore including viscous losses in the regenerator in the total heat that is converted into acoustic energy may predict better expectations for the configuration where viscous losses in the regenerator will increase more with the same power increase than in the other configuration. Indeed the difference between serial and parallel configurations is higher in this quantitative solution (fig.6.3 and 6.4) In section 6.1.3 in the 'acoustic power derived method' a reflection on the quantitative results of this section will be given.

### 6.1.3 Correction of the load power

There are two ways to calculate the theoretical load power that could be dissipated from the system. When no additional power is lost around the unit in a parallel configuration due to the increase in flow velocity amplitude, as the valve to the load is opened further. And the drive ratio is the same for the load and the engine side.

1) *Acoustic power derived method:* The start conditions can be found by use of figures 6.3 and 6.4.

As the power dissipated by the load increases, while the drive ratio and therefore the power going into the units remains constant, the temperature needs to increase. How much the temperature will need to increase depends on the overall amplification factor of the configuration. In this way the data from the first set of experiments (section 4.1) is used together with the viscous losses (section 5.2.3) to reproduce the data from the second set of experiments (section 4.3).

2) *Load streaming derived method*: The simulation can be used to find a correlation between the opening of the valve to the load and the velocity around the unit that is placed on the load side in a parallel configuration. The viscous losses are known when the valve is closed (section 5.2.3). When the load would be placed somewhere else, the load power that can be extracted would increase relative to the experimental results for the parallel configuration by the same amount the viscous losses increased.

### Acoustic power derived symmetrical load power

From figure 6.3 and 6.4 The reference power and start temperature can be found for different drive ratios. From the experimental results a relation between hot temperature and cold temperature of the regenerator can be found. The main mechanism in the regenerator is conduction. The cold temperature is mainly dependent on the hot temperature and partly on the acoustics. The data can be used to create a linear relation between hot and cold temperature as a function of the hot regenerator temperature.

From the linearized model eq.2.13 and 2.17 we know the amplification factor as a function of the ratio between hot and cold temperature. The specific amplification factor increases when the temperature increases. When the conditions (pressure and drive ratio) stay the same the ingoing work to the regenerator stays the same. When the specific amplification factor increases, the power converted in the regenerator will increase above the initial or reference value by the ratio between the amplification factor and the initial amplification factor. The acoustic power converted in the regenerator can be defined as

$$\dot{W}_{ref} \frac{2\tau - 2}{2\tau_{ref} - 2} < \dot{W}_{out,series} < \dot{W}_{ref} \frac{\tau^2 - 1}{\tau_{ref}^2 - 1}$$

$$\dot{W}_{out,parallel} = \dot{W}_{ref} \frac{2\tau - 2}{2\tau_{ref} - 2} \quad (6.5)$$

with:  $\tau = \frac{T_h}{T_c}$ , and  $T_c$  a function of  $T_h$

where  $\dot{W}_{in}$  is the ingoing work,  $\dot{W}_{out}$  is the converted power, and the subscript 'ref' corresponds with the reference value that is found when the operating drive ratio is found.

The characteristics of figure 6.3 & 6.4 can be used to determine the temperature necessary to obtain a certain drive ratio and see what acoustic power needs to be produced in order to maintain these conditions. When a load is applied, but the ingoing conditions of the engine remain the same, the load power can only be produced by a higher temperature difference.

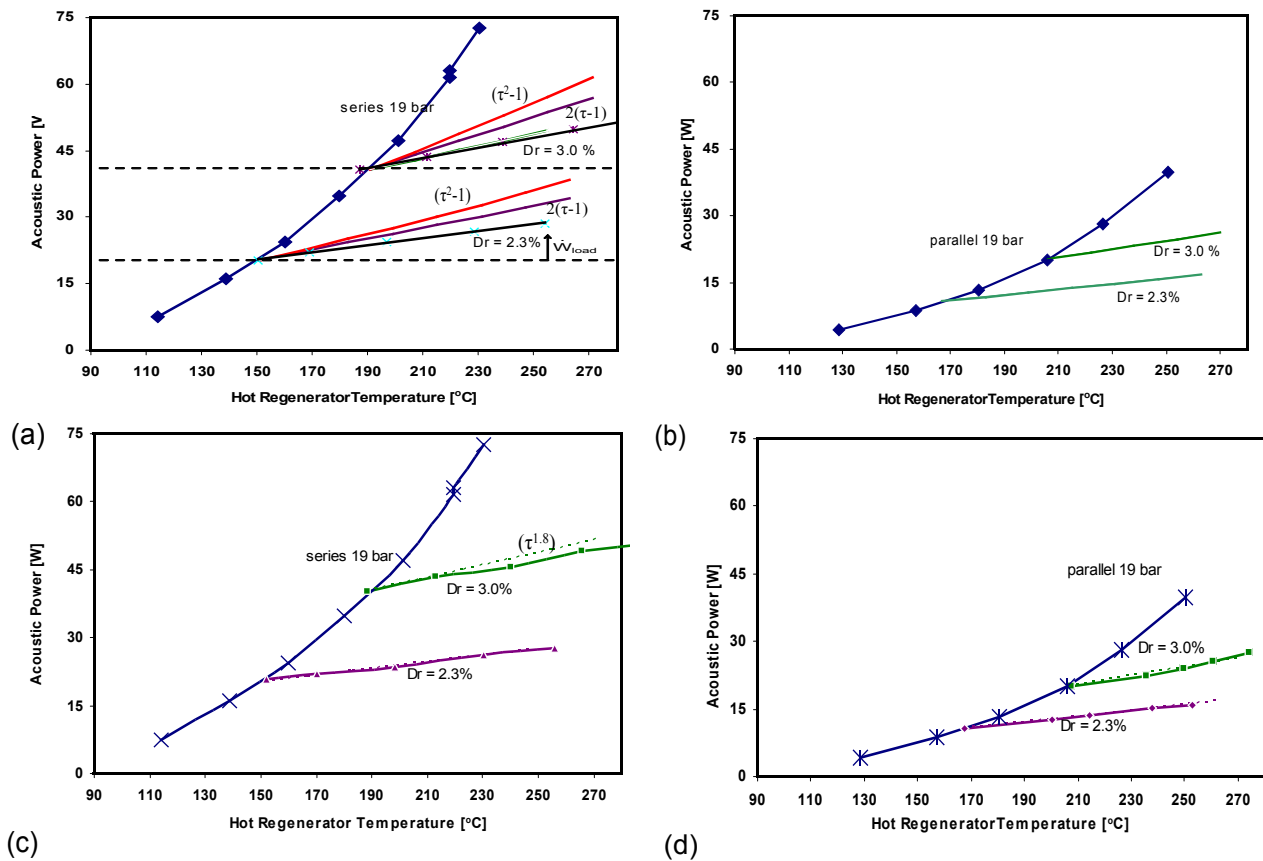


Figure 6.5 Acoustic regenerator power in load and no load conditions. (a) Serial configuration, load conditions calculated by the specific amplification factor (b) Parallel configuration, load conditions calculated by the specific amplification factor (c) Serial configuration, load conditions from experiments (d) Parallel configuration, load conditions from experiments. In (c & d) the calculated values are presented by a dashed line.

In figure 6.5d the load power predicted by eq.2.13 when the total acoustic power converted in the regenerator from figure 6.4 is used for the start condition is plotted as a dotted line (same as 6.5b). When figure 6.5b where the load power is calculated is compared to 6.5d where the load power was measured the similarity is striking. This means that the losses due to asymmetric placement of the load can not have a big influence on the power that can be subtracted from the system. The amount of load power predicted by the linear equation is only correct if reference power at the start conditions are correct. It confirms the values adjusted acoustic power for the parallel configuration (fig.6.4b and d).

In figure 6.5a is shown the load power is the difference between the resonator power (at startup conditions for a certain drive ratio) and the excess power. The theoretical load power in the parallel configuration is given in figure 6.6. The load efficiency depends on how the heat is distributed in the different configurations. The relation between temperature and heat distribution found in the experimental results is used whereas the load power is derived from figure 6.5b.

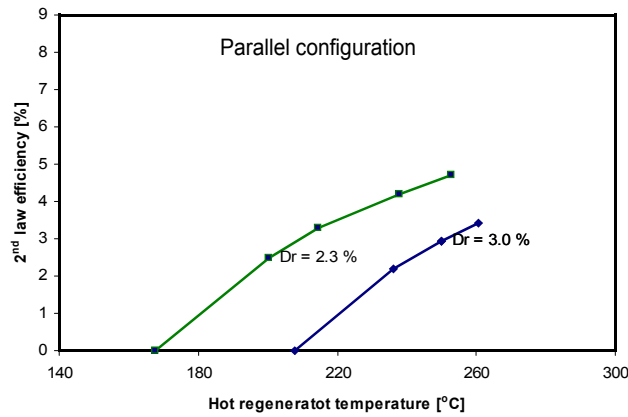


Figure 6.6 Predicted 2<sup>nd</sup> law external efficiency as a function of hot temperature in a parallel configuration

The theoretical load power from the parallel configuration is the same as the experimentally determined load power (fig.6.6).

In figure 6.5a the measured load power (black) is much lower than predicted by the two amplification factors (red and dark purple). This could be because the amplification factor in the serial configuration is much lower than in the parallel configuration, but then the total acoustic power would not increase more rapidly with the increase in temperature than in the parallel configuration. Then this must be because the adjusted acoustic power is not done correctly for the viscous losses around the second unit. Or the acoustic power output behaves quite differently than in any amplification factor model. As an example the power dissipated by the load was compared in figure 6.5c to a fitting amplification equation of  $\tau^{1.8}$ , which is independent from the power input. This could be caused when the temperature increase that is caused by the viscous losses is converted back into acoustic power (the corresponding amplification equation:  $\tau^{1.8}-1+1$ ).

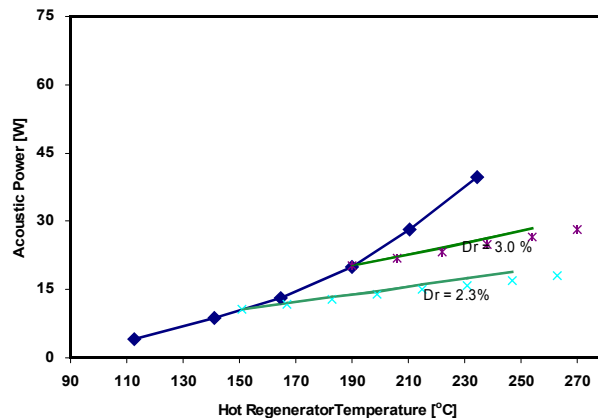


Figure 6.7 Data of acoustic power converted in the parallel configuration with the temperatures 16 K lower

When the adjusted acoustic power levels found in the serial configuration are incorrect the adjusted acoustic power levels in the parallel configuration (fig.6.7) can be used to quantify the error. In figure 6.7 the acoustic power converted in the parallel configuration is used. The x-axis is moved 16K so the start temperatures are equal to the start temperature in the serial configuration (fig.4.2c). The green lines are calculated based on a amplification factor of  $\tau^2-1$  and the crosses are calculated based on an amplification factor of  $2\tau-2$ . For a drive ratio of 3.0% the load power at 268°C then becomes respectively 10.4 W and 8.0 W when the dissipated load power in reality was 10.4 W. This means the converted power at this point which is equal to the sum of all viscous losses are likely to be 0-30% more than in the parallel configuration because of to the location and size of the second unit.

Whatever causes the discrepancy in figure 6.5a, the theoretical excess load power that can be dissipated in the serial configuration is higher than the results found in the experiments. Because the theoretical and experimental values of the power dissipated by the load fit (fig.6.5c) the power that can be dissipated in the load is more likely underestimated in the serial configuration than in the parallel configuration. It is likely that the volumetric flow to the load does not increase the velocity significantly around the unit in the parallel configuration. The results of the external efficiencies are representative.

The discrepancy in figure 6.5a cannot be explained by a single cause. The real quantitative temperature dependent amplification factor of a serial configuration cannot be found.

### Load streaming derived symmetrical load power

DeltaEC is a modeling tool that can accurately predict the acoustic behavior. When an external volume with a control valve is added as a load in the geometry the local increase in velocity can be calculated.

The volumetric velocity at the start and the end of the parallel unit closest to the load is plotted against the load power (fig.6.8).

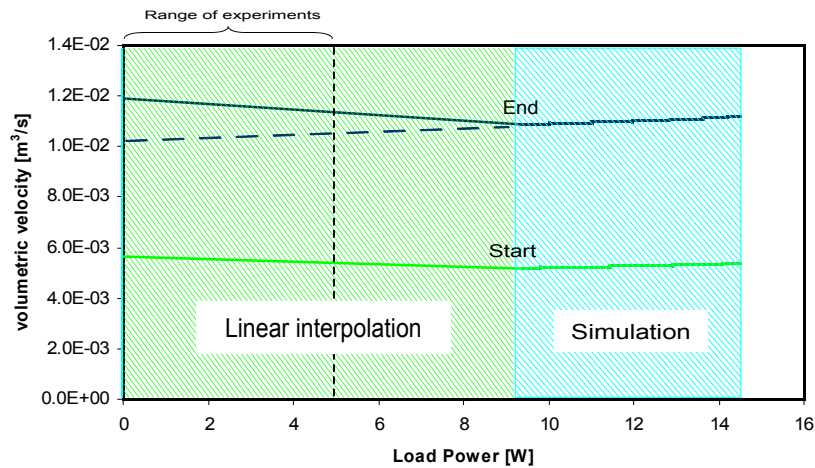


Figure 6.8 volumetric velocity at end and start position of the unit under load conditions.  $Dr = 2.3$

Although the simulation does predict an increase in the velocities when the load power increases from 9 W till 14 W, it also predicts higher velocities when the valve to the load is closed. The simulation was not stable for load powers up to 9 W. Therefore between 0 and 9 watt of load power the velocities were found by linear interpolation.

If the velocity would increase linearly with the load power, based on the data between 9W and 14 W load power, the volumetric velocity amplitude at the end of the unit at load side in the parallel configuration would have been  $0.0104 \text{ m}^3/\text{s}$  under no load conditions and  $0.010703 \text{ m}^3/\text{s}$  under a maximum load of 5 Watt (fig.6.8). The viscous losses are proportional to the velocity squared increase of load power then would have been

$$1778Dr^2 \left( \frac{U_{load}}{U_0} \right)^2 = \frac{1778 \cdot 9}{100 \cdot 100} \left( \frac{1.0703}{1.04} \right)^2 \cong 0.19 \text{ W} \quad (6.6)$$

at a load power of 5 Watt, which would mean the theoretical load power in the parallel configuration could be 4% higher than the measured value. This would still make the serial configuration performs better under all circumstances. When not the dashed line in figure 6.8, which is bases on the results of the simulation between 9 and 14 Watt, is used but the solid line, which is based on the results of 0 and 9 watts. The parallel configuration has even less viscous losses when the load power increases from 0 to 5 Watt. Therefore the theory that increased viscous

losses around the unit at load side causes the parallel configuration to dissipate less power in the load can be dismissed.

## **6.2 Irreversibilities from additional experiments**

In chapter 5 the losses in the system have been analyzed. Heat images (section 5.2.1) showed that the sum of acoustic power, the heat losses to the environment and the cooling water is far less than the heat power input.

The compensated acoustic power that was found in section 6.1.2 was more in line with the results (section 5.2.1). Mechanical power can be dissipated to the environment through vibrations. The difference between ingoing and outgoing heat in section 5.2.1 can not be explained by measurement errors alone and probably exceeds the mechanical energy dissipated to the nearby environment through vibrations.

The production of chaotic mechanical power as suggested in section 5.2.2 is likely.



# 7 Conclusions and Recommendations

## 7.1 Conclusions

The experiments show that the serial configuration produced more acoustic power in the load than the parallel configuration. In contrast the efficiency of the power dissipated in the resonator, which is over half the engine power, is found to be about the same for both configurations. This is because of the assumption that the power dissipated in the resonator is equal to twice the power dissipated in an empty half of the resonator, while in reality the power dissipated in the resonator depends also on the internal geometries in the resonator, and the internal velocity.

In the present experimental setup the pressure and velocity profile are not the same for serial and parallel configurations. The acoustic power measured in the load is used to compute the external efficiency. The internal efficiency is calculated from the resonator losses and the power measured in the load. The resonator losses were originally determined from two microphone measurements of an empty resonator half, without the consideration of internal geometries. Hence internal efficiencies of the two configurations can not be compared, whereas the external efficiencies can be compared to draw conclusions.

In the parallel configuration at a pressure of 19.9 bar, a drive ratio of 3.03 and a heater input of 324 W, 5.96 W of acoustic power can be subtracted while the hot regenerator temperature rises till 274 °C. In the serial configuration at a pressure of 19.5 bar, a drive ratio of 2.95 and a heater input of 367 W, 11.63 W of acoustic power can be subtracted while the hot regenerator temperature rises till 290 °C. This means the 2<sup>nd</sup> law external efficiency of the serial configuration is 47% better than for the parallel configuration. A calculation predicts that the serial configuration could perform as much as 80% better if the load was placed at the engine side.

In cooling, heating, and other processes where the external power is the useful power the serial configuration is the better configuration.

## 7.2 Recommendations

The power dissipated in the resonator in parallel and serial configurations is similar. There is a lot of power lost due to friction around the casing in the serial configuration. In a torus configuration there are no friction losses around the unit. It is likely a serial torus configuration produces more efficiently resonator power than a parallel torus configuration. This could be proven in a new test.

In the discussion (S6.1.2) compensation for friction losses proved to be valuable for the consistency of the experimental data. In section 6.1.1 it was proven that the drive ratio on the engine side was likely to be higher than the model predicted. In any asymmetric system the drive ratio should be measured on both ends for analysis of the system.

The viscous losses around the unit are found to be much higher than the DeltaEC model anticipated. This explains a lot of the differences in performance between the model and reality. This friction however could also cause phase changes that affect the performance of the regenerators. Internally placed microphones can find the phase difference and help to further optimize the serial configuration.

In Section 6.1.3 the amplification factor in the serial configuration could not predict the power that could be dissipated by the load power from the total acoustic power that was produced. This may be due to a misinterpretation of the acoustic power produced. If the viscous losses around a serial configuration dummy engine are to be measured (fig.5.6c) and prove to be much lower than predicted, the experimental results of the acoustic power produced by the regenerators in the serial configuration in combination with the power dissipated by the load could be used to determine the real amplification factor of this serial configuration. This will quantify the difference in performance between serial and parallel configurations in a general form.

The highest amount of heat loss occurs in the inside of the thermal buffer zone. These heat losses are likely to occur also in the more efficient torus configuration. The placement of a wide grid stack inside the thermal buffer zone will reduce the turbulent streaming. It will be interesting to see how a stack that functions as a low resistance flow straightener affects the efficiency and the start temperature of a thermoacoustic engine.

## References

1. Lord Rayleigh: The explanation of certain acoustical phenomena.  
Nature (1878) pp. 318-321
2. N. Rott: Damped and thermally driven acoustic oscillation in wide and narrow tubes.  
Z. Angew. Phys. (1969) pp. 230-243
3. N. Rott: Thermally driven acoustic oscillations, part III Second order heat flux.  
Z. Angew. Phys. (1975) pp. 43-49
4. N. Rott: Thermoacoustics.  
Advanced applied Mechanics (1980) pp. 133-175
5. K.T. Feldman: Review of the literature on Sondhauss thermoacoustic phenomena.  
J. Sound Vib. (1968) pp. 71-82
6. K.T. Feldman: Review of the literature on Rijke thermoacoustic phenomena.  
J. Sound Vib. (1968) pp. 83-89
7. P. H. Ceperly: A pistonless stirling engine  
Acoustic society of America Volume 66 No. 5 (1979)
8. P. H. Ceperly: Gain and efficiency of a short traveling wave heat engine  
Acoustic society of America Volume 77 (1985)
9. E.L. Mikulin, A.A. Tarasov, and M.P. Shkrebyonock: Low Temperature expansion pulse tubes.  
Advanced Cryogenic engineering (1984) pp. 629-637
10. J. Urieli and D.M. Berchowitz: Stirling Cycle Machine  
Adam Hilger, Bristol UK (1984)
11. D.E. Hall: Basic Acoustics  
Wiley New York (1987) pp. 247
12. B. Zinn: Pulsating combustion  
Advanced Combustion Methods (1986) pp. 113-181
13. J. Weathley, T. Hoffler, G.W. Swift, and A. Migliori: Understanding some simple phenomena in thermoacoustics with applications to acoustical heat engines.  
American association of physics teachers (1985)
14. T. Hofler, J.C. Wheatley, G.W. Swift, and A. Migliori: Acoustic cooling engine.  
US Patent No. 4,722,201 (1988)
15. G.W. Swift: Thermoacoustic engines  
Acoustic Society of America Volume 94 (1988) pp. 1145-1179
16. A.M. Fusco, W.C. Ward, and G. W. Swift: Two-sensor power measurement in lossy ducts.  
Acoustic society of America Volume 91 No. 4 (1992) pp. 2229-2235
17. S. Backhaus and G.W. Swift: A thermoacoustic-stirling heat engine  
Acoustic society of America Volume 107 No. 6 (2000)
18. G. Swift: What is thermoacoustics?  
Condensed Matter and Thermal Physics Group Los Alamos Nat. Library (2004)
19. C.M. De Blok: Thermoacoustic system.  
Dutch Patent: International Application No. PCT?NL98?00515. US Patent 6,314,740
20. M.E.H. Tijani, J.C.H. Zeegers, and A.T.A.M. Waele: The optimal stack spacing for thermoacoustic refrigeration  
Acoustic society of America Volume 112 No.1 (2002) pp. 128-133
21. M.E.H. Tijani, S. Spoelstra, and P.W. Bach: Thermal-relaxation dissipation in thermoacoustic systems  
Applied Acoustics 65 (2004) pp. 1-13
22. J.A. Lycklama à Nijeholt, M.E.H. Tijani and S. Spoelstra: Simulation of a traveling-wave thermoacoustic engine using computational fluid dynamics  
Acoustic society of America Volume 116 No.4 (2005) pp. 2265-2270

23. K. I. Matveev, G. W. Swift, and S. Backhaus: Analytical solution for temperature profiles at the ends of thermal buffer tubes  
International Journal of heat and Mass Transfer 50 (2007) pp. 897-901
24. A. Berson, M. Michard, and P. Blanc-Benon: Measurement of acoustic velocity in the stack of a thermoacoustic refrigerator using partial image velocimetry.  
Springer verlag (2007)
25. Q. Li, L. Chen, F. Wu, F. Guo, and D. Gua: Optimal exergy efficiency of a thermoacoustic cooler with a complex heat-transfer exponent.  
Applied Energy (2008)
26. M.E.H. Tijani, S. Spoelstra: Study of a coaxial thermoacoustic-Stirling cooler  
Cryogenics 48 (2008) pp. 77-82
27. L.E. Kinsler, A.R. Frey, A.B. Coppens, J.V. Sanders: Fundamentals of Acoustics 4<sup>th</sup> edition  
Wiley and sons pp. 93
28. J.R. Olsen and G.W. Swift: Acoustic streaming in pulse tube refrigerators. Tapered pulse tubes  
Cryogenics 37 (1998) pp. 769–776
29. A.F. Mills: Heat and Mass Transfer  
Richard D. Irwing Inc. (1995) pp. 293-314